The connectome of medullary sympathetic premotor neurons

MACQUARIE
University

Bowen Richard Dempsey (BSc, Honours 1st)

Faculty of Medicine and Health Sciences

Macquarie University

A thesis submitted to Macquarie University in fulfilment of the requirements for the degree of Doctor of Philosophy

Principal Supervisor: Dr Simon McMullan

Associate Supervisor: Associate Professor Ann Goodchild

Adjunct Supervisor: Professor Andrew Allen

Table of contents

Abstract

The basal and evoked activity of sympathetic nerves, and therefore the physiological consequences of sympathetic nerve activity (e.g. cardiovascular homeostasis), are directly dependent on synaptic drive arising from groups of sympathetic premotor neurons in the medulla and hypothalamus. The central theme of this thesis is the employment of genetic tools, primarily viral based tracing strategies, to map the locations of neurons distributed throughout out the brain that provide synaptic drive to sympathetic premotor neurons in the ventral medulla.

Genetic tools grant researchers the ability to selectively manipulate neuronal populations based on either anatomical criteria or the constitutive expression of specific promoters. In Chapter 2 of this thesis we developed a novel technique that permits the genetic manipulation of single neurons in the rat, based on functional (electrophysiological) criteria. The work described in this chapter is foundational for future experiments that intend to map functionally relevant circuits in combination with tran-synaptic viral tracing strategies.

Sympathetic premotor neurons within the rostral ventrolateral medulla (RVLM) are essential for the generation of vasomotor tone. However, key questions regarding the architecture of the circuits that control their activity remain. In Chapter 3 we address this topic by employing a trans-synaptic viral tracing strategy to identify neurons monosynaptically connected to bulbospinal RVLM neurons. The anatomical data acquired using this approach has allowed us to generate a brainwide map of the neurons that provide monosynaptic input to bulbospinal RVLM neurons, and therefore determine major sources of synaptic drive likely to underlie the generation of SNA. We describe an arrangement for afferent input to RVLM bulbospinal neurons that emphasises input from hitherto unappreciated local medullary sources, but is overall qualitatively similar to currently held circuit schemes.

In Chapter 4 we examine the anatomical substrates that underlie the recruitment of autonomic and motor responses to alerting stimuli. Using an anterograde viral tracing strategy we identify a previously undescribed direct efferent projection from the superior and inferior colliculi to the ventral brainstem. We describe termination of axons originating from the colliculi to regions of the brainstem previously associated with sympathetic, respiratory, and motor functions, and observe putative synaptic

contacts in close apposition to bulbospinal neurons in the rostral ventromedial medulla and medullary raphe nuclei. These observations characterize a potential pathway via which sympathetic, respiratory and motor outflows are coordinated by higher order sensory systems.

The application of genetic approaches in the context of autonomic systems provides an unprecedented opportunity to examine the structure of discrete neural circuits that drive a defined, measurable output. The experiments conducted in this thesis provide a greater understanding of the neuroanatomy that underlies the central control of physiological behaviours, specifically the basal control of blood pressure and the coordination of sympathetic outputs as component of motor responses to the environment.

Declaration of originality

I acknowledge that the work conducted in this thesis entitled "The connectome of medullary sympathetic premotor neurons" has not been submitted for a degree nor has been submitted as part of the requirements for a degree to any other university or institution other than Macquarie University. I declare that the contents of this thesis represent the original experimental and written work of the candidate except where due acknowledgement is made.

All research presented in this thesis were conducted with the consent of the Macquarie University Ethics Committees and conformed to the Australian Code of Practice for the Care and Use of Animals for Scientific Purposes. (Animal research authorities: **2011-055**, **2012-030**, **2014-022**, **2014-028**)

Bowen Richard Dempsey

Declaration of contribution to Chapters containing submitted or published work

Chapter 2

Dr Simon McMullan, Dr Anita Turner and Dr Sheng Li contributed to *in vivo* electrophysiological experiments. The candidate performed all *in vitro* experiments and was the major contributor to the manuscript.

Chapter 3

Dr Simon McMullan, Dr Anita Turner, Mr Phillip Bokiniec and the candidate performed vector injections. The candidate performed all histological processing and imaging. Analysis was performed primarily by Dr Simon McMullan. The candidate was the major contributor to the manuscript.

Chapter 4

Dr Simon McMullan, Dr Anita Turner, Mr Phillip Bokiniec and the candidate performed vector injections. The candidate performed all histological processing and imaging. Analysis was performed primarily by the candidate. The candidate was the major contributor to the manuscript.

Publications arising from thesis

Dempsey B,Turner AJ, Le S, Sun QJ , Bou Farah L, Allen AM, Goodchild AK, McMullan S. (2015). Recording, labeling, and transfection of single neurons in deep brain structures. Physiol Rep 3(1)

In preparation

Manuscripts of chapters 3 and 4 of this thesis are currently in preparation

Communications

Bou Farah L, Turner A, **Dempsey B**, Goodchild AK, McMullan S (2012). The oxygen sensitivity of sympathetic premotor neurons does not involve heme oxygenase-2 (HO-2). Poster presentation at the Macquarie University Biofocus Research Conference, Sydney, Australia.

Bou Farah L, Turner A, **Dempsey B**, Goodchild AK, McMullan S (2013). The oxygen sensitivity of sympathetic premotor neurons does not involve heme oxygenase-2 (HO-2). Poster presentation at the 33rd Annual meeting of the Australasian Neuroscience Society, Melbourne, Australia.

Dempsey B, Turner A, Bou Farah L and McMullan S (2013). A novel technique that combines single cell electroporation with extracellular recordings *in vitro* and *in vivo.* Poster presentation at the 33rd Annual meeting of the Australian Neuroscience Society, Melbourne, Australia.

Bou Farah L, Turner A, **Dempsey B**, Goodchild AK, McMullan S (2013). The oxygen sensitivity of sympathetic premotor neurons is mediated by non-neuronal release of ATP not heme oxygenase-2 (HO-2). Oral presentation at the 8th Congress of the international Society for Autonomic Neuroscience (ISAN) and the 15th Meeting of the European Federation of Autonomic Societies (EFAS), Giessen, Germany.

Dempsey B, Turner A, Bou Farah L and McMullan S (2013). A novel technique that combines single cell electroporation with extracellular recordings *in vitro* and *in vivo*. Poster presentation at the 8th Congress of the international Society for Autonomic

Neuroscience (ISAN) and the 15th Meeting of the European Federation of Autonomic Societies (EFAS), Giessen, Germany.

Bou Farah L, Turner A, **Dempsey B**, Goodchild AK, McMullan S (2013). The oxygen sensitivity of sympathetic premotor neurons is mediated by non-neuronal release of ATP not heme oxygenase-2 (HO-2). Poster presentation at the 37th congress of the International Union of Physiological Sciences (IUPS), Birmingham United Kingdon.

Dempsey B, Turner A, Bou Farah L and McMullan S (2013). A novel technique that combines single cell electroporation with extracellular recordings *in vitro* and *in vivo*. Poster presentation at the 37th congress of the International Union of Physiological Sciences (IUPS), Birmingham United Kingdon.

Bou Farah L, Turner A, **Dempsey B**, Goodchild AK, McMullan S (2013). The oxygen sensitivity of sympathetic premotor neurons is mediated by non-neuronal release of ATP not heme oxygenase-2 (HO-2). Poster presentation at the Central Cardiovascular and Respiratory Control:Future Directions conference, Sydney, Australia.

Dempsey B, Turner A, Bou Farah L and McMullan S (2013). A novel technique that combines single cell electroporation with extracellular recordings *in vitro* and *in vivo*. Poster presentation at the Central Cardiovascular and Respiratory Control:Future Directions (CCRC:FD) conference, Sydney, Australia.

Bou Farah L, Turner A, **Dempsey B**, Goodchild AK, McMullan S (2014). The hypoxia sensitivity of RVLM sympathetic premotor neurons is mediated by glial ATP release. Poster presentation at the Experimental Biology (EB) conference, San Diego, United States of America.

Le S, **Dempsey B**, Turner A , Qi-Jian S, Bou Farah L, Allen AM, Goodchild AK ,McMullan S (2014). Recording and transfection of single neurons in deep brain structures. Oral presentation at the 13th Oxford Breathing meeting, Sydney, Australia.

Dempsey B, Hassan S, Turner A, Allen AM, Dampney R, Goodchild AK, McMullan S (2014). Efferent projections from the inferior colliculus to putative cardiorespiratory control neurons. Oral presentation at the Central Cardiovascular and Respiratory Control:Future Directions (CCRC:FD)conference, Melbourne, Australia.

Dempsey B, Hassan S, Turner A, Allen AM, Dampney R, Goodchild AK, McMullan S (2015). Projections from the inferior colliculus drive putative sympathetic, respiratory and motor populations in the ventral medulla. Poster presentation at the 25th ISN-APSN Joint Biennial Meeting in conjunction with the Australasian Society for Neuroscience (ANS), Cairns, Australia.

McMullan S, **Dempsey B**, Turner A, Wisinski-Bokiniec P, Goodchild AK (2015).Putative sympathetic premotor neurons in the rostral ventrolateral medulla are not somatotopically distributed. Poster presentation at the 25th ISN-APSN Joint Biennial Meeting in conjunction with the Australasian Society for Neuroscience (ANS), Cairns, Australia.

Dempsey B, Turner A, S. Le, Allen AM, Goodchild AK, McMullan S (2015). The connectome of rostral ventrolateral medulla sympathetic premotor neurons. Oral presentation at the meeting of the International Society for Autonomic Neuroscience (ISAN) in conjunction with the American Autonomic Society (AAS), the European Federation of Autonomic Societies (EFAS) and the Japanese Society for Neurovegetative Research (JNSR), Stresa, Italy.

Dempsey B, Hassan S, Turner A, Allen AM, Dampney R, Goodchild AK, McMullan S (2015). Projections from the inferior colliculus drive putative sympathetic, respiratory and motor populations in the ventral medulla. Poster presentation at the meeting of the International Society for Autonomic Neuroscience (ISAN) in conjunction with the American Autonomic Society (AAS), the European Federation of Autonomic Societies (EFAS) and the Japanese Society for Neurovegetative Research (JNSR), Stresa, Italy.

Dempsey B, Turner A, S. Le, Allen AM, Goodchild AK, McMullan S (2015). The connectome of rostral ventrolateral medulla sympathetic premotor neurons. Oral presentation at the Central Cardiovascular and Respiratory Control:Future Directions (CCRC:FD)conference, Sydney, Australia.

Acknowledgments

I would like to thank everybody who made this thesis possible, in particular my supervisors Simon and Ann for their patience and support throughout what was a particularly arduous candidature. My labmates, who have made the past 4 years the best on record. My good friends; Phil, Paul and Mike, for the all great things that happened outside of the lab (eating, drinking and catan). My family, for their continous support and lastly Rebecca, who was always there when I needed her.

I would also like to thank the Adam J Berry Memorial Fund and the Australian Academy of Science for supporting my stay at the National Institutes of Health and Dr Jeff Smith for generously offering to host me.

This thesis is dedicated collectively to the Sprague Dawley rat, may you inherit the earth.

List of Figures

List of Tables

CHAPTER 1: Introduction

The relationship between structure and function is a central theme in the investigation of biological systems. Regardless of scale, resolving the structural characteristics of a biological substrate has often been a critical step in determining the mechanism of action by which its function is served. As deciphering the crystal structure of DNA served in determining the mechanism of inheritance, the histological examination of neuronal tissue provided neuroanatomy pioneers with insights into the key role of the synapse in governing communication between neurons. One of the emergent central tenets of neuroscience is that the physical structure of the brain, and the pattern in which neurons are interconnected, fundamentally underlies its function.

Even the simplest behaviours rely on the coordinated activity of networks of interconnected neurons. The systematic stimulation, lesion and reduction of the brain (e.g. Alexander (1946)) has provided a broad understanding of functional roles served by spatially delineated brain nuclei at a gross level. However, our understanding of the organisation of neural networks, the substrate that definitively underlies behaviour, remains notably primitive in comparison to that of the functional architecture of other organs. These shortcomings reflect both the technical difficulties associated with identifying brain connections and the enormous complexity of the brain. As a result, our understanding of the mechanisms that underlie most pathologies of the nervous system are relatively limited. Indeed, in contrast to the fields of physics, chemistry, much of ecology, and evolutionary biology, there is as yet no grand theory of neuroscience that explains the organisational principles of the brain or that can be used to make predictive models of brain function or animal behaviour.

Efforts to generate a complete wiring diagram of the brain's connections, coined "the connectome" (Sporns *et al.*, 2005), have been hampered due to the sheer magnitude of the brain's intrinsically complex structure. Such a task would require the mapping of approximately 86 billion neurons for the brains of humans (Azevedo *et al.*, 2009; Herculano-Houzel, 2009) and 200 million for those of experimental animals such as the rat (Herculano-Houzel & Lent, 2005) and ultimately, to define the thousands of inputs thought to be received by each neuron (Nimchinsky *et al.*, 2002). At its most basic level, the field of connectomics does not even consider the complex world of synapse biology, but rather attempts to generate simplified circuit diagrams that aim to resolve the nodes

linking neurons, microcircuits, nuclei and brain regions (discussed by Branco and Staras (2009)).

Investigation of even the simplest connectome, notably that of *c elegans* which contains only 302 neurons (White *et al.*, 1986), have relied on ultrastructural approaches that employ electron microscopy to comprehensively define physical synaptic contact between neurons within a given volume of tissue. The circuit structures acquired in this manner for *c elegans* have provided some of our best insight and models into the structure function-relationships of neural circuits (Chalfie *et al.*, 1985; Gray *et al.*, 2005; Chalasani *et al.*, 2007). However the application of these ultrastructural approaches to the examination of complete circuits in the brains of small mammals, although currently underway (Helmstaedter *et al.*, 2013; Kasthuri *et al.*, 2015), appear limited by sampling volume and the enormous time and resource requirements for processing and analysis (discussed by Lichtman & Denk, 2011; Wanner *et al.*, 2015). Ultrastructural technologies such as block-face electron microscopy are enjoying something of a renaissance but although considered definitive, the scale of the workload is still staggering; a cubic millimetre of tissue takes 18 years of acquisition time alone using current state-of-the-art approaches, with a storage requirement of 300 Tb per millimetre. Given the entire data storage capacity of the world was estimated in 2011 at 295 exabytes (1 exabyte = 1 million terabytes) (Hilbert & Lopez, 2011), and given that the volume of the human brain is about 1.4 million cubic millimetres, this means that storage of a single human brain dataset would consume considerably more storage space than is currently available worldwide (~420 exabytes) and more significantly, would take about 25 million years of imaging time.

This kind of approach, in which all of the data are first acquired in an undirected and unbiased way and then the structure of the circuit is determined by painstaking rendering of 2 dimensional images into 3 dimensional structures, is analogous to brute-force 'cracking' of encrypted messages, in which, given enough processing power, the secret message hidden within the data will emerge. Some success has been reported using block-face electron microscopy, particularly for small tractable circuits such as the retina, in which the inputs and outputs are understood and the objective is to understand the organisation of the relatively small number of spatially confined neurons in which processing of input data occurs (Briggman *et al.*, 2011; Denk *et al.*, 2012).

However, this approach is clearly inappropriate for interrogation of large dispersed circuits.

Tracing projections and connections with light microscopy

In contrast to serial-block face microscopy, light microscopy permits the investigation of large volumes of tissue with relatively high speed (particularly for automated systems: see Osten and Margrie (2013)). However a major hurdle in defining the structure of neural networks using this approach is overcoming the sheer density at which neurons, their processes, and the interstitial components within which they are embedded (blood vessels and glia) are arranged. Neural tissue is remarkably compact, rendering the challenge of discerning contact within the jumbled mass of fibres almost impossible. Such is the magnitude of this problem that the early examination of neural tissue based on the Golgi method, which formed an appreciation for the extensive ramification of neuronal processes and ultimately served as the foundation of the neuronal doctrine (reviewed by Llinas, 2003), were only discernible due to the capricious selectivity by which neurons were labelled using this technique (<1% of neurons were labelled: Pasternak & Woolsey, 1975).

A more intractable problem for the reconstruction of neural circuits in the brains of higher order animals is the physical dispersion of neurons within 3 dimensional space and the difficulties inherent in reconstructing those circuits. Recently developed tissue processing techniques such as CLARITY (Chung *et al.*, 2013) and serial block face confocal imaging (Osten & Margrie, 2013)in theory permit investigators to image large blocks of tissue (or even whole brains) in a single contiguous dataset. While both approaches have proven useful in accurately rendering general projection trajectories at a mesoscale level, light microscopy lacks the spatial resolution to reliably define synaptic contacts. What may appear as a typical synapse under high magnification may in fact represent a retracting or immature synapse, or may even represent bulk transmission or even fibres of passage. Best estimates are that only about half the synapses identified under light microscopy are actually synapses (Murphy *et al.*, 1995; Descarries & Mechawar, 2000).

Light microscopy is therefore inherently incapable of resolving connectome structure using brute-force approaches. Instead, anatomists have used tracers to render

subpopulations of neurons conspicuous, enabling visualisation of neuronal morphology and suggesting circuit organisations that, although tempered by the limitations of light microscopy and the properties of the tracers, have provided a mainstay for generations of neuroanatomists.

Tracing techniques form the technical staple of much of the research described in this thesis. Emerging genetic tools have recently expanded the utility of light microscopy: the wide spread availability of viral vectors that can be selectively directed towards particular cell types, and the emergence of variants that are suited for labelling of distal neuronal compartments or even of trans-synaptic spread have led to their adoption as a standard neuroanatomy tool permitting researchers a level of specificity that was previously unavailable. In the following paragraphs I will briefly summarise conventional and viral tracing approaches with a focus on a recently developed approach for monosynaptically restricted circuit tracing.

Labelling neurons using tracers

The focal deposition of a detectable tracer within the brain permits the differential labelling of a neuron's soma and processes, based on the transport of dyes within the neuron. This approach, broadly termed "tract-tracing", is often employed in tandem with stereotaxic atlases (Paxinos & Watson, 2005) to qualitatively assess point connectivity in the brains of experimental animals.

Initial tracing approaches involved the physical or electrical lesion of a spatially defined region of the brain, which rendered the degenerated axons of destroyed soma and fibres differentially susceptible to impregnation with metallic silver (Hoff, 1932). Termed "Wallarian degeneration" appertaining to Augusts Waller's observation of axonal degeneration after transection of the glossopharyngeal and hypoglossal nerves of frogs (Waller, 1850), this approach was increasingly refined to the point where terminal boutons could be resolved (Glees, 1946; Nauta, 1952; Fink & Heimer, 1967).

Wallerian degeneration was subsequently replaced by methods that did not require destructive lesions, relying instead on the axonal transport of injected materials from the site of injection to either the cell body (retrograde tracers) or axonal processes (anterograde tracers). The earliest of these tracers were radiolabelled amino acids that when injected were incorporated into polypeptides by neuronal soma and subsequently

transported to axons and terminal processes to be identified via autoradiography (Grafstein, 1967; Cowan *et al.*, 1972). These approaches were soon surpassed by the application of axon-transportable materials that could be detected with conventional light and fluorescence microscopy (e.g. via immunohistological processing, intrinsic fluorescence, conjugation with a fluorescence or enzymatically active probe), these included plant lectins, dextrans, carbocyanin dyes, inorganic molecules, latex microspheres and bacterial toxins.

This variety of tracer constitutes what would now be referred as "conventional tracers" (in contrast to viral tracers). The variety and utility of conventional tracing techniques are broad and have been extensively reviewed (Kobbert *et al.*, 2000; Jones, 2007; Lanciego & Wouterlood, 2011; Nassi *et al.*, 2015). The mechanism of action for each is highly variable, the appropriateness of a tracer for an application is dependent on its particular characteristics for a desired tracing outcome, the most notable of which is the direction of transport.

Phaseolus vulgaris-leucoagglutinin (Gerfen & Sawchenko, 1984) and dextran amine conjugates (e.g. biotinylated dextran amine) (Reiner *et al.*, 2000) have emerged as the archetypal anterograde tracers, routinely employed for mapping axonal trajectories and the distribution of putative terminal boutons (Hoover & Vertes, 2011; Hellenbrand *et al.*, 2013). A common application of anterograde tracers is to assess the formation of putative synaptic connections between projections that originate at the site of tracer deposition and the somata and dendritic processes of a population in another brain region. This approach is particularly powerful when employed in combination with immunohistochemical detection of vesicular transporter proteins (e.g. vesicular GABA (VGAT) and vesicular glutamate transporters (VGLUT)), which provides information regarding the neurotransmitter content of identified synapses (Rosin *et al.*, 2006; Wouterlood *et al.*, 2014).

Retrograde tracers rely on uptake via binding to components of the axon terminal and pinocytosis, resulting in axoplasmic transport over relatively long distances, for example the labelling of motor neurons after injection into peripheral targets (Kristensson & Olsson, 1971; Stoeckel *et al.*, 1977). Examples include Cholera toxin subunit-β (Stoeckel *et al.*, 1977), fluorogold (Schmued & Fallon, 1986), and fast blue (Kuypers *et al.*, 1979).

Stable for a period of weeks, conventional retrograde tracers offer poor morphological resolution compared to that of anterograde tracers.

As with anterograde tracers, retrograde tracers are most powerful when combined with neurochemical approaches that can identify the phenotype of labelled neurons (immunohistochemistry or *in situ* hybridization). They have also been employed in parallel with retrograde tracing from other regions, enabling the identification of populations of neurons that simultaneously project to multiple brain regions (Stoeckel *et al.*, 1977; Kuypers *et al.*, 1979; Shafton *et al.*, 1998; Apps & Ruigrok, 2007; Gowen *et al.*, 2012). Similarly, anterograde tracing can be combined with retrograde labelling to identify anterogradely labelled putative synaptic contacts from one region impacting on a retrogradely labelled somata that projects to another region (Affleck *et al.*, 2012).

Anterograde and retrograde tracers are a mainstay of neuroscience research. However, as discussed in more detail in Chapter 4, conventional tracers are far from perfect: the direction of axonal transport is often neither exclusively retrograde or anterograde, and some tracers are indiscriminately taken up by fibres of passage, which can lead to spurious interpretation of projection. Many of these shortcomings have been surpassed by the application of viral vectors as tracers.

Viral tracers

Although viral vectors can be used to deliver essentially any transgene to any cell type, neuronal or non-neuronal, many researchers have adopted vectors that express fluorescent reporter proteins (e.g. GFP) under the control of neuron-specific promoters as tracers for neuroscience applications. This is because of the potential for restricting reporter transduction to specific subpopulations of infected neurons depending on their genetic profile, the high (and permanent) levels of reporter expression obtained, and the directional specificity and absence of transduction via fibres of passage (reviewed by Callaway, 2005; Betley & Sternson, 2011). Depending on the application, most aspects of a vector tropism can be defined via modification of the viral genome, capsid or envelope (if applicable). The specific attributes of different viral vector types have been reviewed recently and at length (Nassi *et al.*, 2015), and a comprehensive consideration of this topic is beyond the scope of this thesis. However, a brief overview of some of the vectors commonly employed for viral tracing is warranted.

One of the great utilities of viral vector tracing is the ability to selectively trace neurons of a defined genetic phenotype. This is achieved by "mimicking" the expression of a virally encoded transgene, to that of an endogenously expressed gene (Luo *et al.*, 2008). This process entails the insertion of the cis-regulatory sequence (promoter) for said endogenous gene, upstream of the transgene in the viral genome (Callaway, 2005; Luo *et al.*, 2008). However, promoters are large and occupy considerable amounts of the limited capacity of the viral genome, and so truncated versions of promoters are often used. This works well for constitutively active promoters such as the ubiquitous cytomegalovirus (CMV) promoter or the neuron-specific synapsin promoter (SYN), but often results in poor expression or specificity for cell specific promoters, in particular those based on neurotransmitters (e.g. the vasopressin and oxytocin promoters (Pinol *et al.*, 2012)).

Alternatively, genotype restriction can be achieved using a combination of a transgenic animal that drives the expression of a site specific recombinase (e.g. cre-recombinase) within a genetically defined neuron population (Gofflot *et al.*, 2011), and a vector with recombinase conditional transgene expression, for example a flip excision (FLEX) (Schnutgen *et al.*, 2003) or inverted open reading frame configuration (Saunders *et al.*, 2012). Although dependent on the availability of a suitable "recombinase driver line", this approach has become a popular method of targeting gene expression for tracing or manipulation of a defined population of neurons, due to the degree of control and level of transgene expression that can be achieved. The utility of this technology is exemplified by Fenno *et al.* (2014), who demonstrate an intersectional approach, that requires the action of up to three recombinase variants (e.g. Cre + Flp + Dre) to achieve transgene expression, restricting transduction to a sub-population of neurons defined by expression of two genes, cell body location, and axonal projection.

With the exception of some genetically modified rabies variants, the majority of viral vectors used for research applications are replication-deficient. In general this is achieved using an incomplete viral genome that lacks the components critical for replication (reviewed by Nassi *et al.*, 2015). This offers the benefit of reduced toxicity, which permits stable labelling over long periods of time. Replication deficient vectors have become the gene-delivery work-horses of contemporary biological research (and a considerable number of human clinical trials), prominent among these include adeno-

associated virus (AAV), lentivirus (LV) and herpes simplex virus (HSV) amplicon vectors (reviewed by Nassi *et al.*, 2015).

As with conventional tracers, the reliable identification of terminal appositions under light microscopy remains a limitation of straightforward vector-based tracing strategies in which the cytosol is filled with a fluorescent reporter. A number of elegant approaches that restrict reporter expression to synapses have been developed to circumvent this limitation. The utmost iteration of this approach is a dual vector system in which each vector drives the expression of one half of a GFP-derived dimer that only becomes fluorescent when both halves bind. The only place at which the two components can become physically close enough to bind is the synaptic cleft, so GFP fluorescence at one injection site is interpreted as evidence of synaptic input from neurons that reside at the other injection site (Feinberg *et al.*, 2008; Kim *et al.*, 2012). The interested reader is directed to a recent review by Wickersham and Feinberg (2012) that considers alternative methods for synaptic complementation.

Although elegant for resolving direct point-to-point connection questions, this strategy represents a cumbersome approach to larger scale circuit mapping, and as with standard viral and conventional tracers, are limited in their capacity to contextualize the larger, multi-synaptic neural pathways, those point connections ultimately serve. An alternative and popular approach as been to exploit the mechanisms used by neurotrophic viruses to spread through the central nervous system. Classically, replication-competent neurotrophic vectors, such as rabies (Ugolini, 1995; Kelly & Strick, 2000) and herpes variants, particularly pseudorabies (PRV) (Strack *et al.*, 1989b; Barnett *et al.*, 1995; Card & Enquist, 1995; Aston-Jones & Card, 2000; Kelly & Strick, 2003; Rinaman & Schwartz, 2004; Ekstrand *et al.*, 2008; Song *et al.*, 2009; McGovern *et al.*, 2012a; McGovern *et al.*, 2012b; Vaughan & Bartness, 2012; Wojaczynski *et al.*, 2015), have been employed to trace circuits of connected neurons via the trans-synaptic trafficking of viral progeny.

These viruses although diverse in many aspects, are commonly enveloped by host derived membrane that is incorporated by newly formed viral particles as they “bud” from the host cell (Callaway, 2008). The expression of envelope proteins derived from the viral genome mediates transynaptic trafficking as exocytosed virons interact with

the presynaptic elements of synaptically linked neurons, a process that remains poorly defined ((McGeoch *et al.*, 1988; Lafon, 2005), discussed (Callaway, 2008)).

These vectors present a significant advantage for circuit tracing over conventional tracers, in the sense that labelling can be safely interpreted as indicating synaptic contact. However these approaches suffer from three major drawbacks unique to neurotrophic viruses (in addition to biosafety considerations): first, replication competent vectors are commonly cytopathic, driving deterioration in the structural integrity and function of infected neurons (McCarthy *et al.*, 2009; Ugolini, 2010a). The resulting compromises in morphology and electrophysiology limit the utility of these vectors, in particular alpha-herpesvirus based vectors, for neurochemical analysis or functional investigation to early stages of infection. Second, the virus continues to propagate throughout the central nervous system following infection, so whereas infection denotes synaptic connection, it is difficult to resolve the degree by which labelled neurons are connected i.e. mono- or polysynaptic. Third, classical replication-competent neurotrophic viruses can be targeted to efferent (in the case of vectors that spread in a retrograde direction e.g pseudorabies) or afferent (in the case of vectors that spread in an anterograde direction e.g. HSV-1 H129) pathways by selecting an appropriate peripheral target (such as the adrenal gland: Strack *et al.*, 1989b), however, there is no way to selectively target groups of neurons that are not motoneurons or do not receive primary afferent input; direct CNS injection of these vectors gives rise to non-selective infection. Interestingly, it has been noted that the tropism of rabies based tracers does not include sensory or autonomic nerve terminals, exclusively infecting alpha-motoneurons when injected into the periphery (Ugolini, 2011).

Recently, recombinase dependent constructs, i.e. floxed-stop thymidine kinase PRV genomes (DeFalco *et al.*, 2001) or transgene cassettes i.e. brainbow cassette (Livet *et al.*, 2007) permit transynaptic tracing from genetically defined populations. The former restores viral replication exclusively to virons that infect CRE+neurons, permitting targeted cell injection and the later alters transgene expression (i.e. alternates reporter expression) in virons that are passaged through CRE+ neurons. These recombinase conditional approaches partially circumvent the limitations of targeting polysynaptic viral tracing, however the degree of connectivity between labelled neurons still remains ambiguous. An ideal approach would permit restrict tracing from a defined sub-

population of neurons and limit the degree of viral spread to a defined number (e.g. monosynaptic) of synaptic 'leaps'.

Glycoprotein-deleted rabies: a monosynaptically restricted viral tracer

Rabies is a replication-competent vector that has been infrequently employed in its wild-type state for polysynaptic tracing in the central nervous system (Ugolini, 1995; Kelly & Strick, 2000). Rabies is transmitted in an exclusively retrograde direction in the central nervous system; wild-type rabies rapidly spreads from the site of initial infection (typically a bite when contracted in the wild), via sympathetic postganglionic neurons that innervate vascular smooth muscle at the bite site, to the spinal cord and then retrogradely throughout the central nervous system. Although wild-type rabies is extremely dangerous (only four cases of survival following initial symptoms have been recorded in human patients), a number of attenuated strains have been developed for the generation of vaccines and for research purposes. One such strain is Street Alabama, Dufferin B19 (SADB19), a virus isolated from a symptomatic dog in the 1930s and exclusively maintained on cultured rodent tissue ever since. In the intervening years SADB19 has become rodent-specific with relatively low pathogenicity: oral exposure leads to development of rabies symptoms in only 6% of mice (Vos *et al.*, 1999), although direct injection into muscle or brain leads to fatal rabies in almost all cases (Beckert *et al.*, 2009). In contrast, direct brain injection of SADB19 has never resulted in disease development in fox, cat, stonemarten, ferret, birds or primates (Vos *et al.*, 1999). These features, and the absence of transmission of SADB19 between infected rodents (Vos *et al.*, 1999), make SADB19 an ideal research tool. Indeed, because of the traits described above, SADB19 was developed as a live oral vaccine for wild foxes in Germany in the 1980s: 50 million doses of live SADB19 have now been airdropped over central Europe, and it is an important part of the European rabies control program.

In recent years genetically modified recombinant SADB19 varieties have provided a new generation of tracing tools that avoid the shortcomings of classic replication competent neurotrophic viruses (reviewed by Callaway & Luo, 2015). At the heart of this technology is the key role of the rabies glycoprotein (sometimes called B19G), a single factor that is responsible for the initial infection and trans-synaptic trafficking of rabies (Etessami *et al.*, 2000; Ugolini, 2010b). Deletion of the gene that encodes the rabies glycoprotein renders the virus, so-called SADΔG, practically inert. However, transient re-

expression of the glycoprotein on the viral envelope, achieved via passage through a genetically modified cell line that expresses rabies glycoprotein (Etessami *et al.*, 2000; Wickersham *et al.*, 2007a), temporarily restores terminal tropism to SADΔG but eliminates trans-synaptic spread. This is because, with no means of synthesizing the glycoprotein, the SADΔG progeny are rendered "stuck" within these cells. By substituting a sequence encoding a fluorescent reporter for the rabies glycoprotein gene (SADΔG-GFP), Callaway and colleagues essentially generated a terminal-specific retrograde tracer that, because of the continued replication of the virus within infected neurons, drives extensive reporter expression (Wickersham *et al.*, 2007a) (Figure 1.1).

The key insight made by Wickersham *et al.* (2007b) is that the ability of rabies to trans-synaptically migrate could be transiently restored by expression of the rabies glycoprotein on infected neurons *in trans* using conventional gene delivery techniques or transgenic platform. As demonstrated recently by Esposito *et al.* (2014), by simply expressing the rabies glycoprotein on a population of target neurons (for example motoneurons) and subsequently infecting those neurons with SADΔG (by injecting SADΔG into the muscle), the spread of SADΔG is restricted to neurons monosynaptically connected to the source of the glycoprotein, irrespective of their distance from those neurons.

This approach was further refined by genetically restricting the initial access of SADΔG to neurons that express an extrinsic receptor, TVA, which is expressed in birds but not constitutively in mammals and which is the obligate binding partner for the avian sarcoma leukosis virus (Wickersham *et al.*, 2007b). Thus, when SADΔG is pseudotyped with the envelope protein of the avian sarcoma leukosis virus (EnvA), the tropism of the resultant vector (SADΔG(EnvA)) is restricted to neurons that express the TVA receptor.

The starting point for monosynaptic retrograde tracing strategies that use SADΔG(EnvA) can be defined by co-expression of the genes that encode TVA and the rabies glycoprotein in a target population, which we subsequently refer to as 'seed' neurons. Direct CNS injection of SADΔG(EnvA) will selectively infect seed neurons at the injection site, where the SADΔG will replicate, incorporating the glycoprotein, and spread to monosynaptically connected members of the pre-synaptic network (which we refer to as 'input' neurons). To distinguish input neurons from seed neurons, a reporter that

differs in colour from that contained in the SADΔG genome is often included with the TVA and glycoprotein genes (Marshel *et al.*, 2010). In the experiments described in Chapter 3 we use a cassette that contains the yellow fluorescent protein reporter (YFP) TVA receptor and the rabies glycoprotein to define the seed population, and SADΔG(EnvA)-mCherry to label input neurons.

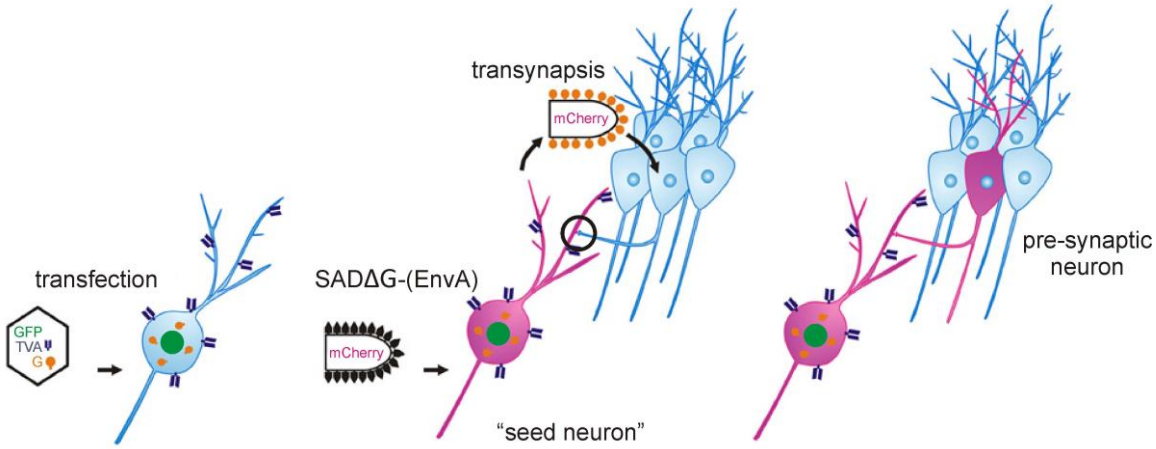

Figure 1.1 Monosynaptically restricted trans-synaptic tracing with SADΔG(EnvA). Neurons are transfected with genes encoding the receptor for EnvA; TVA, the rabies glycoprotein (G) and a reporter protein (e.g. GFP), to permit exclusive entry of SADΔG(EnvA) and subsequently "seed" monosynaptic trafficking of SADΔG to pre-synaptic neurons throughout the brain. Once in a pre-synaptic neuron SADΔG is rendered incapable of further trans-synapsis due to the lack of rabies glycoprotein expression. Pre-synaptic neurons can be distinguished from the seed neuron population by exclusive expression of the SADΔG driven reporter (i.e. mCherry). adapted from (Vivar & van Praag, 2013)

In theory, this approach could be used to identify monosynaptic inputs to any population in which it is possible to selectively drive the TVA and the rabies glycoprotein. As recently reviewed (Callaway & Luo, 2015; Nassi *et al.*, 2015), investigators from diverse branches of neuroscience have used innovative approaches to limit seeding to their populations of interest, using transgenic mice (Takatoh *et al.*, 2013), AAV (Liu *et al.*, 2013), LV (Brennand *et al.*, 2011) and HSV (Yonehara *et al.*, 2013) vectors, and even transfection of single functionally identified neurons recorded *in vivo* (Rancz *et al.*, 2011; Velez-Fort *et al.*, 2014). Although not without its technical confounds, SADΔG(EnvA) represents the current state-of-the-art technique for interrogation of circuit structure.

The overall goal of this thesis is to deploy some of the neuroanatomical tools described above to answer key unresolved questions in the field of autonomic neuroscience. The field of autonomic neuroscience remains a core component of the discipline, in part due

to its continued function under anaesthesia (rendering it accessible), its well defined inputs and outputs (rendering it tractable), its conservation between species (making it translatable) and its role in human disease (making it relevant).

At a macroscopic level, the central nuclei that generate sympathetic nerve activity are critically dependent on the integration of convergent afferent sensory, affective, and tonic inputs at discrete sympathetic premotor nuclei, which in turn drive the activity of sympathetic motor pathways and their effectors in the periphery. The functional attributes of these networks have been extensively examined in anaesthetised animals (Morrison, 2001; Guyenet, 2006). However, key questions remain regarding the organisation of the circuits responsible for generating sympathetic nerve activity. I will next provide some context for the experiments described in this thesis by providing an overview of some key functional and structural aspects of the sympathetic nervous system.

The sympathetic nervous system

The sympathetic nervous system (SNS) is comprised of a network of nerves, ganglia, motor neurons and the central interneurons which they subserve. The output of the SNS, sympathetic nerve activity (SNA), is regulated by afferent feedback and often antagonized by common parasympathetic innervation of peripheral effectors. SNA and its "push-pull" relationship with the parasympathetic nervous system serve to maintain a homeostatic balance, a primary function of which is the maintenance of blood pressure. Blood pressure is regulated in a state-dependent manner to meet metabolic requirements during diverse behaviours. Because blood volume is finite, this is achieved by shunting blood between different vascular compartments. Differential regulation of sympathetic effectors allows the body to cope with dynamic metabolic and thermal demands in a closed-loop system (Adams *et al.*, 1971; Carrive, 1993). For example, during exercise the resistance vessels in the visceral (vasoconstriction) and muscle (vasodilatation) beds are modulated in a reciprocal manner to shunt blood from the former to the latter.

The regulatory action of the SNS on blood pressure is directly mediated via the transmission of noradrenaline from the terminal processes of sympathetic nerves, which acts onα-adrenergic receptors present on smooth muscle within the tunica media of blood vessels and β-adrenergic receptors on skeletal muscle, driving vasoconstriction and vasodilation respectively (Janig, 1988). Sympathetic nerves innervating the vasculature arise from ganglionic neurons within the cervical paravertebral ganglia and the pre-aortic ganglia. These ganglionic neurons receive input from cholinergic sympathetic pre-ganglionic neurons (SPN) in the spinal cord (Janig, 1988) that are organized in clusters predominantly within the intermediolateral cell column (Appel & Elde, 1988; Strack *et al.*, 1988; Pyner & Coote, 1994b, a). SPN that supply the sympathetic innervation of the heart and blood vessels although concentrated at the T2 spinal process, are distributed throughout all levels of the thoracic and lumbar spinal cord (Strack *et al.*, 1988).

Basal blood pressure is maintained via the tonic discharge of sympathetic nerves (vasomotor sympathetic tone), which is dynamically adjusted by behaviour and afferent sensory modalities. The basal discharge of SPN and the sympathetic nerves they supply is driven by tonic excitatory input from supraspinal sources (Meckler & Weaver, 1984;

Dembowsky *et al.*, 1985), as transection at the spinomedullary junction results in the abolition of vasomotor tone, whilst removal of the brain rostral to the medulla is inconsequential to blood pressure (Alexander, 1946). The focal source of vasomotor premotor drive was further isolated to the rostral ventrolateral medulla (RVLM), as indicated by evidence of vasomotor collapse to levels equivalent to spinal transection, after the specific lesion of this nucleus (Guertzenstein & Silver, 1974; Dampney & Moon, 1980; Hilton *et al.*, 1983; Granata *et al.*, 1985; Reis *et al.*, 1988). Conversely the stimulation of the RVLM drives pressor responses (Dampney & Moon, 1980; Goodchild *et al.*, 1982; Hilton *et al.*, 1983; Ross *et al.*, 1984).

The immediate cessation of SNA and collapse of arterial blood pressure that occurs following lesion of the RVLM has understandably led to a focus on this region as the primary centre for the generation of vasomotor tone. However, neurons arising from the adjacent rostral ventromedial medulla (RVMM), caudal medullary raphe, A5 noradrenergic cell group and the paraventricular hypothalamic nucleus (PVN) also contribute to the descending input received by SPN (Strack *et al.*, 1989a). These nuclei are thought to contribute discrete and conditional input to SPN in response to specific stimuli or during particular behaviours, which may be considered as adaptive or supplementary to the RVLM (reviewed by Morrison, 2001). However, the RVMM and raphe are notable for their contribution to basal blood pressure (Varner *et al.*, 1989; Varner *et al.*, 1992) and as a regulatory axis for non-barosensitive vasomotor responses to defined stimuli, i.e. temperature, pain and stress (Blessing & Nalivaiko, 2000; Tanaka *et al.*, 2002; Furlong *et al.*, 2014). These nuclei occupy a poorly delineated region in the ventromedial medulla referred to collectively as the medullary reticular formation (MRf). The MRf is of consequence to the findings of Chapter 4 and is discussed in detail throughout that chapter. Overall, the contribution of these nuclei to generation of basal vasomotor tone are widely considered ancillary to that of the RVLM (Guyenet, 2006), which will form the primary focus of this thesis and the investigation detailed in Chapter 3.

The rostral ventrolateral medulla (RVLM)

In the rat, the RVLM can be spatially defined by a region occupying the ventral surface of the medulla immediately caudal and ventral to the inferior pole of the facial nucleus. Pressor responses can be generated in response to the microinjection of glutamate

within this region along a column that extends approximately 1 mm caudal to the facial pole (approximately 12-13 mm caudal to Bregma), ventral to the compact formation of the nucleus ambiguus, lateral to the pyramid and inferior olive, and medial to the spinal trigeminal tract (Goodchild & Moon, 2009). The strongest pressor responses are generated from the rostral extent of the RVLM immediately adjacent to the facial nucleus, which overlays the concentration of RVLM neurons that project to the spinal cord. The termination of RVLM sympathetic premotor neurons with SPN underlies vasomotor tone and has been extensively characterized using conventional (Amendt *et al.*, 1979; Blessing *et al.*, 1981; Pyner & Coote, 1998) and viral (Card *et al.*, 2006a; Abbott *et al.*, 2013; Stornetta *et al.*, 2015) tracing and electrophysiological approaches (McAllen *et al.*, 1994; Oshima *et al.*, 2006; Oshima *et al.*, 2008).

The majority of RVLM bulbospinal neurons have been found to express mRNA for vesicular glutamate transporter 2 (VGLUT2) (Stornetta & Guyenet, 1999; Stornetta *et al.*, 2002; Stornetta *et al.*, 2004), and thus it is generally accepted that the sympathoexcitatory role of this input is predominantly mediated by glutamatergic transmission (Deuchars *et al.*, 1995; Llewellyn-Smith *et al.*, 1998; Morrison, 2003). Importantly, a population of neurons that express catecholamine biosynthetic enzymes (C1 neurons), such as tyrosine-hydroxylase (TH), dopamine-β-hydroxylase (DβH), and phenylethanolamine-N-methyltransferase (PMNT), occupy a region that spatially overlaps with the RVLM pressor area. Although only 1/3 of C1 neurons form spinal projections, approximately 60-70% of the entire bulbospinal RVLM population are C1 neurons (Hokfelt *et al.*, 1973; Blessing *et al.*, 1981; Ross *et al.*, 1981; Goodchild *et al.*, 1984; Phillips *et al.*, 2001; Stornetta *et al.*, 2002). This population served neuroanatomists and physiologists with a reliable neurochemical marker for the RVLM pressor area; subsequent electrophysiological experiments confirmed the catecholamine synthesis of functionally identified RVLM sympathetic premotor neurons (Schreihofer & Guyenet, 1997) and conversely demonstrated that optogenetic activation of C1 neurons drove sympathoexcitatory effects (Abbott *et al.*, 2009b). The contribution of these neurons to sympathetic output, in particular to the regulation of blood pressure, have been extensively reviewed (Guyenet *et al.*, 2013). Studies that selectively lesion DβH+ neurons using saporin conjugates, delivered retrogradely via spinal injection (Schreihofer & Guyenet, 2000; Ritter *et al.*, 2001; Madden *et al.*, 2006) or locally into the RVLM (Madden *et al.*, 1999; Madden & Sved, 2003), have demonstrated that C1 neurons

although critical for RVLM mediated homeostatic changes (systemic adrenalin release) to glucoprivation, are inconsequential to basal blood pressure. This observation in combination with the marginal increases in blood pressure driven by the selective stimulation of RVLM C1-neurons (Abbott *et al.*, 2009b; Burke *et al.*, 2014), implies that the non-C1 RVLM population alone is sufficient to support basal sympathetic tone.

Input to the RVLM

Antidromic stimulation, lesion and tracing approaches have assisted in establishing the current model of afferent drive to the RVLM sympathetic pre-motor population (Figure 1.2), which includes inputs from structures located along the entire neuroaxis (see table 1.1).

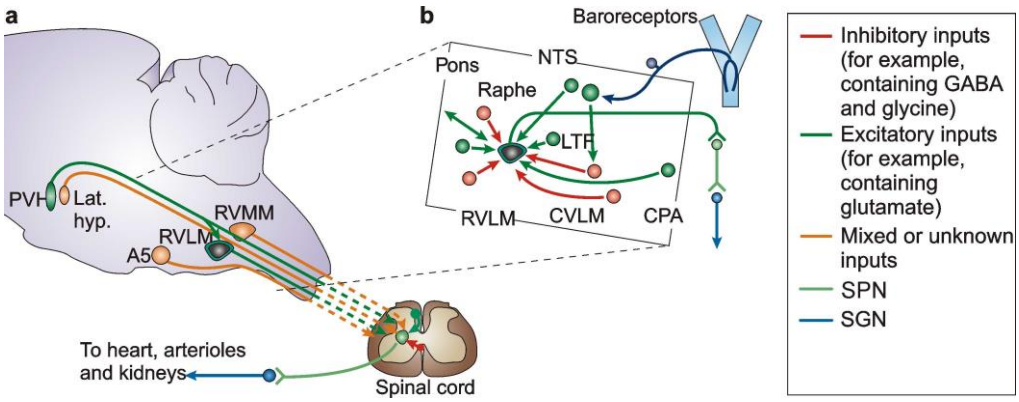

Figure 1.2: Central pathways of sympathetic vasomotor control. A. Input to the SPN arises from a combination of pre-sympathetic nuclei in the medulla: the A5 group, RVLM, RVMM, Raphe (not shown), and hypothalamus: PVH and lateral hypothalamus. B. Sources of excitatory and inhibitory input to the RVLM. A5: A5 noradrenergic group, RVLM: rostral ventrolateral medulla, RVMM: rostral ventromedial medulla, PVH: paraventricular hypothalamic nucleus, CVLM: caudal ventrolateral medulla, NTS: nucleus of the solitary tract, LTF: lateral tegmental field, CPA: central pressor area. Adapted from (Guyenet, 2006).

Table 1.1: Sources of input to the RVLM

Structure	Nuclei	References describing projections to the RVLM
Rhombencephalon	**A5, LC, SubLC, KF, PB**	(Dampney *et al.*, 1982; Lovick, 1986; Dampney *et al.*, 1987; Van Bockstaele *et al.*, 1989; Hayakawa *et al.*, 1999; Goodchild *et al.*, 2001; Card *et al.*, 2011)
	LTF, BötC, C1/RVLM	(Barman & Gebber, 1987; Gebber & Barman, 1988; Nicholas & Hancock, 1991; Bryant *et al.*, 1993; Granata & Chang, 1994; Lipski *et al.*, 1995; Gaytan *et al.*, 1997; Sun *et al.*, 1997; Madden *et al.*, 1999; Card *et al.*, 2006b; Card *et al.*, 2011; Agassandian *et al.*, 2012; McMullan & Pilowsky, 2012; Turner *et al.*, 2013),
	RVMM, mRaphe	(Lovick, 1986; Van Bockstaele *et al.*, 1989; Zagon, 1995; Milner *et al.*, 1996; Babic & Ciriello, 2004; Card *et al.*, 2011)
	NTS	(Dampney *et al.*, 1982; Ross *et al.*, 1985; Lovick, 1986; Dampney *et al.*, 1987; Aicher *et al.*, 1996; Koshiya & Guyenet, 1996
	rVRG, CVLM, PreBötC,	(Willette *et al.*, 1984; Blessing, 1988; Ellenberger & Feldman, 1990; Agarwal & Calaresu, 1991; Gieroba *et al.*, 1992; Li *et al.*, 1992; Gaytan *et al.*, 1997; Chan & Sawchenko, 1998; Tan *et al.*, 2010)
	A1, cVRG/Ramb, MCPA/CPA	Granata *et al.*, 1986; Dampney *et al.*, 1987; Gordon & McCann, 1988; Possas *et al.*, 1994; Chan & Sawchenko, 1998; Sun & Panneton, 2002, 2005)
Midbrain	**VLPAG, LPAG**	(Lovick, 1985; Carrive *et al.*, 1988; Van Bockstaele *et al.*, 1989; Card *et al.*, 2011; Stornetta *et al.*, 2015)
Hypothalamus/ Thalamus	**Pe, LHA, DMH, PVN, ZI**	(Lovick, 1985; Dampney *et al.*, 1987; Van Bockstaele *et al.*, 1989; Hardy, 2001; Card *et al.*, 2011)
Cortex/Sub Cortex	**CeA, MC, SeC, ILC, InC, PrL**	(Westerhaus & Loewy, 2001; Saha, 2005; Bowman *et al.*, 2013)

Abbreviations. **A5**: A5 noradrenergic cell group, **LC**: locus coeruleus, **SubLC**: sub locus coeruleus, **KF**: Kölliker-Fuse nucleus, **PB**: parabrachial nucleus, **LTF**: lateral tegmental field, **BötC**: Bötzinger complex, **C1**: C1 adrenergic cell group, **RVLM**: rostral ventrolateral medulla, **RVMM**: rostral ventromedial medulla, **Raphe**: medullary raphe, **NTS**: nucleus of the solitary tract, **rVRG**: rostral ventral respiratory group, **CVLM**: caudal ventrolateral medulla, **PreBötc**: PreBötzinger complex, **A1**: A1 noradrenergic cell group, **cVRG**: caudal ventral respiratory group, **Ramb**: retroambiguus nucleus, **MCPA**: medullo-cervical pressor area, **CPA**: caudal pressor area, **VLPAG**: ventrolateral periaqueductal grey, **LPAG**: lateral periaqueductal grey, **Pe**: perifornical hypothalamus, **LHA**: lateral hypothalamic area, DMH: dorsal medial hypothalamus, **PVN**: paraventricular hypothalamic nucleus, **ZI:** zona incerta, **CeA**: central nucleus of the hypothalamus, **MC**: motor cortex, **SeC**: sensory cortex, **ILC**: infralimbic cortex, **InC**: insular cortex, **PrL**: prelimbic cortex.

Afferent modalities that modulate sympathetic nerve activity

The output of RVLM sympathetic pre-motor neurons and the sympathetic nerves they supply is patterned in a state dependent manner. Although some aspects of modal regulation are served by the intrinsic sensitivity of the RVLM sympathetic pre-motor neurons (e.g. hypoxia: Sun *et al.*, 1992), SNA and AP are regulated, with respect to immediate physiological demands, via the integration of homeostatic reflex arcs with convergent descending drive (reviewed in Dampney, 1994b; Morrison, 2001; Guyenet, 2006). Thus the activity of RVLM sympathetic pre-motor neurons is sensitive to a range of extrinsic and intrinsic sensory modalities.

Increases in blood pressure are buffered by an immediate decline in SNA. The pathway mediating this response, "the baroreflex arc", is initiated by excitatory drive from baroreceptors within the wall of the aortic arch (Farnham & Pilowsky, 2009). Excitatory baroreceptor drive is conveyed via the aortic depressor nerve (Krieger & Marseillan, 1963) via synapses with second order excitatory neurons in the dorsolateral and medial nucleus of the solitary tract (NTS) (Zhang & Mifflin, 1998), to inhibitory GABAergic neurons in the CVLM (Guyenet *et al.*, 1987; Schreihofer & Guyenet, 2003; Bailey *et al.*, 2006), which subsequently innervate the RVLM (Jeske *et al.*, 1995). The reflex arc coalesces with a transient decrease in the activity of barosensitive sympathetic pre-motor neurons (Brown & Guyenet, 1985; Lipski *et al.*, 1996; Schreihofer & Guyenet, 1997; Verberne *et al.*, 1999a).

RVLM sympathetic pre-motor neurons are differentially activated in response to hypoxic stimuli in order to route blood from peripheral organs to the brain and reduce oxygen consumption by decreasing heart rate (Guyenet, 2000). Chemoreceptors within the carotid bodies detect fluctuations in the oxygen partial pressure within the carotid circulation (Marshall, 1994; Kumar & Prabhakar, 2012), driving excitatory input to the RVLM via the medial and commissural NTS (Mifflin, 1992; Aicher *et al.*, 1996; Koshiya & Guyenet, 1996). The net effects of peripheral chemoreceptor activation are increases in sympathetic nerve outflow to peripheral organs and viscera (Miyawaki *et al.*, 1996; Koganezawa & Terui, 2007) and a reduction in outflow to cardiac tissue (Kollai *et al.*, 1978; Koganezawa & Terui, 2007). This patterned response is also reflected in the activity of the neurons that innervate these targets (McAllen, 1992; Koshiya *et al.*, 1993): the activity of barosensitive cardiac nerve fibres is inhibited, facilitating shunting of

blood to the cerebral circulation and bradycardia respectively. RVLM neurons also drive vasodilation of the cerebral vasculature in response to hypoxia, however this is mediated via the direct oxygen sensitivity of neurons in the RVLM region, including RVLM sympathetic premotor neurons (Kemp, 2006), apparently via collateral projections to higher order brain centres that control the release of yet unknown vasorelaxants (Golanov & Reis, 1996; Reis *et al.*, 1997; Golanov *et al.*, 2001; Ilch & Golanov, 2004).

In addition to these classically defined pathways, the output of RVLM sympathetic pre-motor neurons are regulated by an extensive range of reflex pathways that convey information regarding temperature, body position, mechanical distortion and noxious pain, such as the somatosympathetic (Sato, 1973), viscerosympathetic (Koganezawa *et al.*, 2010), vestibulosympathetic (Yates *et al.*, 1991; Yates, 1992; Yates & Miller, 1994) and diving reflexes (McCulloch & Panneton, 2003), descending input from higher order brain sites, notably the PAG, PVN and CeA conveying psychogenic state (Carrive & Bandler, 1991; Saha, 2005; Carrive, 2013) and changes in blood volume (Gomez *et al.*, 1993; Badoer & Merolli, 1998; Badoer, 2001).

Sources of tonic drive to the RVLM

RVLM sympathetic premotor neurons exhibit a spontaneous discharge between 1 and 40 Hz that is strongly correlated with the discharge of sympathetic nerves (Brown & Guyenet, 1984, 1985; Morrison *et al.*, 1988). Those with the highest basal firing rates also have the highest spinal conduction velocities (~4 m/s) (within the range of lightly myelinated A-fibres) and are predominantly non-TH (Allen & Guyenet, 1993; Schreihofer & Guyenet, 1997; Sartor & Verberne, 2003; Verberne & Sartor, 2010).

Despite the extensive profiling of the discharge properties of these neurons, the origins of spontaneous activity are yet to be determined. These neurons have a demonstrated capacity for autodepolarization in the absence of fast synaptic transmission (Sun *et al.*, 1988; Kangrga & Loewy, 1995; Li *et al.*, 1995; Koganezawa & Paton, 2014), however the contribution of this pacemaker activity is yet to be understood within the context of normal function (discussed in Dampney *et al.*, 2000). Intracellular recordings of bulbospinal RVLM neurons suggest that the spontaneous activity of these neurons is dependent on ongoing synaptic drive (Lipski *et al.*, 1996) from a network of neurons,

that are yet to be defined(Barman & Gebber, 1989; Ito & Sved, 1997; Dampney *et al.*, 2003; Coote, 2007).

Although a popular view, one major paradox confounds straightforward interpretation of the data; blockade of glutamatergic transmission in the RVLM only elicits modest reductions in SNA and blood pressure (Sun & Guyenet, 1986; Kiely & Gordon, 1994; Ito & Sved, 1997; Araujo *et al.*, 1999; Mayorov & Head, 2002; Horiuchi *et al.*, 2004) and does not silence the activity of bulbospinal RVLM neurons (Koganezawa & Paton, 2014), which is not predicted by a network model that is reliant on fast glutamatergic transmission. Thus, it has proven difficult to delineate the source(s) of the spontaneous activity using functional methodologies (i.e. micro-stimulation). Some have posited that this observation is due to a net dis-facilitation of local tonically active inhibitory interneurons (Willette *et al.*, 1983b; Koshiya *et al.*, 1993; Ito & Sved, 1997; Horiuchi *et al.*, 2004). The blockade of GABAergic transmission in the RVLM drives substantial depressor responses (Dampney, 1994a) and drives increases in the firing of bulbospinal RVLM neurons (Sun & Guyenet, 1985). The origin of at least part of this tonic GABAergic inhibition has been determined to arise from the caudal ventrolateral medulla (CVLM), including a non-baroceptive population of neurons in the more caudal CVLM, that is coextensive with the caudal pressor area (CPA) (Cravo *et al.*, 1991; Horiuchi & Dampney, 2002) (discussed in (Schreihofer & Guyenet, 2002)(Dampney *et al.*, 2003)).

Reduced preparations of the brain demonstrate that basal SNA is independent of input arising from structures rostral of the pons (Alexander, 1946; Dampney *et al.*, 1988; Paton, 1996), or contralateral medullary structures (Kubin *et al.*, 1985). It is therefore expected that the ensemble of neurons that provide tonic synaptic drive to RVLM sympathetic premotor neurons (reviewed (Barman & Gebber, 1989; Dampney *et al.*, 2003)), arises from local structures within the brainstem. With the exception of the GABAergic CVLM input described above, local sources of tonic drive remain poorly defined. Probable sources, based on functional observation, include the pontine reticular formation (which encompasses the SubLC, A5) (Krassioukov & Weaver, 1993; Hayes *et al.*, 1994), lateral tegmental field (LTF) (Barman & Gebber, 1987; Gebber & Barman, 1988; Barman *et al.*, 2000), RVMM (Varner *et al.*, 1994), Raphe (Barman & Gebber, 1992) and the ventral respiratory column (VRC) (McAllen, 1987; Haselton & Guyenet, 1989; Kanjhan *et al.*, 1995; Mandel & Schreihofer, 2006; Koganezawa & Paton, 2014).

The anatomical organisation of these most proximal inputs remains unclear due to their coextensive boundaries with the RVLM, notably the LTF, RVMM, rostral most aspects of the VRC and speculative RVLM interneurons. Logistically, this has rendered anatomical data acquired using conventional retrograde tracers permissive to false positive errors (e.g. (Bowman *et al.*, 2013)), and anterograde tracing data of limited value (e.g. (Ellenberger & Feldman, 1990)). Similarly, it has been virtually impossible using conventional and viral tracing methods to selectively delineate the sources of input that form monosynaptic input to the sympathetic pre-motor population. Thus, alternative sources of tonic drive to those previously suggested may presently remain obscured.

Card *et al.* (2011), using a sophisticated recombinase dependent, PRV tracing strategy, were able to label the pre-synaptic network of the renal, pre-sympathetic, RVLM population. Despite the technical eloquence of this approach, this study failed to document in a qualitatively or quantitatively useful manner, the structural of this network, and provided with limited anecdotal evidence, insight regarding input from local sources i.e. RVLM interneurons, the RVMM and Raphe. Input from the CVLM, A5, LC, NTS and PVN were noted, however, input from the VRC was neither noted or discussed. This study highlights a short coming in the still emerging approaches to the documentation and formatting of large connectomic datasets, that is; the tendency for researchers to objectively document pathways that are of interest to particular hypothesis. Overall, key questions still remain regarding the absolute structure of the input networks that underlie evoked and basal drive of RVLM sympathetic pre-motor neurons. Comprehensively resolving the pre-synaptic network of this population using refined tracing approaches like g-deleted rabies and the subsequent generation of a volumetric atlas, will assist in the generation of new hypotheses regarding the emergence of sympathetic drive.

Scope of this thesis

Our primary objective was to map the sources of synaptic input to sympathetic pre-motor neurons in the RVLM. The summative innervation of this population is a critical determinant of basal sympathetic tone, thus a comprehensive appreciation for the anatomical structure of this input network would contribute substantially to the formation and refinement of hypotheses regarding the generation and regulatory control of vasomotor tone.

Initially, we intended to identify the sources of input received by functionally identified RVLM sympathetic premotor neurons, using SADΔG(EnvA), based on promising early work that showed that single cell gene manipulation *in vivo* was possible (Marshel *et al.*, 2010). I first set out to modify the juxtacellular labelling technique to enable plasmid delivery in single neurons recorded under anaesthesia. As described in Chapter 2, that project was ultimately successful, leading to the development of a technique that can be used to genetically modify individual neurons or to label neurons with conventional dyes with improved speed and reliability compared to conventional approaches (Dempsey *et al.*, 2015).

The next stage in the progression of this project was to use this technique to permit infection of SADΔG(EnvA) to RVLM sympathetic pre-motor neurons by first transfecting with the plasmid cassette that encodes TVA and the rabies glycoprotein and then infecting the neuron with SADΔG(EnvA). However, the relatively low success rate of the gene delivery technique, coupled with the availability of novel viral vectors that enable the retrograde transduction of neurons based on their axonal trajectory, led us to pursue the same objective using a different approach.

In Chapter 3 I describe experiments that map brain-wide sources of input to putative RVLM sympathetic premotor neurons that project to the T2 spinal cord. We used an HSV vector to retrogradely drive the expression of YFP, TVA and the rabies glycoprotein in RVLM neurons whose axons terminated within the T2 spinal segment, and subsequently infected them with a focal injection of SADΔG(EnvA) into the RVLM. Using a novel analysis and visualisation platform, I provide a quantitative map of input neurons that control RVLM sympathetic premotor neurons and in so doing, also provide the first anatomically defined "segmentation" model for the RVLM based on the spatial density of bulbospinal C1 neurons. In addition, this is the first time any brain-wide map of inputs has been generated in the rat.

One of the surprising outcomes of that Chapter is that virtually no input is received from the superior colliculus, a region that is capable of recruiting powerful sympathetic, respiratory and somatomotor outputs. Our collaborators had previously hypothesized that the RVLM was a likely relay for collicular sympathetic responses (Muller-Ribeiro *et al.*, 2014). Having undermined that hypothesis with the results of Chapter 3, I then

investigated alternative pathways by directly examining the efferent targets of the inferior colliculus by AAV-mediated anterograde labelling. In Chapter 4 I describe a highly localised and previously unrecognised pathway that links the inferior colliculus to the mRF. I found evidence of a large projection that terminates in close proximity to likely somatomotor and sympathetic premotor neurons, and provide the foundation for ongoing experiments that are beyond the scope of the thesis.

Finally, I summarise the major findings of this thesis and discuss potential avenues for future research in Chapter 5.

CHAPTER 2: Recording, labelling and transfection of single neurons in deep brain structures

Abstract

Genetic tools that permit functional or connectomic analysis of neuronal circuits are rapidly transforming neuroscience. The key to deployment of such tools is selective transfection of target neurons, but to date this has largely been achieved using transgenic animals or viral vectors that transduce subpopulations of cells chosen according to anatomical rather than functional criteria. Here we combine single-cell transfection with conventional electrophysiological recording techniques, resulting in three novel protocols that can be used for reliable delivery of conventional dyes or genetic material *in vitro* and *in vivo*. We report that techniques based on single cell electroporation yield reproducible transfection *in vitro,* and offer a simple, rapid and reliable alternative to established dye-labelling techniques *in vivo*, but are incompatible with targeted transfection in deep brain structures. In contrast, we show that intracellular electrophoresis of plasmid DNA transfects brainstem neurons recorded up to 9 mm deep in the anaesthetized rat. The protocols presented here require minimal, if any, modification to recording hardware, take seconds to deploy, and yield high recovery rates *in vitro* (dye labelling: 89%, plasmid transfection: 49%) and *in vivo* (dye labelling: 66%, plasmid transfection: 27%). They offer improved simplicity compared to the juxtacellular labelling technique and for the first time offer genetic manipulation of functionally characterized neurons in previously inaccessible brain regions.

Introduction

Techniques that combine electrophysiological recording of neuronal activity with dye labelling have been used to address fundamental questions about the relationship between neurochemistry, morphology, and cell behaviour (Schreihofer & Guyenet, 1997; Bevan, 1998; Mileykovskiy *et al.*, 2005; Noseda *et al.*, 2010; Jiang *et al.*, 2013). Historically, investigators have used three main strategies to introduce dye from a recording pipette to the cell interior. In the first, intracellular access is obtained by impalement of the neuron with a sharp electrode and fluorescent dyes or biotin conjugates are deposited by intracellular electrophoresis (Stretton & Kravitz, 1968; Horikawa & Armstrong, 1988). In the second, whole cell access is obtained using a low-resistance patch pipette and dye is passively dialyzed into the cell (Edwards *et al.*, 1989; Pickering *et al.*, 1991). In the third approach an extracellular recording electrode is positioned in close contact to the cell membrane (a "juxtacellular" position) and a train of 200 ms long positive current pulses up to 10 nA in amplitude is used to initiate and maintain membrane electroporation and simultaneously eject positively charged dyes, typically over a period of 2 – 30 minutes (Pinault, 1996; for review, see Pinault, 2011).

All three approaches are technically difficult and require experience and skill for efficient use, particularly *in vivo*. The quality of labelling obtained using the juxtacellular approach is generally inferior to that obtained using intracellular dye deposition; however, the technical difficulty associated with maintaining stable sharp recordings or obtaining whole cell access in deep brain regions *in vivo* has led to the ascendency of Pinault's juxtacellular technique as the gold-standard approach for labelling functionally identified neurons.

Recent advances in molecular biology have provided incentives for the development of single-cell labelling techniques that are compatible with intracellular nucleotide delivery. The major challenge associated with delivery of genetic material is the large molecular weight of gene constructs and the high copy number required for efficient transfection. For example, the molecular weight of the plasmid that encodes yellow fluorescent protein, pCAG-YFP (MW 1.8 MDa) is approximately 6,000 times greater than that of neurobiotin (MW 286 Da). This obstacle has been overcome using two approaches. First, as with traditional dyes, plasmids can be dialyzed into neurons during

low-resistance whole cell recordings (Rancz *et al.*, 2011). Although the transfection rate associated with this approach is high (56%: Rancz *et al.*, 2011) and the use of whole-cell patch recordings *in vivo* is becoming more commonplace, this approach is still restricted to more superficial brain regions as whole-cell recordings become difficult to obtain beyond about 2 mm deep (Margrie *et al.*, 2002; Schramm *et al.*, 2014).

An alternative approach combines conventional electrophysiological recording methods with single cell electroporation (SCE) (Haas *et al.*, 2001; Rae & Levis, 2002; Rathenberg *et al.*, 2003; Bestman *et al.*, 2006; Steinmeyer & Yanik, 2012). In common with the juxtacellular technique, SCE uses voltage trains to induce localized dielectric breakdown of the cell membrane and drive charged molecules from the pipette into the cell, but differs in terms of the duration (~ 1 ms), frequency (50 – 1000 Hz) and amplitude of pulses (~ 10 V, equivalent to ~ 500 nA assuming a series resistance of 20 MΩ). SCE is an efficient and quick transfection method, but suffers some limitations: first, it is critically dependent on gentle contact between the pipette and target cell, meaning its use is largely restricted to preparations in which direct visualization of the cell is possible (Rathenberg *et al.*, 2003; Kitamura *et al.*, 2008; Judkewitz *et al.*, 2009). Furthermore, the voltages required for efficient SCE are beyond the limits of commercially available voltage-clamp amplifiers, meaning SCE cannot readily be combined with electrophysiological characterization of target neurons.

Three recent reports detail amplifier modifications and protocols that combine traditional electrophysiological recordings with SCE, allowing transfection of recorded neurons *in vitro* (Daniel *et al.*, 2013) or, within superficial layers of the cortex, *in vivo* (Cohen *et al.*, 2013; Oyama *et al.*, 2013). These achievements represent an important technical landmark that, in common with the whole-cell transfection technique (Rancz *et al.*, 2011), may prove valuable to investigators studying neurons in easily accessible brain regions. However, their applicability to neurons in deep or fibrous regions of the adult brain is unproven.

Our group has a long-standing interest in the anatomy, behaviour, and network dynamics of autonomic and respiratory nuclei deep in the ventrolateral medulla of the rat (McMullan *et al.*, 2008; Sevigny *et al.*, 2008; Burke *et al.*, 2011). These neurons are located up to 9 mm deep to the cerebellar surface, lie intermingled with large fibre

tracts, and are not amenable to whole-cell recordings in recovery experiments. The objective of the current study was to develop a technique that can be used for the targeted transfection of electrophysiologically profiled neurons in deep brain regions. We first independently developed an approach that combines extracellular recording of unit activity with SCE. We then validated its efficacy *in vitro* and extensively tested its suitability for transfection of neurons recorded >2 mm deep in the brainstem. We report that SCE-based approaches provide good transfection efficiency *in vitro* and can be used *in vivo* for dye-labelling as a simple and reliable alternative to the juxtacellular technique. However, in our hands SCE did not result in reliable transfection *in vivo*. To circumvent this limitation we describe a protocol for intracellular electrophoresis of DNA and show that this is a more useful approach.

Methods

Ethical Approval: All experiments were approved by Macquarie University Animal Ethics Committee and conformed to the Australian Code of Practice for the Care and Use of Animals for Scientific Purposes.

General Preparation

Preparation of brain slices for in vitro electroporation

P 2-8 Sprague Dawley rat pups of either sex were anaesthetized with isoflurane and decapitated when arreflexic. The head was submerged in ice-cold carbogen-bubbled artificial cerebrospinal fluid (ACSF, in mM: 125 NaCl, 25 $NaHCO_3$, 3 KCL, 1.25 $NaH_2PO_4.H_20$, 10 glucose, 2 $CaCl_2$, 1 $MgCl_2$). The brain was dissected and 250 µm slices of hippocampus, cortex or brainstem were cut with a vibratome in ice-cold ACSF. Slices were maintained and recorded at 34 ^oC in ACSF. In some cases spontaneous activity was enhanced by superfusing slices in 5-12 mM [K^+] ACSF (Onimaru & Homma, 2007).

Organotypic slice cultures of hippocampus, cortex, brainstem and cerebellum were prepared as previously described (De Simoni & Yu, 2006). Cultures were maintained on organotypic culture mesh inserts (Millipore, PICM03050) in 6 well dishes, submerged in 1 ml of culture media. Slices were kept in a CO_2 incubator at 37 ^oC, 5 % CO_2 for at least 2 days prior to use.

Animal preparation: acute experiments

Adult Sprague Dawley rats of either sex (250 – 650 g) were anaesthetized with 10 % urethane (1.3 g/kg i.p.) and prepared for single unit recording as previously described (Turner *et al.*, 2013). In brief, vascular access was obtained and rats were intubated and instrumented to record blood pressure, core temperature and end-tidal CO_2. Rats were positioned in a stereotaxic frame in the skull flat or nose-down (~30 ^{o}) position. Bone overlying the brainstem was removed and the dura reflected. In experiments targeting respiratory neurons the caudal pole of the facial nucleus, an anatomical landmark for the respiratory cell column, was mapped by antidromic field potentials as previously described (Brown & Guyenet, 1985). Diaphragmatic EMG was recorded as an index of respiratory phase via fine steel wire hook electrodes inserted through the thoracic wall into the diaphragm using a 26 gauge needle. When indicated by respiratory movements

that interfered with recording stability, rats were artificially ventilated at parameters that maintained end-tidal CO_2 at 3.5 - 4.5 % and movements suppressed by careful titration with pancuronium bromide (0.2 - 2 mg/kg i.v., AstraZeneca) such that diaphragmatic EMG was still observable. In long experiments hydration and electrolyte balance was maintained by intravenous infusion of 0.9 % NaCl or 5 % glucose (5 ml/kg/hr). Anaesthetic depth was carefully monitored by examining autonomic, respiratory and/or motor responses to firm pinch of the hindpaw; supplementary anesthesia (10 % initial dose) was provided as required.

Animal preparation: recovery experiments

Adult Sprague Dawley rats of either sex (85 – 605 g) were anaesthetized with intraperitoneal ketamine (75 mg/kg; Parnell Laboratories, Australia) mixed with medetomidine (0.5 mg/kg; Pfizer Animal Health, Australia). Prophylactic antibiotics (20 mg/kg Cephazolin sodium, i.m.; Mayne Pharma, Australia) and analgesia (2.5 mg/kg Carprofen, s.c.; Norbrook Pharmaceuticals, Australia) were administered and the left femoral artery and vein were cannulated under aseptic conditions. The brain was exposed as described above under minimally invasive conditions, medetomidine was reversed (atipamazole 1 mg; Pfizer Animal Health, Australia, s.c.), and anaesthesia switched to 1 – 3 % isoflurane (Veterinary Companies of Australia Pty Ltd) in 100 % oxygen and monitored as described above for the remainder of the procedure. In some experiments rats were artificially ventilated following endotracheal intubation with a 14 gauge cannula.

After conclusion of recordings, wounds were irrigated and the exposed brain covered with oxidized cellulose haemostat. Neck muscles were sutured and skin closed with stainless steel suture clips. Femoral catheters were removed, vessels tied off and incisions closed. Anaesthesia was discontinued, rats were removed from the stereotaxic frame and, where applicable, extubated. Rats were treated with post-operative carprofen, (2.5 mg/kg s.c.; Norbrook Pharmaceuticals, Australia) and monitored closely for up to 36 hours with additional analgesia as required.

Histology

At the conclusion of *in vivo* experiments rats were euthanized with pentobarbitone (>100 mg/kg i.v. (acute experiments) or i.p.(recovery)), transcardially perfused with

heparinised saline followed by 4 % PFA (4 % paraformaldehyde, 76.7 mM Na_2HPO_4, 26.6 mM NaH_2PO_4, pH 7.4), and the brain removed and postfixed in 4 % PFA solution overnight. At the conclusion of *in vitro* experiments brain slices were briefly immersed in 4 % PFA and transferred into TBPS until imaging.

Brainstems from *in vivo* experiments in which dextran or plasmids encoding fluorescent reporters were used were cut into 50 µm coronal sections with a vibrating microtome, wet-mounted and immediately visualized under epi-fluorescence. As part of a separate study, neurobiotin-labelled neurons were processed for ChAT and somatostatin 2A receptor immunoreactivity before visualization. Sections were washed in 0.01 M phosphate buffered saline containing 0.2 % Triton-100 for 3x15 mins, and incubated in 0.01 M phosphate buffered saline containing 2% bovine serum albumin and 0.2% Triton-100 for 1 h at room temperature. Primary antibodies (Goat-anti-choline acetyltransferase, 1:800 (Chemicon, Millipore, Cat#AB144P), Rabbit anti-SST 2a receptor 1:100 (Bio-trend, ss-8000-rmc, Lot#a080826)), were added to the blocking buffer and sections were incubated for 48 h at 4 °C. Sections were washed in TPBS 3x30 mins and incubated in secondary antibodies (ExtrAvidin®-FITC 1:500 (Sigma-Aldrich, Cat#E2760), Cy3®-conjugated AffiniPure Donkey anti-Goat IgG (H+L) 1:250 (Jackson ImmunoResearch Laboratories, INC, Code#705-165-147, Lot#68839), Alexa Fluor® 647-AffiniPure Donkey Anti-Rabbit IgG (H+L) 1:250 (Jackson ImmunoResearch Laboratories, INC, Code#711-605-152, Lot#105115)) for 12 h at 4 °C. Processed sections were washed again in TPBS 3x30mins before being mounted in serial order on glass slides and coverslipped for imaging with Zeiss Z1 epifluorescent or Leica TCS SP5X confocal microscopes. In two cases CFP and EGFP immunoreactivity were enhanced using Rabbit-anti-GFP (1:1000, Life Technologies Cat# A-6455).

Recording parameters

Recordings were made using an Axoclamp 900A amplifier with HS-9AX1 headstage (Molecular Devices, USA) in current clamp mode. This model has several features that make it suitable: its high maximum current output (1000 nA) is convenient for constant-current electroporation, and the headstage is tolerant of externally generated voltages of up to 10 V.

Extracellular activity was simultaneously measured on two channels, one using conventional extracellular configuration (AC channel: Gain: 20 – 50, Band pass: 100-3000 Hz) and one configured for intracellular recordings (DC channel: Gain: 1, Band pass: DC-3000 Hz). Data were sampled at 10 (AC) or 5 (DC) ksamples/s using a 1401plus or power1401 running Spike 2 version 7 (Cambridge Electronic Design, UK). AC recordings were played back as an audio signal during experiments.

Pipettes were pulled from filamented borosilicate glass (external diameter 1 mm, internal diameter 0.5 mm) using a P-2000 pipette puller (Sutter Instruments). Pipettes with a long taper and tip diameter of approximately 1 µm (Resistance 10-20 MΩ when filled with 0.9 % NaCl) were considered ideal for extracellular recordings. All pipettes were inspected using a microscope with a calibrated graticule.

Intracellular recordings were made using similar pipettes pulled to <1 µm tip diameters and filled with either Tris EDTA buffer or water containing freshly filtered plasmid DNA diluted to a concentration of 250 - 350 ng/µl in 1 M KCl.

Constant voltage switching circuit

A constant voltage generator (DS2A-mkII, Digitimer Ltd.) was connected in parallel to the recording pipette by connecting one pole of the stimulator to the pipette and the other to the experimental preparation. A high-impedance recording circuit was maintained by isolating the stimulator from the pipette assembly with an electromagnet-controlled reed switch. The increased capacitance (~ 7 pF) of the assembly was offset by the amplifier capacitance compensation. For electroporation the electromagnet was engaged with a 5 V TTL pulse and the stimulator triggered to produce the desired voltage train.

In vitro electroporation

Experiments were performed on a patch electrophysiology rig under an Olympus microscope with differential interference contrast optics and immersion lenses. Pipettes were back loaded with plasmid DNA, fluorescent dextran (tetramethylrhodamine- or fluoroscein-conjugated dextran (3000 MW, Invitrogen # D3307 and D3305 respectively, 1-3 % in 0.9 % NaCl) or neurobiotin (1 – 2 % in 0.9 % NaCl) and mounted on the recording headstage. Brain slices were placed in the recording chamber and perfused at 1-2 ml per minute. The pipette tip was guided onto the surface of the target cell until a

dimple was formed. Pipette patency was maintained with positive pressure as required. Following electroporation the pipette was carefully retracted from the cell and reused until clogging occurred.

The same approach was used for transfection of neurons in organotypic culture, except pipettes were filled with freshly filtered plasmid DNA in 0.9 % NaCl (0.3 – 3 μg/μl). SCE of organotypic cultures was typically completed within 15 minutes. Transfected neurons were washed in fresh media and restored to the incubator for 24 – 48 hours before fixation and imaging of reporter-expressing neurons.

In vivo electroporation

Pipettes were prepared as above, mounted on the recording headstage and slowly (~ 10 μm/s) lowered into the brainstem using a piezo microstepper. For extracellular recordings, pipette pressure was maintained at >200 mmHg until a the tip reached a depth of 2 mm at which point the pressure was reduced to 0 – 50 mmHg. The pipette was advanced in 3 μm steps until a spontaneously active neuron was isolated and pressure was released. In many cases no pressure was applied beyond 2 mm deep, without any apparent effect on dye labelling efficiency or quality. Positive pressure was always used in attempted extracellular transfection.

Correct pipette position was verified by induction of an open-cell response to single cell microstimulation. Once a recording from a single cell was isolated the pipette was withdrawn until spike amplitude was 0.2 - 0.5 mV and microstimulation was attempted. If no response was obtained the pipette was advanced and re-tested in 3 μm steps until a response was observed (interpreted as establishment of contact) or the spike height receded (interpreted as passage of the pipette past the cell without making contact.

Electroporation was generally only attempted in neurons in which normal neuronal activity resumed after responses to microstimulation, although electroporation before recovery was still associated with robust labelling (see Figure 2.5C). After electroporation the pipette was slowly withdrawn. Fresh pipettes were used for each track.

For the majority of intracellular recordings no pressure was applied during positioning of the pipette: it was lowered to a depth of 1.5 mm and then advanced in 1 – 5 μm steps

until a extracellular recording of a spontaneously active neuron was isolated. A capacitive buzz was applied to gain intracellular access and the pipette was further maneuvered until a stable membrane potential was obtained. After electrophoresis the pipette was slowly withdrawn in until the membrane potential returned to zero and was then withdrawn completely. New pipettes were used for each track.

Plasmid preparation

Plasmids encoding fluorescent reporter proteins were used to validate electroporation: pCAG-DsRed (Addgene: 11151), pCAG-YFP (Addgene: 11180), pCAG-EGFP (Addgene: 11150), pCAG-CFP (Addgene: 11179), pCBA-TdTomato (Addgene: 28017). Plasmids were amplified and purified according to the suppliers' recommendations, filtered, and stored at -20 ^{o}C until use.

Avoidance of inadvertent neuronal labelling

Partial blockage of recording pipettes is commonly resolved by passing a high-amplitude 'clearing' current through the pipette. In early experiments we occasionally observed false-positive dextran-labelled neurons at locations at which anionic 'clearing' currents had been used; this can be avoided using clearing currents opposite in polarity to that of the dye. As was the case with *in vitro* experiments, *in vivo* electroporation sometimes labelled more than one neuron. This rarely happened with TMR-dextran (2/79 recovered neurons, 2.5 %), but occurred significantly more frequently with neurobiotin (7/51 neurons, 14 %, $P = 0.03$, Fisher's exact test). Inadvertent labelling of neurons due to positive pressure ejection of dextran/neurobiotin was almost never seen; unintentionally labelled neurons were easily identified by their position dorsal to the end of the recording track.

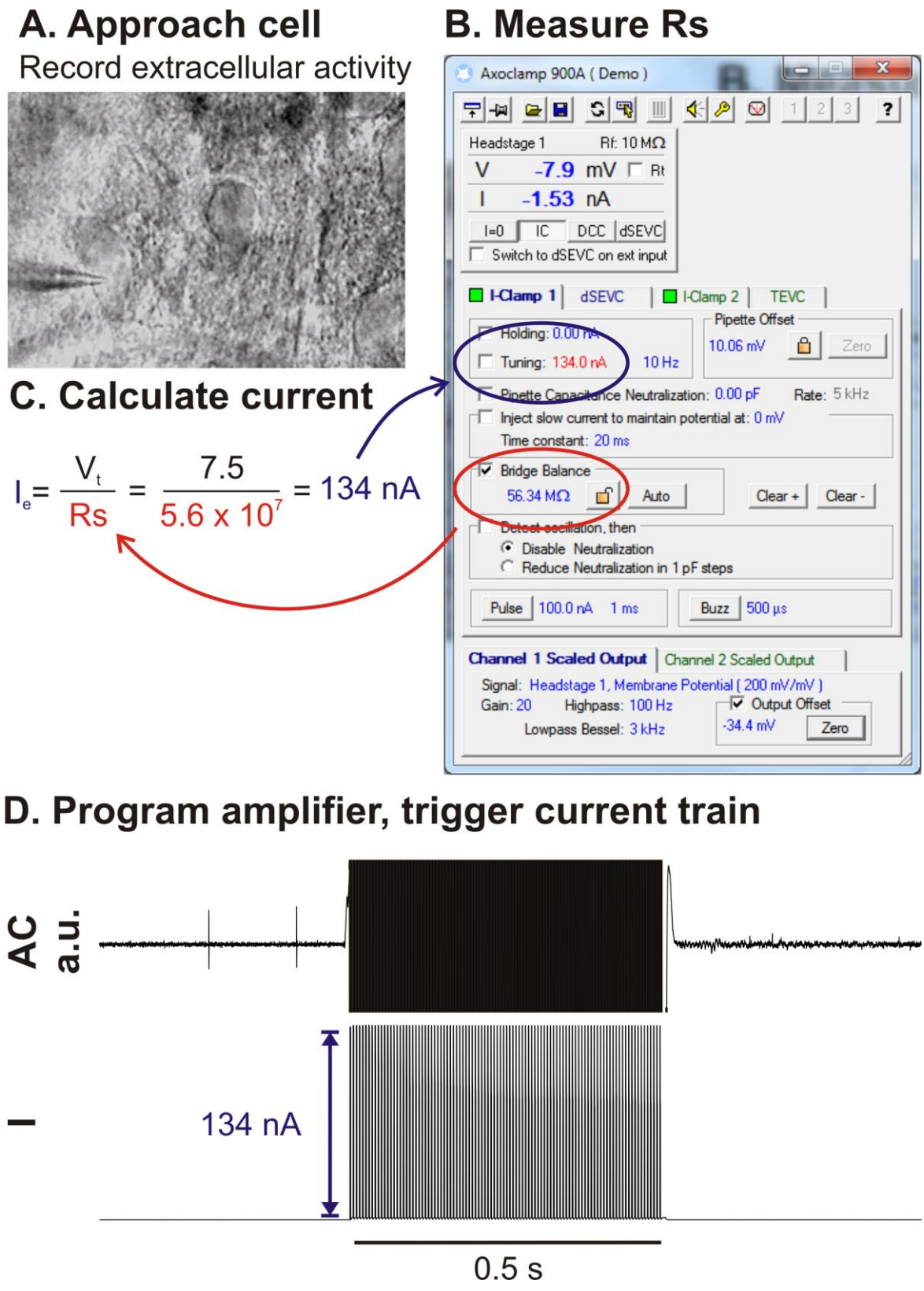

Figure 2.1 Illustration of workflow used for constant-current electroporation *in vitro*. (A) Recording pipette is moved into gentle contact with the target cell under optical guidance. (B). Immediately prior to electroporation Rs is measured using the amplifier bridge-balance function and (C) used to calculate the electroporation current (I_e) required to generate the target voltage (V_t; in this example 7.5 V). (D). The amplifier is programmed to deliver a train of current pulses at I_e.

Results

Dye-labelling *in vitro*

In pilot experiments performed on acute brain slices we first established that SCE was compatible with the micropipettes and recording amplifier used for extracellular recordings. Recording pipettes with a 1 μm tip diameter were filled with 0.9 % NaCl containing 1-3% fluorescein- or tetramethylrhodamine-dextran (TMR-dextran: MW 3000, resistance = 8 – 20 MΩ) and electroporation currents were delivered by the amplifier current ejection system. The pipette was positioned in gentle contact with the target cell under optical guidance and series resistance (Rs) was measured using the amplifier bridge-balance function. The electroporation current (I_e) required to generate the target electroporation voltage (V_t) was calculated by Ohm's Law and programmed into the amplifier current-injection dialogue (Figure 2.1). As the amplitude of currents injected using this approach remain constant over the course of the electroporation train, we term this approach *constant-current electroporation*.

Constant-current electroporation was compatible with high-quality recording of extracellular action potentials and resulted in labelling of the soma and dendritic tree using a wide range of train parameters: reproducible single-cell labelling was obtained with trains of 1 ms pulses delivered at 200 Hz for 0.5 s (V_t = 7.5 V: 36/48 cells labelled on the first attempt, Figure 2, Supplementary Video 2.1). Electroporation with even relatively low (<1 %) concentrations of fluorescent dextrans resulted in extensive filling of fine axons and fibres, allowing resolution of fine morphological details (e.g dendritic spines) that were clearly observable under epifluorescent illumination in the live slice. Resolution was enhanced by increasing the concentration of dextran used. In the vast majority of cases electroporation (successful or unsuccessful) caused an immediate cessation of spontaneous firing that rarely recovered within 10 minutes (although resumption of firing was not systematically investigated).

Electroporation occasionally labelled more than one cell (3/129 cells, 2.4 %). In such cases the intended target was always labelled too, and processes extending from the unintentionally filled cell were always observed in close proximity to the recording pipette, and were therefore presumably labelled *en passant*.

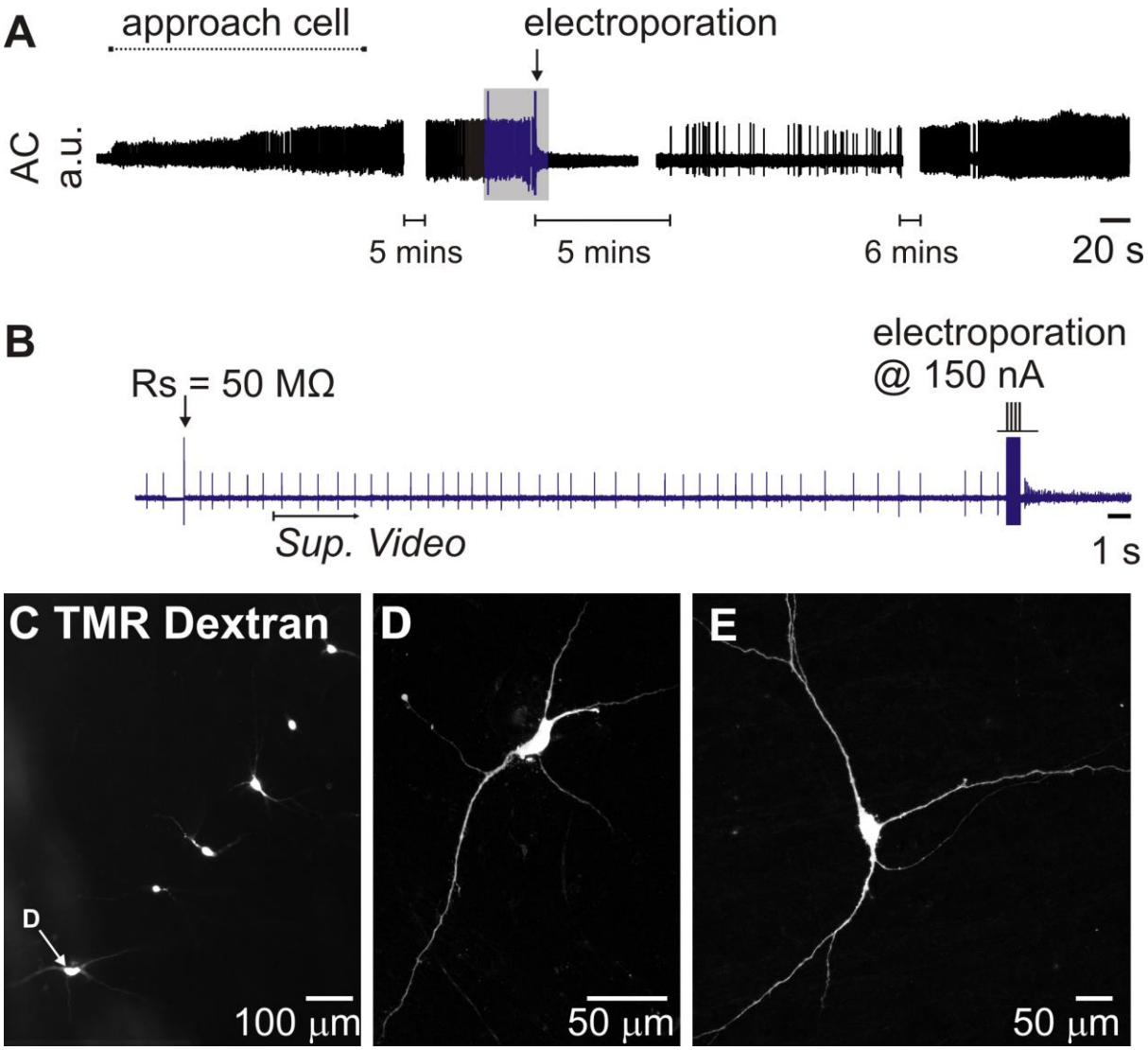

Figure 2.2 Extracellular recording and constant-current electroporation of a spontaneously active neuron in an acute brain slice (same recording as Supplementary Video 1). (A) Overview of entire recording. (B) Detailed view of portion indicated in blue in A. To electroporate Rs was first measured using the amplifier bridge-balance function and used to calculate the appropriate electroporation current (see Figure 2.1). A 200 Hz train of 100 x 150 nA, 1 ms pulses immediately filled the cell with 1% tetramethylrhodoamine (TMR)-dextran and abruptly halted its spontaneous discharge. Spontaneous activity returned after five minutes and was maintained for the remainder of the experiment. *Sup. Video* indicates starting point of Supplementary Video 1. (C) Low-power fluorescence image of six dextran-filled neurons recorded and electroporated in a single slice (D) Confocal image of the neuron indicated in C. (E) Example of a neuron from a different experiment.

Single-cell transfection *in vitro*

Using the same approach we attempted to transfect neurons in organotypic cultures with plasmids that encode fluorescent proteins ($V_{t=}$ -10 to -12 V, 100 x 0.5 - 1 ms pulses, 100 Hz, 1 s train). Although occasionally effective, this approach did not reliably result in protein transcription. As discussed in detail below, we postulated that low transfection efficiency may have resulted from voltage drop-off during pore formation, so we modified our pipette assembly to incorporate a constant-voltage source connected in parallel to the recording pipette by an electronic switch ("*constant-voltage electroporation*", Figure 2.3A).

This modification allows delivery of constant-voltage across the recording electrode (and headstage) when the switch is engaged, irrespective of Rs, but electrically isolates the voltage generator during when disengaged, preserving recording quality. This refinement improved the transfection efficiency achieved in organotypic cultures (reporter expression confirmed in 25/51 cells within 24 hours of electroporation, Figure 2.B), making it equivalent to a commercial standalone SCE device (16/30 cells, Axoporator™, Fisher's Exact Test: $P = 0.82$) using the same electroporation parameters (-10 V, 100 Hz, 1 ms pulses, 1 s train). This modification also simplified the electroporation process, as it eliminated the requirement for measurement of Rs and calculation of I_e prior to electroporation. As described elsewhere, transfection of single neurons with plasmids that encode fluorescent reporters resulted in bright and complete filling of proximal and distal neuronal compartments, in most cases sufficient to clearly visualise fine branching of axons and dendrites, axonal varicosities and terminals, and dendritic spines (Haas *et al.*, 2001).

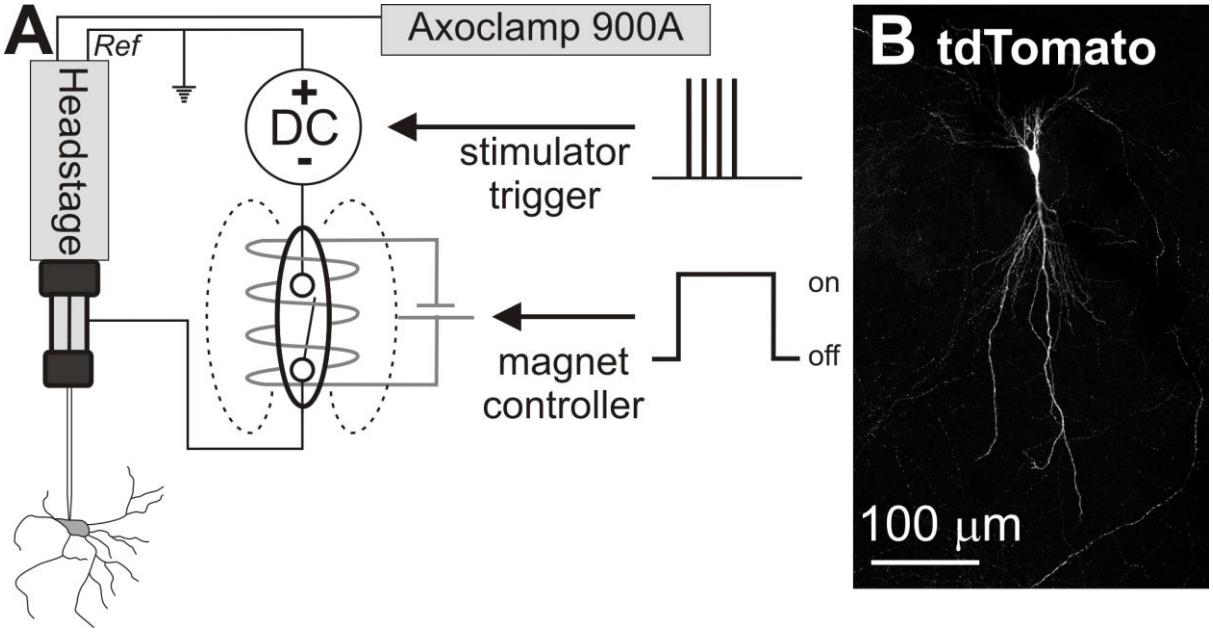

Figure 2.3 (A) Circuit configuration used for recording and constant-voltage electroporation. A DC generator is connected in parallel to the recording and reference terminals of the amplifier headstage and is isolated from the recording electrode by a reed switch placed inside a cylindrical electromagnet. When the electromagnet is engaged the circuit is closed, allowing delivery of electroporation voltages. B. Tdtomato fluorescence 24 hours after transfection of a hippocampal neuron in organotypic culture with pCBA-TdTomato.

Establishing cell contact in blind recordings

SCE is critically dependent on gentle contact between the pipette and target neuron. In fields of view with a high cell density or recordings made deep in the slice it was often difficult to unambiguously determine when the recorded neuron had been correctly identified and contacted. Furthermore, in initial experiments *in vivo,* we were unable to achieve reliable electroporation when using changes in Rs to indicate cell contact (TMR-dextran: 2/29 cells recovered, n = 4 rats), although other investigators have recently reported success using this strategy (Oyama *et al.*, 2013).

To resolve this problem we developed a protocol that uses stereotypical responses to a single 50 - 100 nA, 1 ms pulse ("*single-cell microstimulation*") to definitively identify contact between the recording pipette and soma. In acutely prepared brain slices this stimulus evoked electrophysiological responses characterized by four distinct elements (Figure 2.): (1) Increased discharge rate and altered spike morphology that included (2) an increase in spike height and (3) adoption of an asymmetrical spike shape with a conspicuous after-hyperpolarization (4) a 1-20 mV reduction in potential recorded in DC mode. All four components were *always* apparent in spontaneously active cells, but sometimes transient changes in pipette potential (with or without a short burst of action

potentials) were the only features apparent in silent cells. Electrophysiological changes evoked by microstimulation typically recovered within 10 s and were never observed in the absence of physical contact between pipette and cell, confirmed as a dimpling of the cell membrane.

Although single-cell microstimulation was apparently innocuous *in vitro* (where gentle contact between pipette and cell were closely monitored), microstimulation of spontaneously active neurons *in vivo* was initially associated with loss of recordings and presumed cell rupture and death. This was mitigated by withdrawal of the pipette from the cell once stable recordings were established such that spikes were <0.5 mV in amplitude prior to microstimulation. Where no response to microstimulation was observed the pipette was advanced in 1-3 μm increments and stimulation repeated until a response was obtained. Using this approach transient responses, in which normal neuronal activity resumed within ~10 s, were achieved in approximately 50% of neurons (see Figure 2.4 & 2.5).

Responses to single-cell microstimulation were a reliable indicator of contact between the pipette and cell and were predictive of successful electroporation. Under blind conditions *in vitro,* the probability of achieving dextran labelling on the first attempt was 89 % (55/62 cells) following a positive response to single-cell microstimulation, and rapidly declined as the pipette was withdrawn from the cell membrane (Figure 2.4E). Positive responses to microstimulation were also correlated with successful constant-current electroporation in randomly sampled spontaneously active neurons encountered 0.3 – 9.7 mm deep *in vivo* (dextran electroporation in 82/137 neurons, 60 %, n = 26 rats, V_t = 5 – 10 V, 200 Hz, 1 ms pulses, 0.5 s train). A similar proportion (49/74, 66%, *P* = 0.37, Fisher's exact test) were labelled using dextran or neurobiotin in a second cohort of experiments (n = 21 rats) in which neurons in the ventrolateral medulla with respiratory-related activity were preferentially targeted with constant-voltage electroporation (7.5 – 10 V, 200 Hz, 1 ms pulses, 0.5 s train: Figure 25).

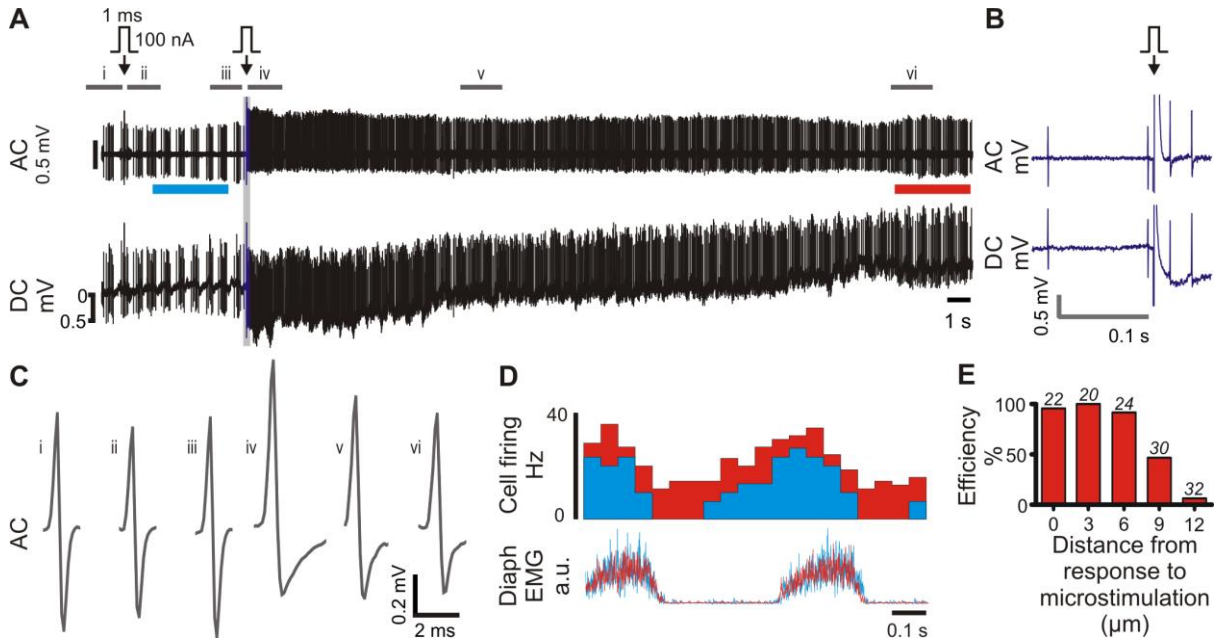

Figure 2.4 Single-cell microstimulation of a medullary respiratory neuron *in vivo*. (A) 100 nA microstimulation (arrow) initially evoked no effect on neuronal firing. The pipette was advanced 3 µm and stimulation repeated. This time the stimulus evoked transient stereotypical changes in firing frequency, spike amplitude and spike shape, apparent in the AC trace, and a small hyperpolarization of the pipette, visible as a 1 mV shift in the DC trace. (B) Expanded view of region drawn in blue in A. (C) Average spike waveforms; source data indicated in A. (D) Diaphragm-triggered histograms of neuronal firing before (cyan, bar indicated in A) and after (red, bar indicated in A) microstimulation: the firing pattern is maintained over the recording. (E) Response to single-cell microstimulation (0 µm) is correlated with high labelling efficiency (TMR-dextran, *in vitro*), which decreases as the pipette is withdrawn from the cell membrane. Number of replicates shown over each series.

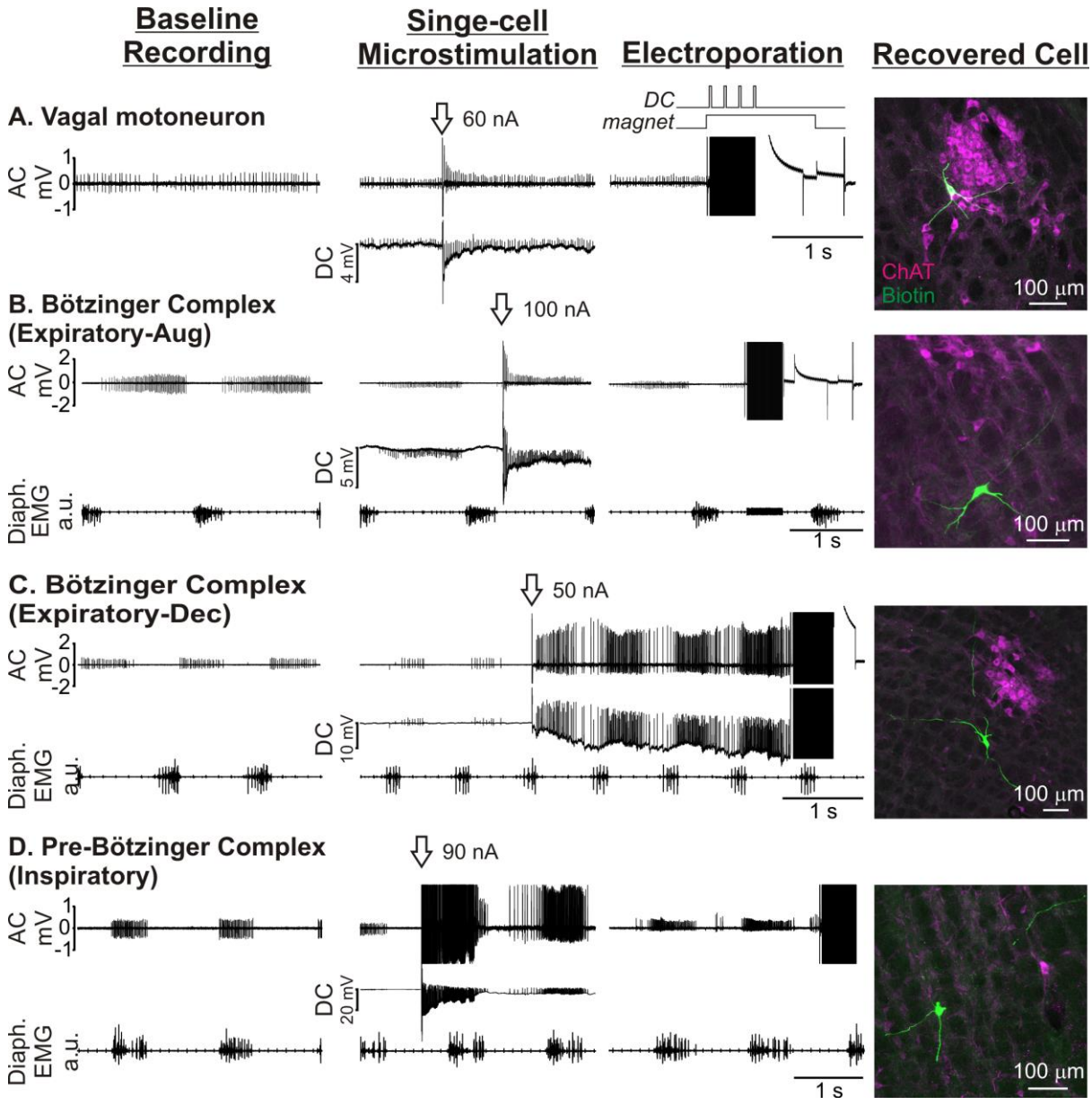

Figure 2.5 Examples of non-respiratory (A) and respiratory (B-D) neurons recorded in extracellular mode in the ventrolateral medulla and labelled with neurobiotin by constant-voltage electroporation *in vivo*. After establishment of baseline recordings and repositioning of the recording pipette such that spike height was <0.5 mV, single-cell microstimulation (arrow) was used to verify cell contact. In most cases neurons were allowed to recover from microstimulation prior to electroporation (100 x 1 ms pulses, 200 Hz, +7.5 to +10 V). Photomicrographs show neurobiotin-filled neurons (green) recovered at the appropriate stereotaxic co-ordinates; magenta channel shows immunoreactivity for choline acetyl transferase (ChAT). Diaphragmatic EMG activity indicates inspiration, permitting functional identification of respiratory neurons. (A) Tonically active ChAT-immunoreactive neuron in the nucleus ambiguus; (B) Augmenting expiratory neuron recorded ventral to nucleus ambiguus; (C) Decrementing expiratory neuron recorded ventral to nucleus ambiguus; (D) inspiratory-locked neuron.

Single-cell transfection *in vivo*:

Having verified that constant-voltage electroporation is capable of reliable single-cell transfection *in vitro* and established a protocol that results in reproducible dye-labelling *in vivo*, we then examined its suitability for single-cell transfection *in vivo.*

Brainstem neurons were recorded 1.6 – 9.8 mm deep in either non-recovery experiments, in which urethane anaesthesia was maintained for 12-18 hours after electroporation (n = 5 rats), or recovery experiments (n = 7 rats), in which anaesthesia was reversed at the conclusion of recording and rats were recovered for 1-2 days. Contact between the pipette and target neuron was first verified by observing a positive response to single-cell microstimulation, and neurons that recovered were electroporated at negative polarity (-10 V, 50 – 100 Hz, 0.5 – 1 ms pulses, 1 s). Regardless of surgical preparation, electroporation parameters, or plasmid construct used, this approach rarely resulted in reporter expression (6/87 neurons, 7%).

We initially hypothesized that the low success rate may have reflected an incorrect assumption regarding the predictive value of our microstimulation technique. We adopted an approach similar to that used for electroporation of superficial cortical neurons (Judkewitz *et al.*, 2009; Oyama *et al.*, 2013), in which the pipette is manoeuvred such that Rs is increased by 30 %, and attempted SCE in 31 neurons in 5 recovery experiments; no transfected cells were subsequently identified.

Review of recordings from successfully transfected neurons revealed that microstimulation had in some cases resulted in full intracellular access prior to electroporation (5/6 neurons), suggesting that transfection could be achieved by direct intracellular plasmid electrophoresis. This hypothesis was examined in experiments in which brainstem neurons were targeted for intracellular recordings using semi-sharp pipettes (tip diameter: <1 μm, resistance 18 ± 3 MΩ). This configuration was compatible with stable recording of unit activity in extracellular mode prior to brief (typically <10 s) intracellular access and plasmid ejection (-10 V, 50 Hz, 1 ms pulses, 1 s train or -10 V, 1000 Hz, 0.1 ms pulses, 0.1 s train: Steinmeyer and Yanik (2012)). Transfection was achieved in 13/48 (27 %) neurons in which intracellular access (membrane potential -30 to -70 mV) was obtained prior to electrophoresis (Figure 2.). Transfected neurons were recorded 1.6 – 8.3 mm deep to the brain surface using pipettes between 8 and 37

MΩ in resistance. 3/13 neurons were silent; the remainder showed spontaneous activity between 1 and 20 Hz. Cross sectional areas of transfected neurons were 141 – 1178 μm^2, equivalent to 13 – 39 µm in diameter.

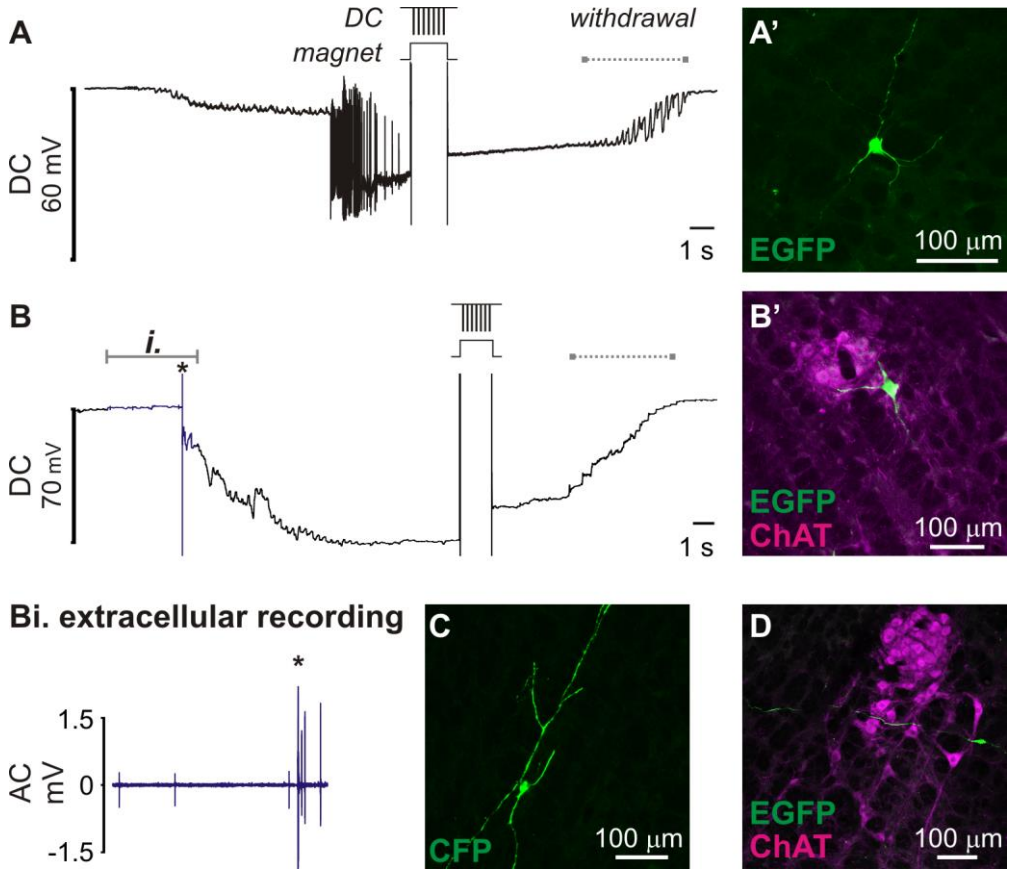

Figure 2.6 Transfection of ventrolateral brainstem neurons following intracellular penetration *in vivo*. Once membrane potential had stabilized plasmid DNA encoding fluorescent protein was electrophoretically injected by -10 V pulses (50 x 1 ms pulses, 1 s). Membrane potential was retained after electrophoresis until withdrawal of the pipette (indicated by dashed lines). (A) Electrophysiological recording from a silent neuron that started firing after penetration. A' shows EGFP-labelled neuron recovered at the corresponding stereotaxic coordinates. (B) Slowly firing spontaneously active neuron: extracellular spikes (blue data, detailed in Bi.) were resolved prior to cell penetration (*). (B') Colocalization of EGFP with ChAT immunoreactivity indicates that this example is a cholinergic motor neuron in nucleus ambiguus. (C + D) show examples of other neurons transfected using the same approach.

Discussion

The current study provides researchers with three novel protocols that can be used for reliable dye-labelling or transfection of functionally identified neurons in deep brain regions *in vivo*. Constant-current electroporation can be performed without any customization of the recording amplifier and yields rapid and high quality dye labelling *in vitro* and *in vivo*. Constant-voltage electroporation requires minimal modification of hardware and yields *in vitro* transfection at efficiency equivalent to a widely-used proprietary device, but in our hands this approach was incompatible with high transfection efficiency *in vivo*. In contrast, we found that intracellular electrophoresis of genetic material may instead offer a more reliable method for transfection of functional identified neurons in inaccessible brain regions.

In establishing our transfection methodology we developed dye-labelling techniques that offer some advantages to the juxtacellular method in terms of simplicity and speed. Successful juxtacellular labelling is indicated by 'entrainment' of neuronal firing to regular anodal pulsing of the recording pipette, which must be maintained for several minutes for reasonable labelling to occur. Longer periods of entrainment are associated with more complete labelling (up to 60 minutes: Noseda *et al.*, 2010). Although the juxtacellular approach can yield efficient labelling in the hands of the technically elite (100/115 cells: Pinault, 1996; 45/50 cells: Guyenet & Wang, 2001), establishing and maintaining entrainment requires considerable finesse, and recordings are often lost before or during entrainment. It is notable that the number of neurons lost during attempted labelling is often omitted from reports that use this approach, perhaps boosting the apparent efficiency of the technique: in unpublished pilot experiments we found that recordings were lost before or during entrainment in 145/248 (58%) attempts.

In contrast to the imprecise cues used to guide entrainment over minutes of juxtacellular labelling, single-cell microstimulation provides an instant binary output; a cell either responds with an unambiguous electrophysiological signature, in which case it may be immediately electroporated with a high probability of recovery, or does not, in which case the pipette is manoeuvred and stimulation repeated (in cases where there is no response) or another cell is sought (in cases where the recording is lost). This makes

the protocol quick to perform and easy to learn: most of the experiments targeting respiratory neurons were performed by a graduate student (SL) who learned the technique in a week and recovered two labelled neurons in his first experiment.

The increase in neuronal excitability and effects on spike shape and amplitude seen in response to microstimulation are consistent with induction of an "open-cell" state by the stimulus, a transient permeabilisation of the neuronal membrane evoked by its partial electroporation (Braeken *et al.*, 2012; Spira & Hai, 2013). Our observation that such responses only occur when the pipette is in contact with the neuron are supported by similar reports by Santos et al. (2007; 2009), who found that 30-100 nA, 1 ms pulses could be used to effectively stimulate spinal cord neurons in loose-seal mode, but not in the absence of physical contact between the pipette and cell. We conclude that single-cell microstimulation provides a reliable and objective indicator of contact between the pipette and neuron. The major shortcoming associated with using single-cell microstimulation to guide electroporation is its high attrition rate *in vivo*; this is most likely due to excessive contact between the pipette and target cell, as it does not seem to occur *in vitro* (where contact can be closely monitored), although factors such as cell size and pipette geometry may also contribute to the effect.

Constant-current and constant-voltage electroporation offer dye-labelling with similar efficiencies *in vitro* and *in vivo*; both result in labelling that is at least equivalent in quality to that offered by the juxtacellular technique *in vivo* and comparable to standard SCE *in vitro*, where fine morphological features such as dendritic spines and terminals are consistently revealed (Haas *et al.*, 2001; Umeda *et al.*, 2005). The quality of labelling obtained using the juxtacellular technique varies according to the brain region targeted and tissue processing, hampering direct comparison with the protocols described here. However, extensive filling of brainstem neurons juxtacellularly labelled with neurobiotin and visualised with fluorescent avidin conjugates is rare in the literature (Sartor & Verberne, 2003; Abbott & Pilowsky, 2009; Kanbar *et al.*, 2011; Boucetta *et al.*, 2014; Iceman & Harris, 2014) and in our own experience (unpublished data). In contrast, although variability in labelling quality was observed using the approaches described here, we often saw extensively filled neurons that projected across dozens of histological sections in which fine morphological details were visible. We did not extensively investigate the quality of labelling possible using diaminobenzidine

visualisation, but details such as terminals and dendritic spines were visible in one of three neurons processed that way. Constant-current electroporation may be conducted without modification to hardware provided the recording amplifier is capable of generating sufficiently high currents (400 - 800 nA), making it fast and cheap to adopt. However, we found it more convenient to use the constant-voltage approach, as it eliminates measurement of Rs and current calculation from the workflow, speeding up the protocol, and is compatible with single-cell transfection *in vitro*.

Why doesn't constant-current electroporation result in transfection? In constant-current mode the measured value of Rs has a critical influence on voltage output. Constant-current pulses may initially succeed in generating V_t for a given Rs; however, pores are formed in the membrane within microseconds of voltage application (see DeBruin & Krassowska, 1999; Wang *et al.*, 2010), lowering membrane resistance and consequently Rs, resulting in a proportionate reduction in trans-membrane voltage. As a consequence of this voltage drop-off, constant-current electroporation may fail to sustain the voltages required for large and stable pore formation, which are crucial for efficient plasmid delivery (Rae & Levis, 2002).

In vitro transfection efficiency was restored by integration of a constant-voltage generator to the recording circuit. This modification allowed the delivery of up to ±10 V without risk to the recording headstage (following advice from the manufacturer), and made transfection efficiency equivalent to that obtained with a commercial single-cell electroporator and comparable to that reported elsewhere (Rae & Levis, 2002; Rathenberg *et al.*, 2003; Steinmeyer & Yanik, 2012). However, exhaustive attempts to translate it for single-cell gene delivery *in vivo* were fruitless. This is surprising, given the similarities between our approach and protocols recently described by other investigators, in which some level of transfection was observed under all parameters tested (Cohen *et al.*, 2013; Oyama *et al.*, 2013). Differences in the brain regions and, perhaps crucially, the depths at which neurons were targeted, may underlie this disparity, as Cohen *et al.* (2013) and Oyama *et al.* (2013) restricted their attempts to neurons within 450 μm or 1.5 mm of the brain surface respectively, where pipette patency is easier to manage.

We conclude that techniques based on SCE are unlikely to yield reliable transfection of neurons in deep brain structures, and speculate that blockage of pipettes is most likely responsible for the poor transfection efficiency seen *in vivo*. Despite applying high positive pressure to the internal solution during brain penetration and cell hunting, we rarely saw any evidence of dye leakage or hydraulic injury along pipette tracks, both of which indicate pipette patency *in vivo* (Rancz *et al.*, 2011), and the quality and efficiency of dye-labelling and reporter expression were consistently higher *in vitro* than *in vivo*. Although we were able to use SCE for efficient dye-labelling nearly 10 mm deep to the brain surface, this does not necessarily mean that recording pipettes were patent: in our experience electrophoretic ejection of fluorescent dextran is consistently possible from clogged pipettes in which no dextran may be pressure-ejected, and we were able to produce robust labelling with such pipettes *in vitro*. However, we and others have found that blocked pipettes absolutely preclude transfection by SCE (Haas *et al.*, 2001; Rae & Levis, 2002; Rathenberg *et al.*, 2003; Bestman *et al.*, 2006; Kitamura *et al.*, 2008; Judkewitz *et al.*, 2009).

If patency is the main issue affecting the efficiency of SCE in deep brain regions, pipette clogging probably reduces rather than completely obstructs plasmid ejection, as intracellular plasmid electrophoresis reproducibly transfected neurons up to 8.3 mm deep. Stable intracellular access is difficult to achieve even in acute preparations, where extensive craniotomy or pneumothoraces are commonly used to reduce movement. However, we found that brief access, sufficient for transfection, could be gained in minimally invasive preparations (although we found tracheal intubation with neuromuscular block and artificial ventilation useful) and that large neurons could be impaled and transfected using low-resistance pipettes. The current data provide a proof-of-principle that intracellular recording may be used to transfect neurons in deep brain regions, but the efficiency of the approach will ultimately dependent on factors including operator experience, animal age, brain region targeted and the size of targeted neurons.

The current data provide relatively simple protocols that can be used for reliable and robust labelling of recorded neurons and a novel approach for transfection of neurons in deep brain regions. The clear-cut criteria used to guide electroporation and the rapidity at which labelling can be performed may prove particularly attractive to novice

investigators, whereas the potential to select neurons for genetic modification based on their functional properties may prove useful to investigators interested in applying advanced connectome-tracing technologies at single-cell resolution (Wickersham *et al.*, 2007b; Marshel *et al.*, 2010; Rancz *et al.*, 2011)

Supplementary Video 2.1. Extracellular recording and constant-current electroporation *in vitro*. The electrophysiological recording (same recording shown in Figure 2.2) has been converted into audio and embedded into the video file; action potentials are audible as clicks. URL: https://www.youtube.com/watch?v=pS6yRxDQH4Y

CHAPTER 3: Mapping sources of pre-synaptic input to bulbospinal RVLM neurons

Abstract

Spinally projecting neurons in the rostral ventrolateral medulla (RVLM) are thought to play a critical role in the generation of vasomotor sympathetic tone and represent a major site of convergence for multiple descending and reflex pathways that coordinate sympathetic nerve activity. Elucidating the organization of the circuits that drive these neurons is key to understanding the mechanisms that underlie the central control of blood pressure. Here we present a brain-wide connectomic map of the neurons that provide monosynaptic drive to a putative RVLM sympathetic premotor population, generated using a two-step restricted trans-synaptic viral tracing strategy. We made focal microinjections of a genetically restricted reporter-expressing rabies vector, SADΔG(EnvA)-mCherry, into the RVLM, and restricted its entry to neurons that project to the T2 spinal cord by first transducing them with a cassette (YTB) encoding complementary genes required for conditional rabies entry and trans-synapsis. We observed reproducible patterns of inputs arising from the dorsal, contralateral, and midline medulla, and local RVLM interneurons including catecholaminergic non-bulbospinal neurons and neurons likely to reside within the ventral respiratory column. Distant inputs albeit sparse, were identified in the pons, cerebellum and midbrain, and included previously suspected sites of monosynaptic drive such as the paraventricular nucleus of the hypothalamus. These observations suggest that the RVLM predominantly receives synaptic drive from local sources.

Introduction

The central command of blood pressure arises from sympathetic premotor populations distributed throughout the brainstem and hypothalamus. Those tasked with regulating the activity of sympathetic vasomotor nerves are concentrated within the rostral ventrolateral medulla (RVLM), immediately caudal to the facial motor nucleus (nVII). This population alone appears critical to basal and reflex command as demonstrated by stimulation and lesion of the region; the former drives increases in arterial blood pressure (AP) and sympathetic nerve activity (Goodchild *et al.*, 1982; Willette *et al.*, 1983a; Ross *et al.*, 1984) and the later reduces AP and SNA to levels equivalent to those seen following cervical transection or ganglionic blockade (Guertzenstein & Silver, 1974; Feldberg & Guertzenstein, 1976; Dampney & Moon, 1980; Ross *et al.*, 1984; Pilowsky *et al.*, 1985).

The sympathetic pre-motor function is reflected by the functional and anatomical attributes of this population, in that they form descending monosynaptic excitatory input to SPN (Strack *et al.*, 1989a; Jansen *et al.*, 1995; Pyner & Coote, 1998; Oshima *et al.*, 2008), are spontaneously active, (Brown & Guyenet, 1984, 1985; McAllen, 1986; Morrison *et al.*, 1988; Reis *et al.*, 1988) and are sensitive to exteroceptive and interoceptive stimuli that modulate sympathetic nerve activity, such as the baroreceptor, chemoreceptor, and somatosympathetic reflexes (Brown & Guyenet, 1985; Morrison *et al.*, 1988; Morrison & Reis, 1989; Sun *et al.*, 1992), as well as temperature (McAllen & May, 1994), body position (Sugiyama *et al.*, 2011), hypercapnia (Koshiya *et al.*, 1993; Marshall, 1994; Guyenet, 2000; Koganezawa & Paton, 2014), osmolarity (Stocker *et al.*, 2008) and glucoprivation (Verberne & Sartor, 2010).These functional characteristics are correlated well with bulbospinal RVLM neurons that express enzymes required for adrenaline synthesis (C1-neurons) (Schreihofer & Guyenet, 1997).

Although our understanding of the functional modalities that influence RVLM sympathetic premotor neuronal activity is comprehensive (at least in anaesthetised preparations), the organisation of the pathways that ultimately underlie the high functional diversity of RVLM sympathetic premotor neurons remains poorly resolved. For example, the on-going spontaneous activity of RVLM sympathetic premotor neurons

is dependent on excitatory and inhibitory input (Barman & Gebber, 1989; Lipski *et al.*, 1996; Ito & Sved, 1997; Dampney *et al.*, 2003; Coote, 2007). Although the 'network theory' of action potential generation (discussed in Dampney (1994b) was widely adopted in the 1990s, the source of the synaptic drive that supposedly underlies spontaneous activity remains largely unknown over twenty years later.

A central tenet of neuroscience is that the structure of a neuronal circuit underlies the behaviour of its output. The field of connectomics, still in its infancy, posits that insights regarding the function of neuronal circuits can be gained by definitively resolving network architecture (Carandini, 2012; Denk *et al.*, 2012). We believe that employing a structural approach to unambiguously define the sources of monosynaptic input to RVLM sympathetic premotor neurons may resolve some of the impasses associated with this field and serve as a platform for hypothesis generation.

Here we use a genetically modified rabies variant, SADΔG, to unambiguously label neurons that form monosynaptic connections with putative RVLM sympathetic premotor neurons. SADΔG, initially developed by the Callaway laboratory, (Wickersham *et al.*, 2007a; Wickersham *et al.*, 2007b) exploits the exclusive trans-synaptic and retrograde trafficking of the rabies virus in the central nervous system. The key innovation of SADΔG is that the ability of the virus to enter a target neuron, and its ability to retrogradely infect monosynaptically connected pre-synaptic neurons, can be conferred by genetic modification of the target neuron using conventional gene delivery techniques (as recently reviewed by Callaway & Luo, 2015). Our strategy was to first drive the expression of the cassette, YTB, that contained the components required for cell entry (TVA receptor) and trans-synapsis (rabies glycoprotein), in spinally projecting neurons. This was achieved by microinjecting a recombinant herpes vector (HSV) with a retrograde transduction profile at the intermediolateral cell column (IML) of the spinal cord, a major site of termination of sympathetic premotor neurons. We then selectively infected YTB-expressing neurons using a reporter-driving variant of SADΔG that is dependent on the expression of TVA for cell entry (SADΔG(EnvA)-mCherry). By restricting the infection of YTB-expressing neurons with SADΔG(EnvA)-mCherry to those residing within the RVLM we were able to control the access of SADΔG to putative sympathetic premotor neurons, and then map brain-wide sources of drive received by those neurons.

Methods

Ethical Approval: All experiments were approved by Macquarie University Animal Ethics Committee and conformed to the Australian Code of Practice for the Care and Use of Animals for Scientific Purposes.

Vector preparation

SADΔG production

SADΔG was produced at Macquarie University within a quarantine containment level 2 facility, following the protocol described in Osakada and Callaway (2013). Briefly, EnvA-pseudotyped SADΔG was derived from the pSADΔG-mCherry genome plasmid (Addgene 32636) and assembled with the pcDNA-SADB19N (Addgene 32630), pcDNA-SADB19P (Addgene 32631), pcDNA-SADB19L (Addgene 32632), and pcDNA-SADB19G (Addgene 32633) helper plasmids. The vector was packaged in a baby hamster kidney cell line, B7GG, that expresses T7 RNA polymerase, rabies glycoprotein and histone-tagged GFP. Packaged SADΔG-mCherry was then pseudotyped with the EnvA envelope protein from the avian sarcoma leucosis virus, via passage through an EnvA-expressing cell line, EnvA-BHK. SADΔG(EnvA)-mCherry was titrated via serial dilution and infection of a human embryonic kidney cell line, TVA-HEK, that expresses the receptor for the EnvA envelope protein. The titre of SADΔG(EnvA)-mCherry used for injections was $6.8x10^7$ IU/ml. SADΔG(EnvA)-mCherry purity was determined by infection of naïve HEK cells and determined to contain approximately $5.33x10^3$ unpseudotyped virions per ml. Vector was stored in 3 µl aliquots at -80^{o}C until microinjection.

Plasmids were acquired from addgene and amplified and purified according to the suppliers' recommendations. B7GG, EnvA-BHK and TVA-HEK cell lines were kindly provided by Professor Ed Callaway.

Retrograde HSV vectors

We used a recombinant herpes simplex type1 (HSV1) vector with a retrograde tropism to drive expression of rabies glycoprotein, TVA receptor, and YFP reporter protein (HSV-hCMV-YTB). The gene cassette was derived from the pCAG-YTB plasmid (Addgene 26721) and cloned into recombinant HSV amplicons under the control of the human

cytomegalovirus promoter at the Massachusetts Institute of Technology vector core, using a modified version of the protocol described by Lim and Neve (2001). Control vectors that drive the expression of reporter proteins (HSV-hCMV-GFP, HSV-hCMV-mCherry) were used in initial experiments to determine the time course of protein translation and determine the anatomical boundaries of spinally-projecting RVLM neurons. The titre of the HSV vectors as reported by the vector core are 3 x 10^8 IU/ml. Immediately prior to injection vectors were diluted in normal physiological saline containing blue fluorescent polystyrene spheres to label the injection site (1 μm diameter: Thermo Scientific, Australia, 09980508) to ¼ of their original concentration.

Animals

Animals were obtained from the Animal Resources Centre (Perth, WA) and were housed at the Macquarie University Central Animal Facility. Male Sprague-Dawley rats weighing 150-500g at the onset of experiments were used for anatomical studies. Animals were housed in groups of 4 in individually ventilated cages containing environment enrichment material (blocks of wood, shaved cardboard, plastic tubes), with food and water available *ad libitum*. Cages were kept in a temperature- and humidity-controlled room (21°C ± 2°C, 60 % humidity) with fixed 12 h light and dark cycles. Animals were transported to the PC2 laboratories at the Australian School of Advanced Medicine (Macquarie University) for stereotaxic injections and electrophysiology experiments.

Vector injections

Spinal cord injections of retrograde herpes vectors

Rats were anaesthetized with intraperitoneal ketamine (75 mg/kg; Parnell Laboratories, Australia) mixed with medetomidine (0.75 mg/kg; Pfizer Animal Health, Australia) and treated with prophylactic antibiotics (100 mg/kg Cephazolin sodium, i.m.; Mayne Pharma, Australia) and analgesia (2.5-10 mg/kg Carprofen, s.c.; Norbrook Pharmaceuticals, Australia).

In initial experiments using HSV-hCMV-reporter variants, rats were mounted in a stereotaxic frame and tail clamped to maintain the spine in a horizontal and elevated position. The spinal cord was exposed at the T2 and T7 vertebrae following minimal dissection of the intravertebral ligaments and reflection of the dura. At each vertebral level 4 x 500 nl pneumatic vector injections (2 on each side, spaced 1 mm apart

rostrocaudally) were made using a glass micropipette with an approximately 20 μm diameter tip at co-ordinates corresponding to the IML (0.75 mm lateral to the midline and 1 mm deep to the dorsal surface of the spinal cord). Vectors were injected over a 5 - 10 minute period and the pipette was left in position for approximately five minutes before slow retraction. At the conclusion of injections exposed spinal cord sites were irrigated with sterile physiological saline, covered with oxidized cellulose haemostat, and the wound closed with suture clips. Both vectors resulted in equivalent labelling, irrespective of the spinal level at which they were injected, but in most cases the GFP-driving variant was targeted at the T2 IML, and the mCherry-driving variant targeted at the T7 vertebrae (equivalent to the T10 spinal segment). Rats were recovered for 1 – 7 days.

For experiments in which HSV-hCMV-YTB was used the same general surgical approach was employed, but vector injections were limited to 2x 500 nl injections in the left IML at the T2 spinal segment.

At the end of surgery anaesthesia was reversed with atipamazole (1 mg/kg s.c., Pfizer Animal Health, Australia) and rats were monitored until ambulatory and then returned to their home cage. Rats were monitored closely for the remainder of the experiment with additional analgesia as required.

Brainstem injections of SADΔG(EnvA)

1 – 5 days after injection of HSV-hCMV-YTB at the T2 spinal cord level, rats a were re-anaesthetised and treated with analgesia and antibiotics as described above and positioned in a stereotaxic frame in the skull flat position. An incision was made along the skull overlying the brainstem and a 2 mm diameter hole was made in the skull 2 mm lateral to midline, approximately overlaying the RVLM, and the dura reflected. The left facial nucleus, an anatomical landmark for the rostral extent of the RVLM, was mapped by recording antidromic field potentials evoked by stimulation of the facial nerve, as previously described (Brown & Guyenet, 1985). The most caudal position at which facial field potentials could still be evoked was determined as the caudal pole of the facial motor nucleus. 50 – 75 nl of SADΔG(EnvA)-mCherry was microinjected 100 – 300 μm caudal to the caudal pole of the facial nucleus at a depth equivalent to the ventral surface of the facial nucleus. The pipette was left in position for ~5 min prior to withdrawal.

Wounds were irrigated and the exposed brain covered with oxidized cellulose haemostat and the wound closed with suture clips and anaesthesia reversed with atipamazole. Rats were allowed to recover for up to 7 days following SADΔG injection.

Histology

Transcardial Perfusion

Animals were anaesthetized with sodium pentobarbital (>150 mg/kg, 20% lethabarb (Virbac, Australia) in 0.9 % saline). When responses to hind-paw pinch were absent the chest cavity was opened and heart exposed. An 18 gauge needle was inserted into the ascending aorta via the left ventricle and clamped in position with a haemostat. The right atrium was then cut and 1 ml of heparin (1000 IU/ml) injected into the aorta. The animal was then perfused with 300 ml ice cold saline followed by 300 ml of 4 % PFA. The brain and thoracic spinal cord were then removed and post-fixed overnight.

Tissue processing

With the assistance of a brain matrix, the brains were blocked 2 mm caudal to the olfactory bulb and mounted frontal pole down on a vibratome plate so that the ventral surface of the brain was approximately perpendicular to the plate. Slices were sectioned in the coronal plane using a Leica VT1200S vibrating microtome at 50 µm and collected in 4 pots in 0.01 M Tris-phosphate buffered saline (TPBS). For HSV-hCMV-YTB/ SADΔG(EnvA)-mCherry injected animals, pot 1 was mounted directly onto glass slides to maintain section order. Brainstem sections from a second pot were processed for YFP and TH immunoreactivity, so that 'seed' neurons (i.e. neurons infected by both HSV-hCMV-YTB and SADΔG(EnvA)-mCherry) could be identified. The other pots were transferred to cryoprotectant solution (500 µM polyvinylpyrrolidone, 76.7 mM Na_2HPO_4, 26.6 mM NaH_2PO_4, 876 mM sucrose, 5 mM ethylene glycol) for storage at -20^{o}C.

Immunohistochemistry

Sections were permeabilized in TPBS containing 0.2 % Triton ‑ 100 for 3 × 15 min and blocked for nonspecific binding in TPBS containing 2 % bovine serum albumin and 0.2 % Triton ‑ 100 for 1 h at room temperature. Primary antibodies (see Table 3.1) were added to the blocking buffer and sections were incubated for 48 h at 4 °C. Sections were washed in TPBS 3 × 30 min and incubated in secondary antibodies for 12 h at 4 °C.

Processed sections were washed again in TPBS 3 × 30 min before being mounted on glass slides with Dako fluorescence mounting medium and cover slipped.

Table 3.1: Primary and Secondary antibodies

Application	Antigen	Species	Conjugate	Concentration	Clonality	Manufacturer	Code
1°	Tyrosine-Hydroxylase (TH)	Mouse	N/A	1:1000	Mono	Sigma	T1299
1°	Tryptophan-Hydroxylase (TPH)	Mouse	N/A	1:500	Mono	Sigma	T0678
1°	Neurokinin-1 Receptor (NK1R)	Rabbit	N/A	1:1000	Poly	Sigma	S8305
2°	Rabbit IgG (H+L chain)	Donkey	Alexa Fluor® 488	1:500	Poly	Life Technologies	A21206
2°	Rabbit IgG (H+L chain)	Donkey	Alexa Fluor® 647	1:500	Poly	Life Technologies	A31573
2°	Goat IgG (H+L chain)	Donkey	Alexa Fluor® 647	1:500	Poly	Life Technologies	A21447
2°	Mouse IgG (H+L chain)	Donkey	Alexa Fluor® 647	1:500	Poly	Life Technologies	A31571

In situ Hybridization (ISH)

ISH was conducted to examine double labelling of rabies-infected input neurons with GAD67 mRNA, a marker of GABAergic neurons, and GLYT2 mRNA, a marker of glycinergic neurons. ISH probes were identical to those described by Bowman *et al.* (2013) and Le *et al.* (2015) respectively. Sections were incubated for 30 minutes at 37 °C and 1 hour at 58 °C in hybridization solution (5 % dextran sulfate, 5 SSC [pH 7.0]), 50% formamide, 250 µg/ml herring sperm DNA, 1x Denhardt's solution, 0.1 % Tween-20) under RNase-free conditions. The riboprobe was then added to the solution to a final

concentration of 200–500 ng/ml and sections were incubated with gentle agitation at 58 °C overnight. After hybridization, sections were washed twice for 30 minutes in 2x SSC / 0.1% Tween-20 at 58 °C, then twice for 30 minutes in 0.1x SSC / 0.1 % Tween-20 at 58 °C.

Sections were incubated in maleic acid buffer containing 2 % Boehringer Blocking Reagent (BBR, Roche) and alkaline phosphatase-conjugated sheep anti-DIG (Roche, Australia) 1:1,000 for 48 hours at 4 °C. Sections were acclimatized in alkaline buffer (0.1 M NaCl, 0.1 M Tris-HCl, pH 9.5, 0.1M MgCl2, 0.1 % Tween-20, 2 mM levamisole) for 3x 30 min washes.

DIG labels were developed by reaction with a nitroblue tetrazolium (NBT) and 5-bromo-4-chloro-3-indolyl phosphate (BCIP) salt solution (Roche). The development of a dark purple cytoplasmic precipitate was monitored under brightfield until intense with minimal background staining. The reaction was stopped with a 15-min wash in 0.1 M Tris (pH 8.5) with 1 mM EDTA.

CLARITY processing

The brains of 2 animals that received T2 spinal cord injections of HSV-hCMV-GFP were optically cleared for thick block imaging using a passive CLARITY protocol (Tomer *et al.*, 2014). Briefly, animals were perfused with an acrylamide/PFA based hydrogel solution, brains removed and incubated in hydrogel for 2 days at 4 °C. Hydrogel-embedded brains were polymerised at 37 °C for 3 h in the absence of oxygen. Excess polymerized hydrogel was removed from the brain surface with a spatula and the medulla was cut into serial 1 mm thick blocks using a brain matrix. The slices were then passively cleared in a sodium dodecyl sulphate based clearing solution with constant low intensity shaking at 37 °C for 10 days. Slices were washed in PBS for 4 h and then mounted in 85 % glycerol for imaging.

Imaging

For whole-brain reconstruction of rabies-infected neurons, every histological section lying between the cervical spinal cord and the most rostral section in which rabies-labelled neurons were identified was imaged under epifluorescence using 10x objective lens (AxioImager Z2 microscope running ZEN 2011 software, Zeiss, Gottingen, Germany). Whole-brain images were obtained from sections that were immediately

mounted during cutting, preserving order; immediately mounted sections that spanned the RVLM region were not used for mapping of input neurons or seed neurons. Rather, these data were obtained from alternative sections that were processed for YFP and TH immunoreactivity. Neurons that contained both YFP and mCherry were classified as seed neurons and were further sub-classified as TH-immunoreactive or TH-negative.

Confocal images were taken of regions of interest and CLARITY processed slices using a Leica TCS SP5X confocal microscope (Leica Microsystems Pty Ltd, North Ryde, NSW, Australia) and acquired using Leica Application Suite Advanced Fluorescence software (LAS:AF, Leica, Germany)

Images were optimised using ImageJ and FIJI plugin package (NIH, Bethesda, Maryland, USA) and figures prepared using CorelDraw x4.

Epifluorescence imaging at 10x permitted efficient imaging of whole-brain datasets at the expense of biasing against lightly labelled or small neurons. This was particularly problematic for detection of lightly-labelled TH-immunoreactive starter neurons; confocal reimaging (20x objective, Leica TCS SP5X) of three sections containing starter neurons previously imaged and analyzed as described above, indicated that approximately a third of the C1 starter neurons detected under confocal had been identified as non-C1 under epifluorescence (19/27 vs. 13/27). This problem did not apply to detection of rabies-infected neurons, which were unambiguously labelled.

Control Experiments

SADΔG(EnvA)-mCherry was injected into the RVLM of 2 animals that had not previously received injections of HSV-hCMV-YTB, as a control for TVA/rabies glycoprotein-independent infection. No labelled neurons were observed in either animal. Thus we determined that the concentration of contaminating, unpseudotyped particles mentioned above were of an insufficient concentration to cause non-specific labelling.

In another animal HSV-GFP was co-injected into the sciatic nerve with cholera toxin B subunit (CTB) to examine whether HSV variants were capable of transducing fibres of passage (Figure 3.1A). The sciatic nerve was exposed at mid-thigh from a dorsolateral approach and isolated from surrounding connective tissue. A small incision was made through the nerve sheath and a 2 µl co-injection of HSV-hCMV-GFP (at 50 %

concentration used for spinal cord injections) and CTB (0.5 % in normal saline, List Biological Laboratories, USA) were made into the exposed nerve. The exposed area was irrigated with sterile physiological saline and the wound closed with suture clips. In another experiment a rat received bilateral microinjection of HSV-hCMV-GFP mixed with HSV-hCMV-mCherry (1:1,500 nl at 2 sites on each side of the T2 IML) to examine the proportion of double-labelled RVLM neurons (so that an estimate of the proportion of local terminals infected by retrograde HSV variants could be made (Figure 3.1B).

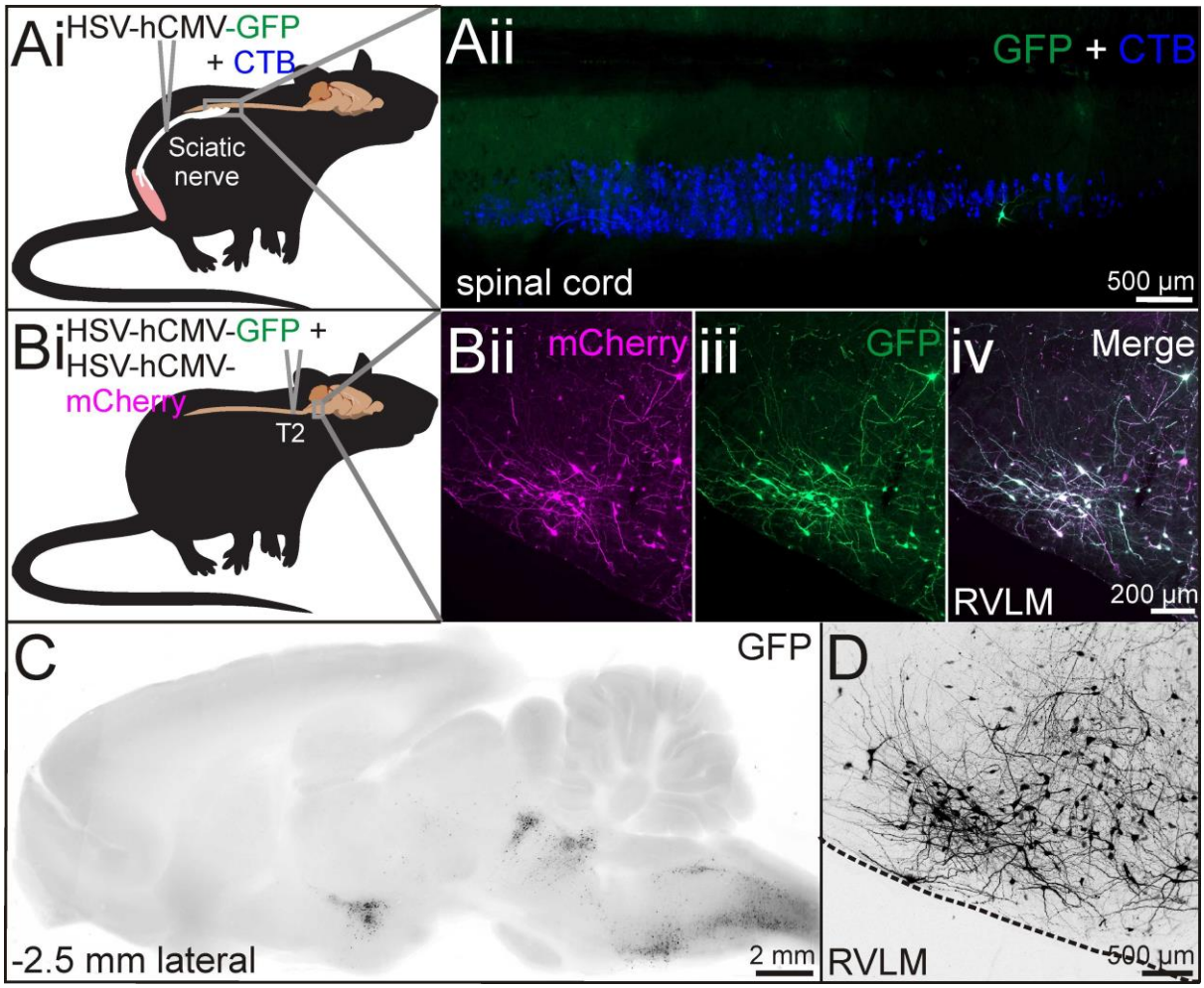

Figure 3.1: Characterization of HSV retrograde tropism. A. Co-injection of HSV-hCMV-GFP and cholera toxin subunit B (CTB) into the sciatic nerve results in extensive retrograde CTB labelling of putative α-motoneurons (Aii, horizontal section), but virtually no GFP expression, suggesting that fibres of passage are not readily transduced by HSV vectors. B. Co-injection of HSV-hCMV-GFP and HSV-hCMV-mCherry into the T2 spinal cord resulted in double-labelling of the majority of RVLM neurons (Bi-iii), indicating that the titre used is sufficient to transfect the majority of neurons that project to the injection site. C. 1 mm thick CLARITY-processed parasagittal (epifluorescence) and coronal (D, confocal maximum projection, 494 optical sections at 2 µm intervals) brain sections demonstrate extensive and robust GFP expression, 5 days after injection of HSV-hCMV-GFP into the T2 spinal segment.

Analysis

Image alignment and anchoring

Image alignment and anchoring was achieved using a beta version of the N3 Navigator system, a web-based data management tool currently under the development of the University of Oslo Neuroinformatics group, kindly provided by Prof Jan Bjaalie. An overview of the image alignment workflow is provided in Figure 3.2: in brief, microscope images of whole brain sections were contrast-optimised for differentiation of grey and white matter and uploaded to N3 in virtual tissue blocks of sequentially cut images spaced at 200 μm. Each image was aligned to an interactive 7T MRI whole brain dataset obtained from a male Sprague Dawley rat (Papp *et al.*, 2014) that allows the user to make virtual cuts through the MRI brain at any angle. This allows the user to align histological sections cut at any plane to the reference dataset, allowing compensation for deviation in cutting plane or tissue distortion. Once each image was optimally aligned to its MRI equivalent the image was considered 'anchored'; geometric vectors corresponding to the rostrocaudal level of the image origin (i.e. the left lower corner of each image), deviation from the vertical and horizontal planes, scaling and rotation were calculated by the N3 platform. With this information the position of any point in the histological image could be converted to 3-dimensional Waxholm co-ordinates using a simple algorithm. Waxholm co-ordinates presented correspond to voxel positions in the original Waxholm dataset, which are by convention presented in the xyz format lateral, rostrocaudal, dorsoventral, with a voxel resolution of 39 μm. The interested reader is directed towards CutNii, a freely downloadable explorer and custom-angle slicer for the Waxholm dataset (Csucs & Bjaalie, 2015), which is similar to the N3 tool used for image alignment (although it does not allow overlay or anchoring of histological images).

Images containing reporter-expressing neurons were manually annotated using Axiovision Zen software. Metadata containing the pixel co-ordinates of each annotated neuron were imported to Microsoft Excel. *x,y* pixel co-ordinates were transformed into *x,y,z* Waxholm co-ordinates following 'anchoring' of each microscope image into Waxholm Space.

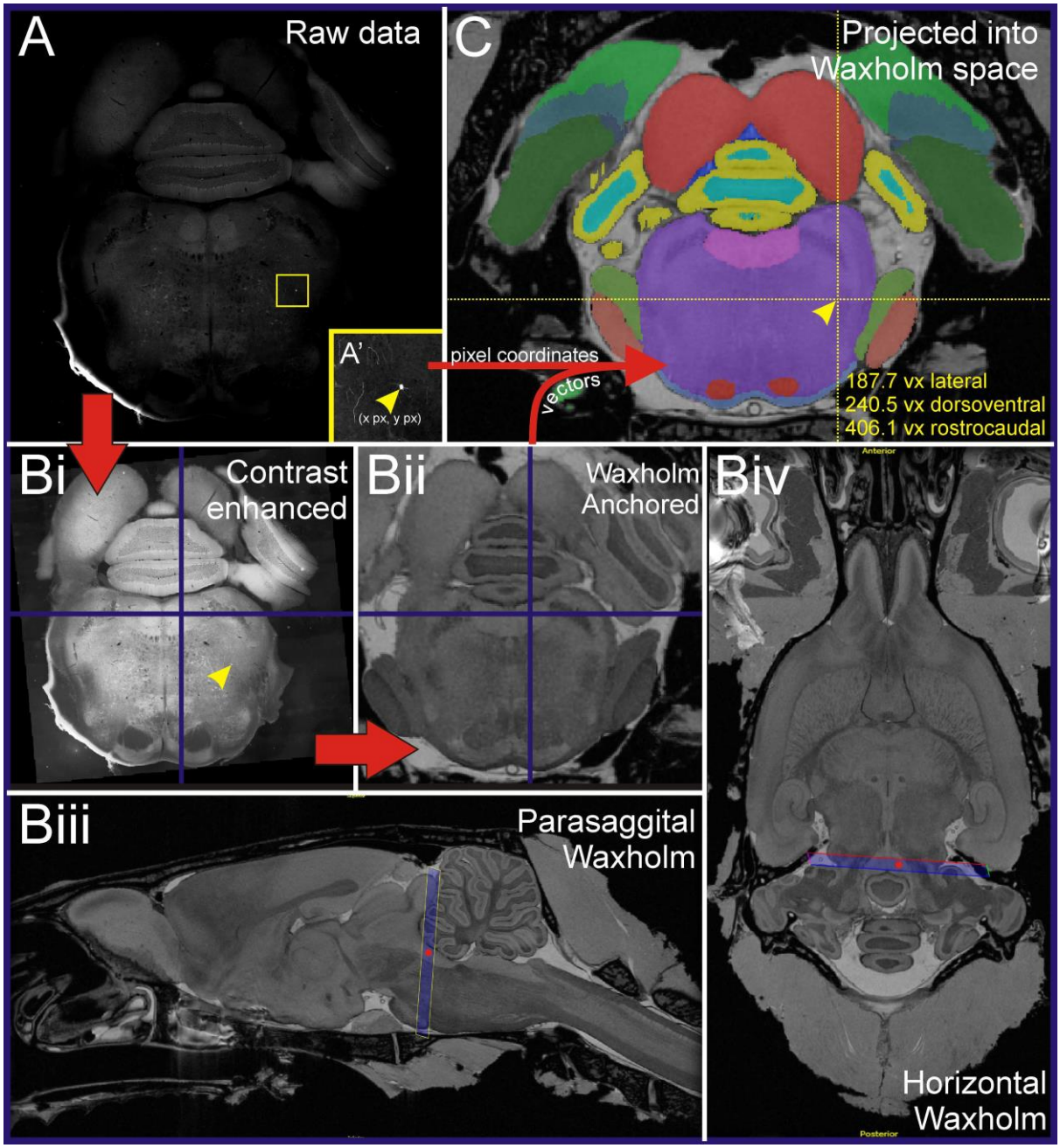

Figure 3.2: Anchoring workflow. A. Original coronal epifluorescence image showing the location of a single rabies-labelled input neuron (yellow box, inset in A'). Following manual annotation, the pixel co-ordinates of the neuron were exported to a spreadsheet and the image contrast adjusted for optimal visualisation of anatomical landmarks (Bi). The image was then uploaded to N3 and anchored to the corresponding section of the Waxholm dataset (Bii: blue crosshairs in Bi and Bii denote centre of section only) following adjustment of the cut angle of the MRI section in the dorsoventral (Biii) and lateral (Biv) planes. The blue boxes in Biii and Biv indicate the region shown in Bii; note offset in rostrocaudal levels in the left and right sides of the image in both the raw histology (Bi) and anchored virtual section (Bii). Anchoring vectors generated by N3 were then used to translate the pixel co-ordinates of annotated neurons into xyz Waxholm co-ordinates and analysed with respect to the Waxholm segmentation model (C).

Segmentation of RVLM region in Waxholm space

The current Waxholm segmentation model does not differentiate brainstem subnuclei. To define the anatomical boundaries of the RVLM in Waxholm space, we used the locations of RVLM sympathetic premotor neurons identified in a previous study that were TH-positive and retrogradely transduced by HSV-hCMV-GFP or -mCherry variants injected at the T2 or T7 vertebral levels (Figure 3.3A). Data were generated by counting labelled neurons bilaterally (except in one case where labelling was restricted to one side of the brainstem) in sections separated by 200 μm intervals in six animals. However, the lateral co-ordinates of all neurons are represented as being on *both* sides of the brainstem for RVLM segmentation (i.e. each neuron was 'mirrored' so that it was simultaneously represented on both left and right sides of the brainstem to avoid asymmetry between left and right sided segmentation models). Two-dimensional contour maps indicating the density of labelling were then generated for each dorsoventral level, using the Plotly visualization tool (https://plot.ly, 10 voxel resolution, see Figure 3.3B'). Contours enclosing pixels that contained >2 neurons/10 pixel radius in the horizontal plane were converted to an image stack and imported into a volumetric model of the Waxholm rat brain using the Imaris software platform (Imaris 8.1, Bitplane AG, Switzerland, Figure 3.3E-G).

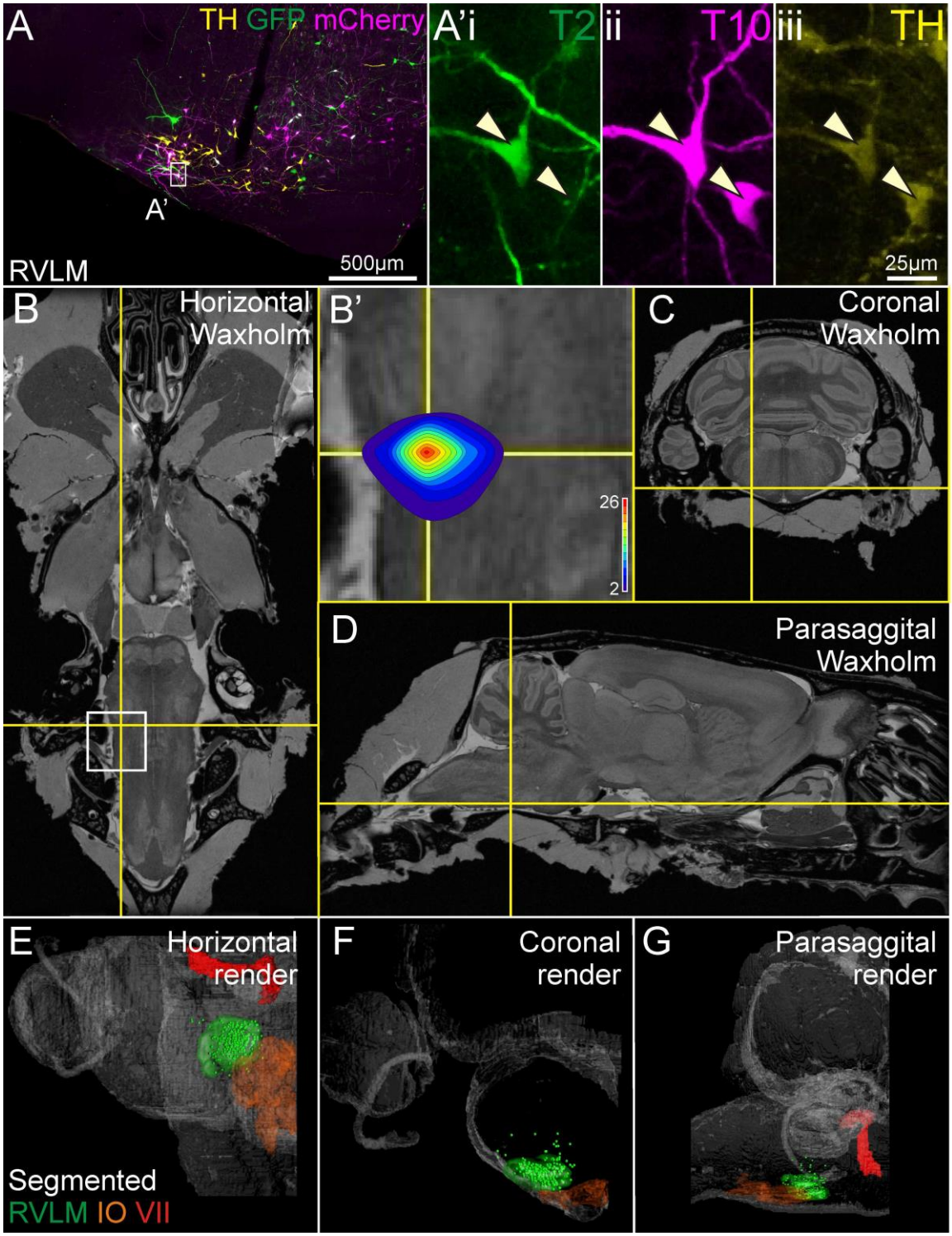

Figure 3.3 Segmentation of the RVLM in Waxholm space. The locations of TH-positive neurons that were retrogradely transduced by HSV-reporter driving vectors from the T2 and/or T10 spinal segments (arrowheads in A'i-iii) were used to denote the boundaries of the RVLM. Waxholm co-ordinates of 273 TH-positive bulbospinal neurons were plotted as 2d heatmaps in the horizontal plane (B: the epicentre of the TH-positive bulbospinal population is indicated by crosshairs in the corresponding horizontal (B), coronal (C) and parasagittal (D) sections through the Waxholm MRI dataset. Heatmap is overdrawn on inset shown in B'. Co-ordinates of individual TH-positive bulbospinal neurons (green spheres, E-G) and the serial heatmaps that enclosed 86%of TH-positive bulbospinal neurons (green surface, E-G) were imported to a 3d-rendered model of the Waxholm brain. Regional landmarks in E-G are the facial nerve (red) and inferior olive (orange).

Connectome map construction

The Waxholm Sprague Dawley brain has thus far been segmented into approximately 70 brain regions (Papp *et al.*, 2014). Having employed the N3 tool to accurately transform the locations of labelled neurons into three dimensional Waxholm coordinates, we then employed the Waxholm segmentation model (Figure 3.2C) to quantify the anatomical distribution of labelled neurons in a semi-automated manner using the Imaris volumetric imaging platform. To do this the most up-to-date segmentation model (Waxholm v2) was downloaded from the International Neuroinformatics Coordinating Facility Software Center (Papp *et al.*, 2015) and imported into Imaris following conversion to the Biorad format in ImageJ, resulting in a surface-rendered model that incorporates all of the regions demarcated in Waxholm space.

The Waxholm coordinates of Input, non-C1 seed, and C1 seed neurons were then imported from Microsoft Excel into Imaris using an open-source Python script (Guyer, 2013), resulting in a 3d model of the Waxholm brain populated with points corresponding to the neurons identified in our histological sections. Another script was then used to automatically quantify the number of input neurons that lay within each segmented region (Bitplane Development, 2013).

Results

Characterizing hCMV promotor driven HSV vectors for retrograde neuronal transduction

Reporter expression was observable in the medulla as early as 24 h after HSV injection into the spinal cord and robust at day 5 (Figure 3.1C & D). The morphological integrity of HSV infected neurons declined rapidly beyond day 7, neurons with shrunken, spherical somata and blebbed processes were common beyond day 8 post-infection.

Defining the specificity of HSV-mediated retrograde transduction was critical to the interpretation of data acquired using these vectors. To examine if transduction was possible following uptake by fibres of passage we co-injected HSV-hCMV-GFP with CTB directly into the sciatic nerve. Inspection of the lumbar spinal cord 4 days later revealed many CTB+ neurons in the ventral horn, presumably representing retrogradely labelled motoneurons. However, only one GFP+ neuron was identified (Figure 3.1A), suggesting that axons *en passage* are essentially resistant to HSV infection. Thus we propose that neurons retrogradely transduced by HSV probably represent neurons that form synaptic terminals at the site of vector injection rather than neurons with axons that traverse the injection site However this may be representative of a more inert axonal environment in the periphery provided by Schwann cells and may not appropriately reflect what would occur during an injection into the CNS.

To determine whether the number of cells retrogradely labelled by the vector truly reflected the total number of cells that projected to the injection site we co-injected a HSV vector expressing GFP and another expressing mCherry into the T2 IML (at half the titre used for the concurrent retrograde tracing in this study). Examination of the RVLM revealed that the vast majority of retrogradely transduced neurons expressed both reporters (Figure 3.1B). We infer that vector concentration within the injection site was sufficient to saturate the majority of available terminals.

Anatomical segmentation of the RVLM premotor area

Despite many years of intense study, to date no objective structural definition of the RVLM region has been made. A key consideration for the interpretation of the current study (or indeed any study in which reagents such as viral vectors, tracers or drugs are

deployed at RVLM sympathetic premotor neurons) is validation that neurons in the appropriate anatomical structure are being targeted. We therefore generated a quantitative map of the distribution of bulbospinal catecholaminergic neurons, which are considered putative sympathetic premotor neurons.

273 bulbospinal TH-immunoreactive neurons were identified in the ventrolateral medullae of six rats previously injected with reporter-driving HSV vectors in the T2 or T10 spinal cord (Figure 3.3). The geometric epicenter of the region containing sympathetic premotor neurons was located at Waxholm coordinates 198 lateral, 313 rostrocaudal, 182 dorsoventral, corresponding to a position 1.78 mm lateral to the midline, 117 μm rostral to the caudal pole of the facial nucleus, and 339 μm dorsal to the ventral surface of the medulla immediately beneath the epicenter (Figure 3.3B). As indicated by the 5th and 95th percentiles of this dataset, RVLM sympathetic premotor neurons spanned Waxholm co-ordinates 185 - 210 lateral (2.28 – 1.31 mm lateral to midline), 301 – 324 rostrocaudal (351 μm caudal to 546 μm rostral to caudal pole of the facial nucleus) and 178 – 193 dorsoventral (117 – 702 μm from the ventral surface of the brainstem). The RVLM segmented model generated from these co-ordinates is density-encoded, and therefore differs slightly from the geometric boundaries indicated above. Our segmentation encloses a dorsoventrally flattened ovoid in which the long axis runs medial in more rostral sections and spans Waxholm coordinates 176 – 218 lateral (2.6 – 1 mm lateral to midline), 287 - 327 rostrocaudal (900 μm caudal to 663 μm rostral to caudal pole of the facial nucleus) and 174 – 198 dorsoventral (39 μm ventral – 897 μm from the ventral surface of the brainstem). This region contained 86 % of TH-positive bulbospinal neurons (n = 236). We noted that this region also included 621 non-C1 bulbospinal neurons; therefore 28 % of bulbospinal RVLM neurons were identified as TH-positive.

Monosynaptic tracing from RVLM sympathetic pre-motor neurons

We plotted brain-wide sources of monosynaptic input to RVLM sympathetic premotor neurons in 3 animals (selected from an experimental cohort of 15) that exhibited the greatest seed to input ratios and in which seed neurons were predominantly confined to the RVLM. 44 (23 - 67) seed neurons were identified per animal (132 total) counting every fourth section, of which 41 % (30 - 45 %) were TH-positive. 79 % of seed neurons (104/132) were identified as residing within the RVLM using the segmentation model

described above, (Figure 3.4 and supplementary files 3.1) and 75 % (99/132) using traditional RVLM boundaries (Goodchild & Moon, 2009).

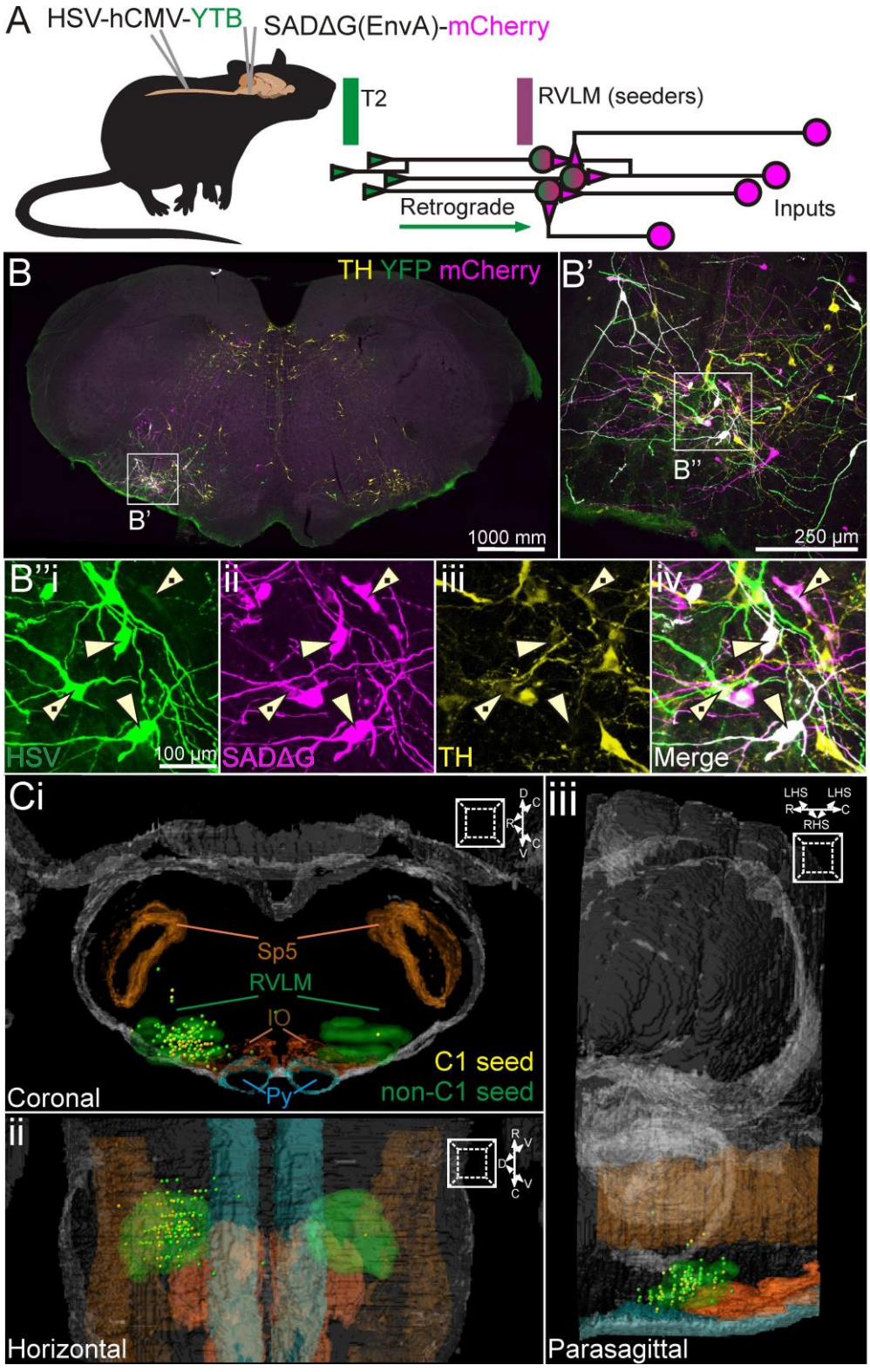

Figure 3.4 Experimental strategy and seed neuron characterisation. A: HSV-hCMV-YTB is injected at the T2 IML, retrogradely transducing spinally projecting neurons to express rabies glycoprotein, TVA and YFP. SADΔG(EnvA)-mCherry is subsequently injected into the RVLM, exclusively infecting neurons that express TVA, and seeding transynaptic infection of monosynaptically connected input neurons . Seed neurons are distinguished by the expression of both YFP and mCherry. B. Coronal brainstem section at the level of the RVLM processed for immunoreactivity to tyrosine-hydroxylase (TH) and YFP. Insets in B' and B'' show detail of confocal image from the same section illustrating examples of C1 (dotted arrowheads) and non- C1 (solid arrowheads) seed neurons. C. C1 (yellow spheres) and non-C1 (green spheres) seed neurons from three experiments plotted in Waxholm space shown from coronal (Ci), horizontal (Cii) and parasagittal (Ciii) perspectives. Anatomical landmarks are Waxholm-segmented boundaries of the inferior olive (IO), spinal trigeminal nucleus (Sp5), RVLM and pyramidal tract (Py).

340 (range 239 - 560) rabies-labelled input neurons were identified per animal (1019 total), corresponding to an average input: seed ratio of 8:1 (4:1 – 13:1)-. Trans-synaptically labelled neurons were encountered from the thoracic spinal cord (although only spinal cord neurons that lay at the medullary-cervical junction are quantified) to the hypothalamus at the level of the optic chiasm, but the vast majority of neurons were identified within the brainstem; analysis of the distance from each rabies-labelled neuron to the epicentre of the RVLM produced a skewed distribution with a median distance of 65 voxels (2533 μm), with the 95 % of neurons lying within 160 voxels (6244 μm) of the RVLM (Figure 3.5B). Using the Waxholm segmentation model to quantify the distribution of input neurons throughout the brain we found that the brainstem, as defined by the Waxholm segments *Pyramidal tract, Medulla, Periventricular grey, Inferior olive, Spinal trigeminal nucleus & tract*, and our newly generated *RVLM* segmentation, accounted for 93 % of input neurons (see Table 3.2). 37 input neurons were not identified by Imaris as lying within any defined brain region are therefore omitted from quantitative analysis; some of these neurons lay on the brain surface or junctions between different segments.

Within the brainstem, input neurons were concentrated in the immediate vicinity and caudal to the seed population, and extended in long bilateral columns that engrossed the lateral reticular formation, extending from the ventral surface to an apex at the dorsal midline (Figure 3.5A',C and 3.6B-E). Of the Waxholm segments currently defined, the RVLM region had the highest density of any region surveyed by a factor of about 5, 94 % of which were ipsilateral to the injection site (Figure 3.5F and 3.6D,E). The majority of RVLM input neurons were non-C1, although examples of catecholaminergic rabies-infected neurons that stained negative for YFP, and are therefore not considered seed neurons, were encountered in all experiments (including those that did not meet quality control criteria for full quantification, Figure 3.7D&E).

The incomplete segmentation of brainstem subnuclei in the current version of the Waxholm atlas misrepresents the true density of inputs within the medulla; inputs were not evenly distributed throughout the region demarcated as medulla in the Waxholm brain, and our subjective assessment is that input density in the regions of the brainstem corresponding to the CVLM/pre-Bötzinger Complex and nucleus prepositus were at least equivalent to that seen in the RVLM; this observation is supported by the heat map presented in Figure 3.5C, in which a dorsal hot spot and extended ventral column are clearly visible.

Inputs constituting the caudal aspect of the column overlaid a region located immediately dorsal of the ventral surface of the medulla spanning the loose, subcompact and caudal most compact formations of the nAmb, corresponding to the CVLM, a small portion of which expressed mRNA for glutamic acid decarboxylase 67 (GAD67), a putative phenotype marker for inhibitory neurons (Figure 3.7E). High input density was also observed in regions corresponding to components of the ventral respiratory column (Figure 3.6B-D), including the Pre-Bötzinger complex and Bötzinger, that form a coextensive rostrocaudal column immediately ventral of the compact formation of the nAmb, but these neurons did not appear to express neurochemical markers that define respiratory neurons in either region; a few Pre-Bötzinger complex neurons were immunoreactive for neurokinin receptor-1 (NK1R), but the vast majority were not (Figure 3.7 A &B), and no Bötzinger neurons expressed mRNA for glycine transporter 2 (GLYT2, Figure 7F). A dense column of highly arborized input neurons with small somata were consistently observed at the ventrolateral boundary of the nucleus prepositus (Figure 3.6E”), and neurons were also observed in the nucleus of the solitary tract (NTS) (Figure 3.6A’), A1 adrenergic cell group region (although most were not TH immunoreactive, Figure 3.6A”) and the midline raphe (Figure 3.6C’’).

Rostral to the RVLM, input neurons were predominantly observed in the ipsilateral hemisphere of the brainstem, occupying a region with boundaries that extended along the medial circumference of the facial nucleus dorsaly to the nucleus prepositus. >500 μm rostral to the seed population, input neurons became sparse and were mostly observed within the ventral medial medulla immediately dorsal to the pyramidal tract. With the exception of the paraventricular nucleus of the hypothalamus (PVN), we rarely observed more than a single input neuron per section rostral to the facial genu. Inputs

arising from the forebrain and midbrain, although sparse, reproducibly included the superior colliculus, periaqueducutal grey, and hypothalamus. The most prominent and rostral source of input we noted was located within the paraventricular nucleus of the hypothalamus (PVN). These inputs were few but consistent across all animals examined (including those not quantified) and occasionally immunoreactive for vasopressin (Figure 3.8A').

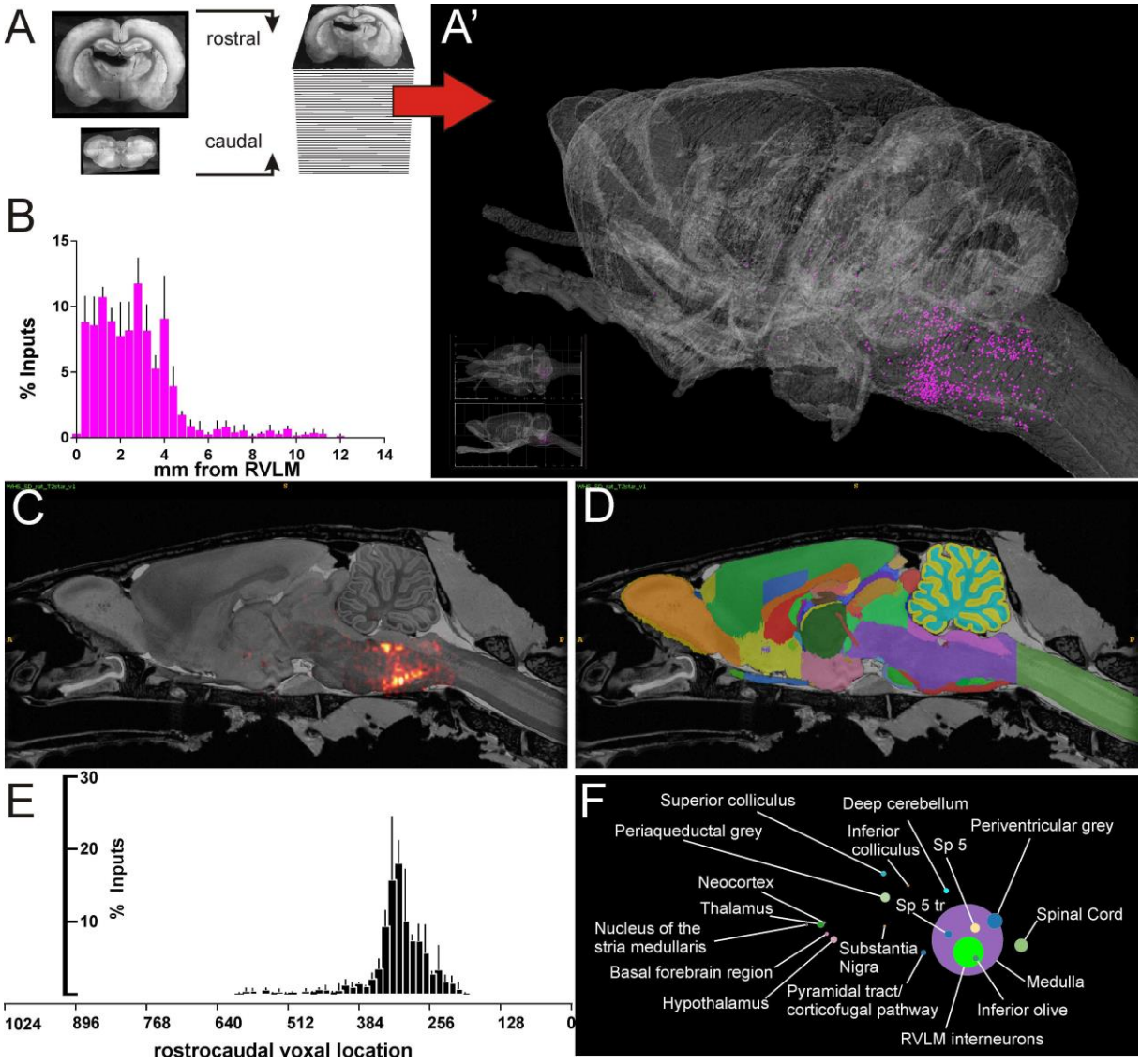

Figure 3.5 Brain wide distribution of input neurons. A. Workflow for input map construction. Neurons identified in epifluorescence images were annotated and anchored in Waxholm space and their 3d co-ordinates imported to a 3d model of the Waxholm rat brain (A'). B. As-the-crow-flies distances of input neurons relative to the geometric center of the RVLM. C. Flattened input density map overlaid on a parasagittal cross-section of the Waxholm MRI illustrating the uneven distribution of inputs throughout the brain and the presence of discrete foci in the ventral and dorsal medulla. D. Reference section at the same level as C illustrating regions demarcated in the current Waxholm segmentation model, including the RVLM segment (bright green region immediately dorsal to the inferior olive) generated in the current study. E. Histogram showing the rostrocaudal distribution of inputs in Waxholm space (same scale as Panel C; for reference the caudal pole of the facial nucleus lies at 310 voxels). F. Input distribution per Waxholm-defined segment, number of neurons represented by sphere size.

Table 3.2 RVLM input neurons sorted according to Waxholm-defined region

Brain Region/*Subnuclei*	*# neurons (mean ± SEM)*	*Volume of region (kvoxels)*	*% inputs (total)*	*Input Density (neurons/Mvoxel)*
Forebrain	4 ± 2		**1.2**	
Neocortex	0	10500	0.1	0.1
Nucleus of the stria medullaris	0	1.6	0.1	623.4
Thalamus	0	1390	0.8	5.8
Basal forebrain region	2 ± 1	1250	0.2	1.6
Midbrain	**9 ± 5**		**2.5**	
Hypothalamus	2 ± 1	388	0.7	18.0
Periaqueductal grey	4 ± 3	269	1.3	48.3
Superior colliculus	2 ± 1	390	0.4	10.3
Inferior colliculus	0	451	0.1	2.2
Substantia Nigra	0	114	0.1	8.8
Cerebellum	***1* ± 1**		***0.4***	
Deep cerebellum	*1* ± 1	2730	0.4	1.5
Brainstem	***323* ± 187**		***93.4***	
Pyramidal tract/corticofugal pathway	1 ± .4	461	0.4	8.7
Periventricular grey	12 ± 7	226	3.5	159.3
Inferior olive	1 ± 1	33.1	0.6	181.3
Spinal trigeminal nucleus	4 ± 2	252	1.3	51.6
Spinal trigeminal tract	3 ± 2	1560	0.9	5.8
RVLM	46 ± 27	46.6	13.5	3004.3
Medulla	243 ± 140	3390	73.4	224.5
Spinal Cord	**8 ± 5**	**1590**	**2.5**	**16.352**

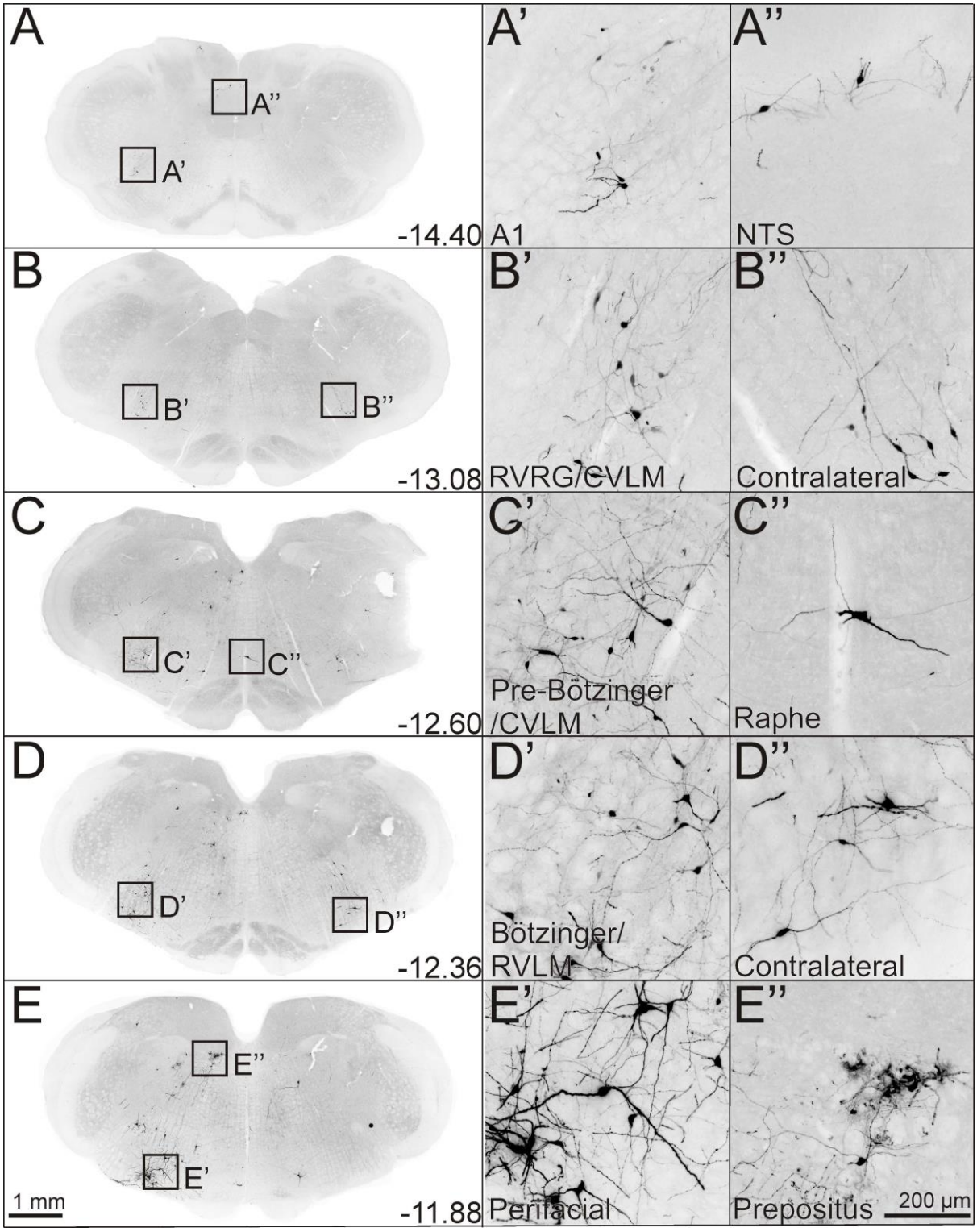

Figure 3.6 Medullary inputs to RVLM sympathetic premotor neurons. Epifluorescence micrographs of the coronal medulla and high power insets (inverted monochrome images). Inputs were most concentrated locally within the ipsilateral (D') and contralateral RVLM (D''), perifacial zone (E'), and within a dorsal population overlaying the nucleus prepositus (E''). A dense band of inputs were distributed bilaterally throughout the nuclei of the ventral respiratory column (B' & B'': rostral ventral respiratory group (RVRG: C': Pre-Bötzinger complex, D' & D'': Bötzinger complex) and the adjacent caudal ventrolateral medulla (CVLM: B', B'', C'). Inputs were also consistently identified in the A1 cell group (A'), nucleus of the solitary tract (NTS: A'') and raphe nuclei (C''). Numbers in lower right corners of low-power images denote rostrocaudal level with respect to Bregma.

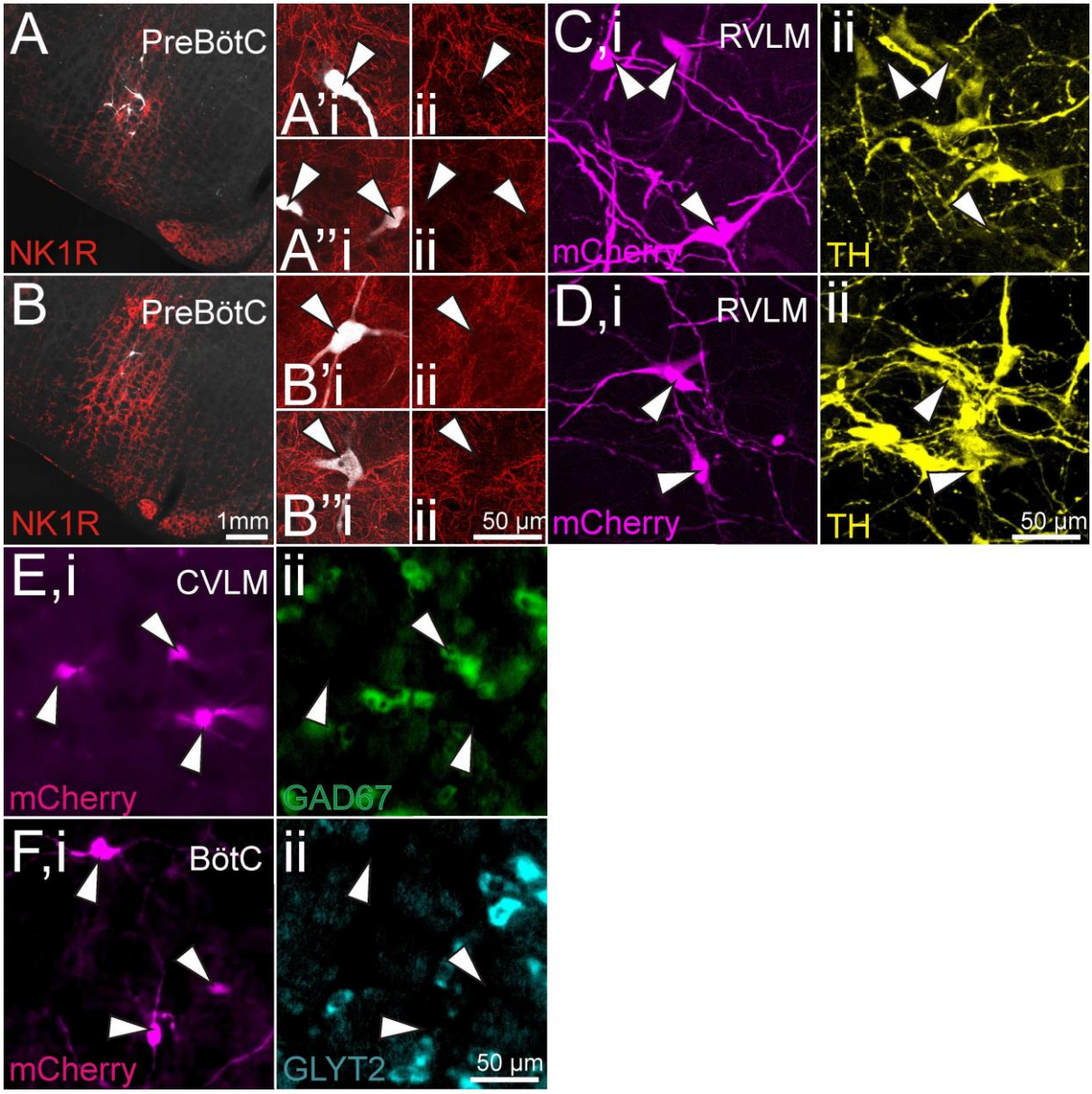

Figure 3.7: Neurochemical phenotypes of medullary input neurons. A & B (and confocal insets). Inputs arising in the pre-Bötzinger complex were not neurokinin-1 receptor immunoreactive (NK1R). Local RVLM inputs were of both non-C1 (C) and C1 neurons (D). E: Input neurons both positive and negative for glutamic acid decarboxylase 67 (GAD67) mRNA were observed within the CVLM (epifluorescence micrographs). F: Input neurons in the Bötzinger complex did not stain for glycine transporter 2 (GLYT2) mRNA (epifluorescence micrographs).

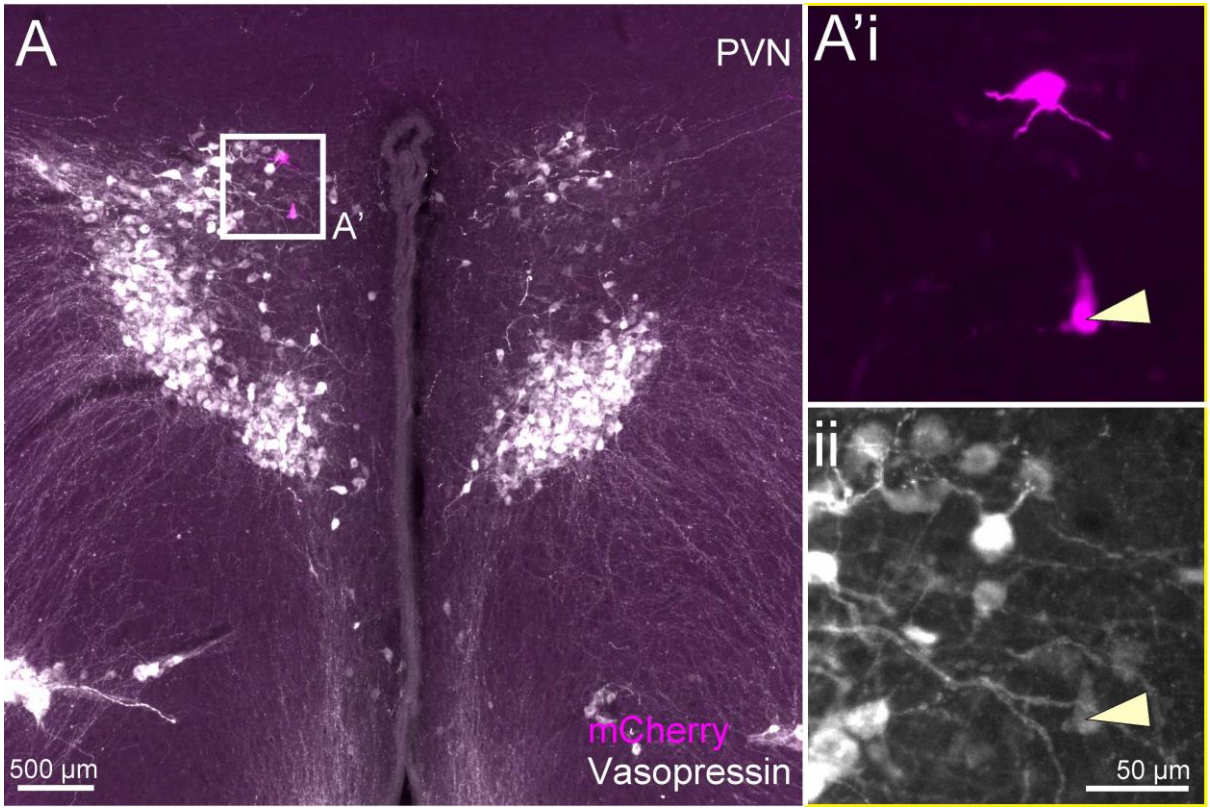

Figure 3.8: Inputs from the paraventricular nucleus of the hypothalamus were sparse but reproducible and included vasopressin-immunoreactive neurons (arrow). A. Low power merged epifluorescent photomicrograph of the paraventricular nucleus of the hypothalamus with vasopressin immunoreactivity (white) and rabies-labelled input neurons (magenta). A'. Magnified inset of boxed region in individual channels.

Discussion

RVLM sympathetic pre-motor neurons are a regulatory axis by which convergent input regarding physiological and psychological state are integrated to drive immediate responses in the periphery via sympathetic effectors (Guyenet, 2006), along with tonic inputs that ostensibly determine the spontaneous discharge of this population and hence set baseline vasomotor tone (Morrison *et al.*, 1988; Lipski *et al.*, 1996; Ito & Sved, 1997). The network of neurons that govern the basal and state-dependent activity of the RVLM sympathetic premotor population arises from a diverse range of brain regions, many of which are associated with the relay of sensory input. However many aspects of this input network remained undefined. Until the recent development of genetic tools that permit targeted and restricted transynaptic tracing (Wickersham *et al.*, 2007a), we have lacked the technical capacity to unambiguously trace direct inputs to anatomically or phenotypically defined populations. In this study we describe the comprehensive network of neurons that provide direct synaptic input to RVLM sympathetic pre-motor neurons innervating the T2 spinal segment in the rat.

Overall, our observations indicate that sources of input to putative RVLM sympathetic premotor neurons arise predominantly within the medulla, from nuclei associated with afferent sensory integration and the regulation of autonomic and respiratory drive. At face value these findings satisfy many predictions of the current network model. However, the sparsity (PAG, PVN) or complete absence (central nucleus of the amygdala) of inputs from midbrain and forebrain nuclei previously identified using traditional neuroanatomical tracing techniques (and which functional data implicate in the control of sympathetic nerve activity) suggest that inputs from numerous local brainstem structures probably play a more critical role in determining the activity of bulbospinal RVLM neurons than inputs from more distant regions.

The discussion of this dataset will focus on the functional implications of prominent inputs we identified, the consonance and dissonance of these findings with the current network model of input to the RVLM, with consideration of the limitations inherent to present and past studies. Lastly, we will contemplate the most appropriate platforms for the analysis and dissemination of large anatomical datasets akin to those described in

the current study, a topic that is emerging as a priority to allow comparative analysis between independently acquired anatomical datasets.

Most synaptic drive to bulbospinal RVLM neurons originates in the brainstem

Previous functional and anatomical studies demonstrate forebrain and midbrain nuclei that regulate sympathetic output via a projection to the RVLM (Dampney, 1994b). Prominent among those described are extensively described inputs from the CeA (Saha, 2005), PVN (Stocker *et al.*, 2008; Carrive, 2013) and PAG (Carrive, 1993) that facilitate the regulation of blood pressure to psychogenic stressors and blood osmolality (in the case of the PVN). Although previous transectional studies have demonstrated that supramedullary inputs are not critical for the generation of SNA (Alexander, 1946; Paton, 1996), we expected to observe major sources of input from these rostral brain regions. However inputs from the CeA were absent and we noted only a handful of neurons scattered throughout the PAG. The PVN was the most rostral region of the brain we observed inputs neurons, they were consistent but sparse, approximately 4 neurons per animal.

When accounting for these differences, we must first appreciate the specificity of the tracing stratagem employed in the present study. We selectively targeted input tracing to a population of RVLM neurons that discretely innervated the IML and adjacent nuclei at the T2 spinal segment, an output that provides sympathetic innervation of the heart and thoracic vasculature as well as other sympathetic effector sites including the adrenal gland and kidney (Strack *et al.*, 1988). The average number of RVLM neurons from which trans-synaptic tracing initiated was only 35 per animal, while the estimated size of the of the hemispheric bulbospinal RVLM population is estimated to be >250 neurons (estimated from the RVLM neurons that supply input to the adrenal gland described in Strack *et al.* (1989b). Sympathetic nerves emerging from different spinal segments have overlapping but distinct functional profiles (for example, differential sensitivity to baroreceptive, nociceptive or metabolic stimuli (Beacham & Perl, 1964; Sato, 1973; Weaver *et al.*, 1984; Dorward *et al.*, 1987; Morrison, 2001; McMullan *et al.*, 2008; Burke *et al.*, 2011), suggestive of highly differentiated organization of the circuits that control the premotor neurons which give rise to these outputs. Secondly, differences in the selectivity of the tracers used to label RVLM-projecting neurons should be considered.

Traditional retrograde tracers (e.g. Bowman *et al.*, 2013) label neurons irrespective of whether they form synapses in the region of the tracer injection or simply pass through *en route* and cannot be used to identify local interneurons. In contrast, the g-deleted rabies used in the current study only labels neurons that form monosynaptic connections with the genetically modified seed population, including local interneurons that are inaccessible to traditional tracers, although only a fraction (2 – 4%) of pre-synaptic neurons are thought to be trans-synaptically infected by SADΔG (Callaway & Luo, 2015). A comprehensive study conducted by our laboratory identified retrogradely labelled neurons in cortical nuclei and the forebrain, including the CeA, PAG and PVN, following microinjection of CTB in the RVLM (Bowman *et al.*, 2013). These areas were were sparsely labelled or absent in the present study. Given the region with the highest density of input neurons identified in the present study was the RVLM, it seems plausible that putative inputs previously identified using traditional tracers microinjected to the RVLM may in fact represent polysynaptic inputs that project to local monosynaptically connected interneurons. These interneurons may well constitute a component of the RVLM population with ascending projections to the midbrain and hypothalamus which includes C1 neurons (Sawchenko & Swanson, 1982; Tucker *et al.*, 1987; Haselton & Guyenet, 1990; Petrov *et al.*, 1993; Verberne *et al.*, 1999b; Card *et al.*, 2006b)). Thus, this speculative arrangement would constitute a feedback loop that provides reciprocal gain control for higher order sources of drive to the RVLM.

Although an expected observation, this study is among the first to document the existence of this population, thus is difficult to speculate upon the functional role served by this hypothetical, gated arrangement or the function role of RVLM interneurons in general. Functional evidence suggests that tonic drive to the RVLM sympathetic pre-motor population is supported by local sources (Barman & Gebber, 1989; Dampney *et al.*, 2003), of which these neurons may be representative. However, the capacity to selectively manipulate these neurons (through genetic means or otherwise), and thus delineate their true functional role, is presently lacking.

The most technically comparable approach to the current study is a limited but nonetheless valuable investigation by Stornetta *et al.* (2015) who used a similar approach to ours to trace inputs to C1 RVLM neurons by restricting entry of rabies to spinally or rostrally projecting neurons using a conditional TH-cre transgenic mouse

and limiting expression of TVA/rabies G with a cre-dependent AAV. The level of transynapsis reported in that study was too low to use for detailed quantification of the distribution of inputs (they saw 1.7 input neurons per seed neuron, less than a quarter of the level of trans-synapsis reported here). However, it is worth noting that their results were qualitatively similar to those reported here, with the majority of inputs arising from the RVLM region. Also worthy of consideration is a pseudorabies -based approach employed by (Card *et al.*, 2011), which mapped retrograde reporter expression in neurons that formed polysynaptic input to RVLM C1 neurons connected to the kidney. As the trans-synaptic expression of reporter labelling observed using this strategy was not monosynaptically restricted, the distribution of inputs at different time points are interpreted as corresponding to the number of synapses crossed. In common with the current study, the distribution of neurons described at early time points, which may be equivalent to one order of synaptic transport, was similar to those of the present study i.e. concentrated to adjacent medullary regions and sparsely labelled within the PVN.

Technical considerations

So, although our findings are qualitatively consistent with those described by Stornetta *et al.* (2015) and (Card *et al.*, 2011), we must also consider vector-specific biases that could contribute to the distribution of labelling we observed. An obvious explanation for the disparate predominance of inputs from within the medulla compared to midbrain centres historically associated with the behaviour of RVLM sympathetic premotor neurons may be the greater distances required for viral transport (to the forebrain and midbrain). However, other studies that employ SADΔG report input labelling across comparable distances (Schwarz *et al.*, 2015).

The restrictions imposed by the deleterious effects of HSV infection beyond day 7 mean that we had to terminate experiments 6 days after rabies infection. Wertz *et al.* (2015) report a 2-fold increase in the number of input neurons observable between days 6 and 10, suggesting that a longer period of rabies incubation would probably improve the yield of trans-synaptically labelled neurons. However, there is no evidence that an increase in the incubation period disproportionately drives infection in more distant neurons (Callaway & Luo, 2015). We frequently observed labelling in the thoracic spinal cord under the current tracing scheme (not shown) and labelling of neurons in the

cortex and amygdala (and among other rostrally equivalent structures) in the experiments where unpseudotyped SADΔG was injected into the RVLM (not included in thesis). Although rabies spread is proportional to synaptic strength (Ugolini, 2008), it does not reflect levels of synaptic activity *per se* (spread is unaffected by incubation of cultured neurons in tetrodotoxin or potassium chloride, which prevent and drive depolarisation respecitvely: Brennand *et al.*, 2011). We therefore assume that the inputs detected in the current study reflect the relative density of synaptic inputs received by RVLM sympathetic premotor neurons, but not necessarily the functional significance of those inputs.

Nonetheless, we must consider the possibility that transport of the virus may be biased towards certain types of input neurons. Callaway, who pioneered the application of G-deleted rabies as a tracer, has stated that "*If rabies does not label all of the inputs to each starter cell, then it naturally follows that the probability of labeling is likely to be different for different input cells*." (Callaway & Luo, 2015) The number of input neurons we observed per seed neuron could not feasibly represent the total number of inputs one would expect this population to receive (although this is a difficult number to estimate: previous studies examining the synaptology of C1 neurons describe approximately 40 synaptic inputs to each neuron that originated from RVLM catecholaminergic neurons (Agassandian *et al.*, 2012). Given we identified only a few C1 input neurons *per experiment*, it is clear that trans-synaptic spread is limited to only a tiny fraction of pre-synaptic partners). There is therefore plenty of scope for variables such as the density and subcellular location of synaptic contacts made by a particular input on seed neurons, or the differential expression of intrinsic binding partners for the rabies glycoprotein (which currently remain to be defined: Callaway & Luo, 2015) to influence the outcome of this kind of study.

Overall, the factor that seems to have the greatest effect on rabies tracing efficiency appears to be the level of available rabies G protein in the seeder population. Tracing approaches that use helper vectors to drive expression of TVA and rabies-G, in particular those with a smaller cassette size like AAVs often report substantial seeder population sizes but a poor input ratio. Approaches that employ a multiple, helper vector system to drive the expression of TVA and rabies G separately (Schwarz et al., 2015) or a transgenic animal e.g. the Rosa26Lox-stop-Lox HTB mouse (Li *et al.*, 2013),

seem to yield the highest rates of transynaptic labelling. Newly developed variants of the g-deleted rabies system, report to have improved transynaptic labelling efficiency by 20 fold through codon optimisation of the rabies g protein (Kim et al., 2016) and the generation of new mutant rabies strains (Reardon et al., 2016)

Functional implications

Inputs from the rostral ventrolateral medulla (RVLM) and the caudal ventrolateral medulla (CVLM)

Tonic synaptic drive to sympathetic premotor neurons is a critical determinate of basal SNA, however clarifying the sources from which these inputs arise is a difficult task. Past efforts indicate that tonic inhibitory drive to RVLM sympathetic pre-motor neurons arises from the CVLM (Ito & Sved, 1997), caudal pressor area (CPA) (Campos & McAllen, 1999) and the caudal region of the contralateral and ipsilateral RVLM (McMullan & Pilowsky, 2012; Turner *et al.*, 2013). All of these hypotheses were supported in the current study: we observed inputs arising bilaterally from the caudal aspect of the RVLM and entire CVLM and from neurons at the most caudal aspects of the medulla in the region corresponding to the CPA. We suspect that a subset of these neurons constitute the population responsible for tonic control of RVLM sympathetic premotor neurons, particularly CVLM neurons that relay baroreceptor drive to the RVLM. CVLM inputs overlaid a region described to contain neurons that project to the RVLM and express c-fos in response to baroreceptor loading (Minson *et al.*, 1997; Chan & Sawchenko, 1998; Schreihofer & Guyenet, 2002) and some monosynaptically connected CVLM neurons were positively identified as containing GAD67 mRNA.

Inputs arising from the rostral aspects of the RVLM were largely restricted to the ipsilateral hemisphere and were mostly non-C1 neurons, whereas input from the caudal RVLM were a mix of C1 and non-C1 neurons. Insitu staining for GAD67 mRNA was not performed on RVLM sections as their availability was exhausted by IHC staining for alternative phenotypes (data not shown). The functional roles of local RVLM inputs has remained a tantalising but inaccessible topic for many years because of the difficulty inherent in selectively manipulating their behaviour, and thus the functional role of these inputs is currently unknown. One avenue for future work, beyond the scope of the

current thesis, is to examine the neurochemical phenotype of these neurons in more detail for clues to the consequences of their activation.

Inputs from the ventral respiratory column (VRC)

Respiratory drive has a profound influence on sympathetic outflow: The activity of many RVLM sympathetic pre-motor neurons is modulated by the respiratory cycle, typically with a depression of firing during the inspiratory period with a post-inspiratory excitation (McAllen, 1987; Haselton & Guyenet, 1989; Miyawaki *et al.*, 1995; Mandel & Schreihofer, 2006; Moraes *et al.*, 2013) that is independent of afferent vagal input from lung stretch receptors and thought to reflect direct input from central respiratory centres. Unsurprisingly, rhythmic respiratory modulation is present in SPN (Gilbey *et al.*, 1986) and sympathetic nerves (Adrian *et al.*, 1932; Habler *et al.*, 1994; Gilbey, 2007; Simms *et al.*, 2009).

In the current study we observed robust input from the ventral respiratory column, throughout the regions immediately ventral to the nucleus ambiguus corresponding to the rostral ventral respiratory group (RVRG), pre-Bötzinger Complex and Bötzinger region. These nuclei constitute the central respiratory pattern generator, which drives and co-ordinates respiratory rhythm generation and phase transition (Smith *et al.*, 2009; Smith *et al.*, 2013).

Glutamatergic pre-Bötzinger Complex neurons are active in the inspiratory phase of breathing and are thought to generate inspiratory drive (Smith *et al.*, 1991), and many express NK1R (Gray *et al.*, 1999; Guyenet & Wang, 2001). Consistent with the inspiratory-depression characteristic of respiratory-sympathetic coupling, few NK1R-positive input neurons were seen in the pre-Bötzinger Complex, although GAD67 positive input neurons were seen in the same region, at first glance compatible with the functional profile of respiratory-sympathetic coupling and the inhibitory neurochemical phenotype of some pre-Bötzinger Complex respiratory neurons (Koizumi *et al.*, 2013), the overlap between this area and the CVLM, and the lack of any neurochemical marker distinct for respiratory inhibitory neurons, makes meaningful interpretation of these data difficult.

Glycinergic Bötzinger neurons are active during the expiratory phase (Schreihofer *et al.*, 1999; Ezure *et al.*, 2003) and have been implicated in respiratory phase transition from

inspiration to expiration (for recent reviews see Smith *et al.*, 2009; Feldman *et al.*, 2013; Smith *et al.*, 2013). Rabies-labelled neurons in the Bötzinger complex did not express mRNA for glycine transporter 2 (GLYT2), suggesting that the RVLM sympathetic pre-motor population probably doesn't receive direct innervation from expiratory-locked inhibitory neurons, again consistent with the functional data.

The pre-Bötzinger Complex and Bötzinger Complex are both coextensive with the RVLM making interpretation of conventional tracing data in regard to establishing connectivity between these regions difficult (Smith *et al.*, 1989b; Ellenberger & Feldman, 1990; Bowman *et al.*, 2013). Card *et al.* (2011) make no mention of inputs from any of the VRC nuclei in their study.

NTS

Inputs were distributed throughout the NTS with a focal concentration in the sub-postremal medial NTS. As the NTS serves as a primary site of afferent termination for visceral reflex pathways that influence sympathetic output (Andresen & Yang, 1995), this observation was unsurprising. Previous studies describe direct projections from the NTS towards C1 (Hancock, 1988; Aicher *et al.*, 1996) and bulbospinal RVLM neurons (Ross *et al.*, 1985). As described in previous paragraphs, the canonical baroflex pathway is mediated by inhibitory CVLM neurons that relay NTS afferent input to the RVLM (Guyenet, 2006), however NTS neurons that express c-fos after baroloading and project directly to the RVLM have been identified in past studies (Minson *et al.*, 1997; Chan & Sawchenko, 1998). Similarly, the chemoreflex control of sympathetic output is mediated via direct excitatory projections from the NTS to the RVLM (Koshiya & Guyenet, 1996; Kline *et al.*, 2010) and recent anterograde polysynaptic tracing studies detail afferent inputs from the airway to RVLM from the airways that are relayed via the NTS (McGovern *et al.*, 2012a; McGovern *et al.*, 2015). Therefore the NTS inputs identified in the present study could feasibly represent sensory afferent innervation from a variety of sources.

Nucleus Prepositus

Blood pressure is regulated with respect to body position, via the activation of receptors in the vestibular system that are sensitive to changes in rotation and acceleration (Yates & Miller, 1994). Lesion studies have demonstrated that the RVLM is critical component

of the vestibulo-sympathetic reflex (Steinbacher & Yates, 1996) and receives vestibular input via a polysynaptic pathway (Yates *et al.*, 1991). Proposed pathways that could mediate this reflex involve a projection from the vestibular nucleus directly to the RVLM or one relayed via the CVLM (Holstein *et al.*, 2011). We did not observe inputs arising from the vestibular nucleus, however we observed a striking source of input from the medially adjacent nucleus prepositus. This nucleus receives integrative input from the vestibular system via the medial vestibular nucleus and is traditionally associated with head orientation and gaze tracking movements of the eyes (Yoder & Taube, 2014). We observed input neurons extending the entire length of the nucleus from the rostral pole of hypoglossal nucleus to the genu of facial nerve, concentrated to the magnocellular part of the nucleus. Many neurons displayed the distinct multi-dendritic morphology of "principal" prepositus neurons (McCrea & Baker, 1985b). Past studies involving the intracellular deposition of dye into prepositus neurons have describe a generic axonal projection to the ventral medulla in the cat (McCrea & Baker, 1985a). The synaptic input from prepositus inputs may occur on the distal dendrites of bulbospinal RVLM neurons that lie outside of the RVLM, offering a possible explanation as to why this source of input has eluded identification in previous tracer studies.

Hypothalamus

Projections from the PVN to the RVLM have previously been implicated in the regulation of sympathetic output in response to changes in blood osmolality (Stocker *et al.*, 2008), blood pressure (Badoer & Merolli, 1998; Chen & Toney, 2010), chemoreceptor activation (Cruz *et al.*, 2008) and stress (Carrive, 2013). Although inputs were sparse, they were consistent across all animals. We found that some of these inputs were immuno-reactive for vasopressin: these neurons may constitute a central vasopressinergic pathway that regulates sympathetic output in response to haemorrhage (Gomez *et al.*, 1993).

Conclusions and Future directions

Ultimately, the purpose of this study was to map the anatomical substrates that underlie the activity of RVLM sympathetic premotor neurons. We identified a comprehensive network of neurons that directly innervate putative RVLM sympathetic pre-motor neurons. As the output of these neurons and subsequently sympathetic drive is derivative of the summative synaptic input to this population, the network we have

identified constitutes the anatomical correlates for modal and basal command of sympathetic vasomotor output. However it is difficult to comprehend the contribution of a particular input to the circuit without assessing the outcomes of perturbation on sympathetic output.

The application of glycoprotein-deleted rabies variants that express functional transgenes (e.g. channelrhodopsin2: Osakada *et al.*, 2011) would serve as an appropriate platform for the selective manipulation of inputs that are spatially distinct. For example, examining the contribution of the nucleus prepositus input to the vestibulo-sympathetic reflex would involve optically inhibiting neurons within the nucleus transfected transynaptically with an inhibitory opsin (halorhodopsin or archaerhodopsin) and titrating blood pressure responses to vestibular nerve stimulation. However, the efficacy of glycoprotein-deleted rabies variants for circuit manipulation is still unproven, despite their longstanding availability (Osakada *et al.*, 2011). Alternatively, substituting another vector system to introduce opsins (e.g. AAV, HSV) or pharmacological approaches (e.g. muscimol) may prove a more simple, although less precise, means of testing the hypotheses suggested by the current dataset.

In addition to employing a SADΔG seeding strategy based on the anatomical projection of the target population, we have also generated the first brain-wide quantitative map of inputs made in the rat, described the first quantitative 3d segmentation for the RVLM region, and described a relatively straightforward workflow for image registration that, coupled with the Imaris platform, may prove useful to other researchers. One of the advantages of our approach is it provides a platform by which huge datasets of thousands of neurons can be easily shared, explored, and analyzed by other researchers.

Although the Waxholm segmentation model is relatively immature, composed of only 70 distinct regions compared to the 400+ regions in Paxinos & Watson-space (Paxinos & Watson, 2006). However, the development of a 3d alignment tool that can convert 2d images captured using low-tech hardware into a common 3d space that can then be automatically quantified and plotted, and shared in a data-efficient manner (this approach expresses the locations of neurons contained in 200+Gb of imaging data in just 100 kb of Cartesian co-ordinates) shows the potential of such an approach. Importantly, this approach is flexible enough to be compatible with contemporary and emerging

approaches to imaging neuronal tissue (e.g. CLARITY). It should serve as an incentive for continued improvement of the Waxholm segmentation model or development of an analagous alignment tool that can be used with more comprehensively delineated rat brain atlases, or emergence of standardised data viewing, sharing and registration tools similar to the Allen Brain Explorer for mice (Lein *et al.*, 2007).

The development of tools that allow the reader to interact directly with the full dataset, rather than relying on other investigators' ability to correctly identify the locations of labelled neurons, or brain atlases in which segmentation is derived from the gross appearance of the brain, will reduce the subjective nature of anatomical datasets and allow appreciation of the complexity of entire datasets, reducing bias and oversimplification. Furthermore, our system, which allows users to define novel segmentations according to density-encoded distributions of neurons with a particular anatomical (e.g. projection to the spinal cord), neurochemical (e.g. expression of TH) or functional (e.g. fos expression in response to a certain stimulus) may lead to the development of next generation crowd-sourced brain atlases that capture the expertise of investigators who have dedicated decades in refining their understanding of a particular nucleus of interest and also integrate gene expression and function into what are currently purely structural atlases.

Supplementary Files 3.1: Supplementary video, Imaris model and complete data in spreadsheet format of the data described in figures 3.4 and 3.5

https://www.dropbox.com/sh/afmu2uin2t2yezn/AAC0rtMIBv72nEMr63NPPRHPa?dl=0

CHAPTER 4 Direct projections from the midbrain colliculi innervate putative pre-motor sympathetic, respiratory and somatomotor populations in the ventral medulla.

Abstract

We have recently shown that disinhibition of a circumscribed region encompassing the superior and inferior colliculi unmasks coordinated cardiovascular, somatomotor, and respiratory responses to multimodal sensory stimuli in the anesthetized rat. These effects were maintained following extensive decerebration, suggesting the existence of a previously undescribed pathway that links the midbrain colliculi to cardiorespiratory and motor control nuclei in the brainstem and/or spinal cord. Here we examine the targets of collicular output neurons using an AAV vector that drives the expression of a fluorescent reporter protein within the axons, synaptic terminals and cell bodies of infected neurons. Following sufficient time for reporter transduction, rats were sacrificed and regions of the brain containing putative sympathetic, respiratory or motor circuits were examined for reporter-labelled terminal fields. Vector injections confined to the region that drives physiological responses resulted in extensive projections throughout the ventral brainstem, with little evidence of projections innervating targets in the spinal cord. The greatest density of terminal labelling was observed within in a region that spanned the medullary reticular formation and raphe nuclei, in which we observed putative synaptic contacts with neurons retrogradely labelled from the thoracic spinal cord. In contrast, no labelling was apparent in other classical respiratory or cardiovascular control nuclei in the ventrolateral medulla. We conclude that coordinated command of sympathetic, respiratory and somatomotor outflow from the colliculi may be mediated by a monosynaptic projection to pre-motor neurons in the ventral medial medulla.

Introduction

The ability to generate rapid behavioural responses to environmental stimuli is critical for survival. The superior and inferior colliculi (SC and IC) of the dorsal midbrain play key roles in the immediate processing of alerting sensory stimuli and the coordination of motor commands appropriate for orientation, defence or escape (Dean *et al.*, 1989; Stein *et al.*, 1995; Casseday & Covey, 1996). Activation of SC neurons via electrical stimulation or disinhibition with $GABA_A$ antagonists (e.g. bicuculline or picrotoxin) in behaving animals is sufficient to drive a variety responses including cowering, vocalization and escape in primates (DesJardin *et al.*, 2013) and approach and avoidance rodents (Sahibzada *et al.*, 1986; Dean *et al.*, 1989). Lesion of the SC produces contrary results, inhibiting normal avoidance behaviours (Maior *et al.*, 2011) and fleeing responses to visual threats (Dean & Redgrave, 1984)

Neurons located within the deep and intermediate layers of the SC (DLSC) are responsible for coupling sensory and motor systems. This population of neurons are sensitive to multiple modes of sensory stimuli (McHaffie *et al.*, 1989), receive direct input from visual, auditory and somatosensory pathways (Huerta & Harting, 1984; Meredith & Stein, 1986), and project extensively to motor circuits throughout the brain and spinal cord (Huerta & Harting, 1982; Rhoades *et al.*, 1987; Sparks, 1988; Munoz *et al.*, 1991; Meredith *et al.*, 1992). Many of these neurons also exhibit phasic bursts of activity immediately before the onset of orienting motor commands (Munoz *et al.*, 1991).

The inferior colliculus (IC) primarily receives convergent sensory input from brainstem auditory nuclei (Casseday & Covey, 1996). Although activation of this region alone is sufficient to evoke orienting and defensive behaviours (Brandao *et al.*, 1988; Cardoso *et al.*, 1994), any sensorimotor capacity attributed to the IC is most likely mediated via a direct projection from this region to the DLSC (Powell & Hatton, 1969; Carey & Webster, 1971).

In addition to driving motor behaviour, activation of the colliculi drives complimentary autonomic effects, including immediate increases in blood pressure, heart rate and respiratory activity (Brandao *et al.*, 1988; Keay *et al.*, 1988; Keay *et al.*, 1990). The parallel recruitment of cardiorespiratory systems suggests that the colliculi are capable

of coordinating supportive functions in preparation for immediate physical activity i.e. redirection of blood to skeletal muscle (Adams *et al.*, 1971; Rowell, 1974; Carrive *et al.*, 1989; Turner, 1991; Carrive, 1993; McAllister, 1998). To appropriately satisfy the physiological demands of motor behaviour (e.g. ventilation and perfusion), accompanying autonomic drive needs to be coordinated with precision (Turner, 1991). A mechanism by which to achieve unified output is for activation of both autonomic and motor drive to arise from a common set of neurons, sometimes conceptualised as 'command neurons' (Kupfermann, 1978).

Our laboratory recently demonstrated that disinhibition of a circumscribed region of the colliculi with bicuculline evoked spontaneous and highly synchronized bursts of sciatic (scNA), phrenic (pNA), and splanchnic sympathetic nerve activities (sSNA) (Iigaya *et al.*, 2012). Essentially identical responses could be evoked in response to multimodal (visual, auditory and somatosensory) sensory stimulation in the absence of any spontaneous activity when the GABA receptor antagonist picrotoxin was substituted for bicuculline (Muller-Ribeiro *et al.*, 2014).The latencies of scNA, sSNA and pNA responses to acoustic or visual stimuli differed by less than 50 ms and were observed under conditions of paralysis and vagotomy, suggesting that all three modes of output were dependent on a common central pathway, rather than, for example, sciatic nerve output alone being driven by a pathway originating in the colliculi, and respiratory and sympathetic responses resulting from somatosensory stimuli related to muscle recruitment (Potts & Mitchell, 1998).

These observations, although novel, were not entirely unexpected, as qualitatively similar autonomic responses have been observed in response to collicular stimulation at sites that also evoke defensive behaviours (Keay *et al.*, 1988) and cardiovascular and respiratory effects which are considered components of the classically defined defence response (Hilton & Redfern, 1986) (although the close synchronization of cardiovascular, respiratory and motor outputs has not previously been reported). However, synchronized bursting responses to polymodal sensory stimulation that were unmasked by collicular disinhibition unexpectedly persisted after extensive pre-collicular decerebration (Muller-Ribeiro *et al.*, 2014), which included removal of the hypothalamus. This suggests the existence of collicular circuits that can directly

orchestrate cardiovascular, respiratory and motor responses to sensory inputs independent of relays in the hypothalamus or forebrain.

The focus of the current study was to identify putative targets of collicular output neurons within the brainstem or spinal cord that could conceivably drive the cardiovascular, respiratory and motor activation we previously observed. We employed an anterograde tracing strategy to identify efferent projections of collicular neurons arising from the region circumscribed previously by (Muller-Ribeiro *et al.*, 2014) and subsequently examined regions of the brainstem and spinal cord classically associated with sympathetic and respiratory control for evidence of synaptic termination. Expected targets included the RVLM and pre-Bötzinger Complex.

Methods

Ethics

Ethical Approval: All experiments were approved by Macquarie University Animal Ethics Committee and conformed to the Australian Code of Practice for the Care and Use of Animals for Scientific Purposes.

Animals

Animals were obtained from the Animal Resources Centre (Perth, WA) and were housed at the Macquarie University Central Animal Facility. Male and female Sprague-Dawley rats weighing 200-600g at the onset of experiments were used for anatomical studies. Animals were housed in groups of 4 in individually ventilated cages containing environment enrichment material (blocks of wood, shaved cardboard, plastic tubes), with food and water available *ad libitum*. Cages were kept in a temperature- and humidity-controlled room (21°C ± 2°C, 60 % humidity) with fixed 12 h light and dark cycles. Animals were transported to the PC2 laboratories at the Australian School of Advanced Medicine (Macquarie University) for stereotaxic injections and electrophysiology experiments.

AAV vector

AAV2-CBa-tdTomato was prepared in the laboratory of A/Prof Andrew Allen at the physiology department of the University of Melbourne and injected at an approximate concentration of $1x10^{11}$ IU/mL.

Surgery

Stereotaxic AAV Injections

Rats were anesthetized with ketamine (75 mg/kg i.p.; Parnell Laboratories, Alexandria, NSW, Australia) mixed with medetomidine (0.5 mg/kg; Pfizer Animal Health, West Ryde, NSW, Australia). Prophylactic antibiotics (100 mg/kg cephazolin sodium, i.m.; Mayne Pharma, Salisbury South, SA, Australia) and analgesia (5 mg/kg Carprofen, s.c.; Norbrook Pharmaceuticals, Tullamarine, VIC, Australia) were administered prior to surgery. Anaesthetic depth was carefully monitored by examining motor responses to firm pinch of the hindpaw. Supplementary ketamine (10% initial dose) was provided as required to maintain anaesthetic plane. Rectal temperature was monitored and

maintained between 36.5 – 37.5 °C with a thermostatically controlled heating pad (Harvard Apparatus, USA).

Rats were positioned in a stereotaxic frame in the skull flat position and an incision was made along the skull to expose Bregma and Lambda. Using a stereomicroscope, a 2 mm diameter hole was made over the target area by thinning the skull with a fine drill burr. The remaining layer of bone above the pial surface was peeled away using fine forceps and the dura punctured using a 26 gauge needle.

Microinjection pipettes with a ~10 µm tip diameter were pulled from borosilicate glass capillaries (O.D. 1.0 mm, I.D. 0.25 mm; SDR Clinical Technology, Australia) using a P2000 laser pipette puller (Sutter Instrument Company, USA) and scored with 50 nl increments (1 mm = 50 nl). The pipette was mounted in a micromanipulator and the AAV2-CBa-tdTomato vector was aspirated using a syringe attached to the pipette with polyethylene tubing. Relative zero for the rostral-caudal and medial-lateral axes was established by lowering the pipette tip to the bone surface at Bregma. The pipette was positioned -1.8 mm lateral and 7.8 mm caudal to Bregma and slowly lowered 4.2 mm ventral to the pial surface. 250 nl of vector was manually injected over a period of 5 minutes and pipette left in place for a further 5 min before withdrawal.

The wound was irrigated with sterile physiological saline and oxidized cellulose haemostat (Surgicel; Johnson & Johnson,USA) placed over the skull exposure. The wound was closed using surgical staples and cleaned with betadine antiseptic (Faulding Pharmaceuticals, Australia). The animal was removed from the stereotaxic frame and anaesthesia reversed with atipamazole (1 mg/kg s.c., Pfizer Animal Health, Australia). The animal was monitored closely until ambulatory and then returned to the animal housing facility. Comprehensive observations of the animals health were conducted twice daily for 1 week post-surgery and twice weekly until the end of the experiment. Additional analgesia (carprofen, 5 mg/kg s.c.) was administered as required.

Thoracic spinal cord injections

Three weeks after AAV injections, rats were re-anaesthetised and prepared for surgery as described above. Once mounted in a stereotaxic frame the sacral vertebral processes were exposed and clamped to maintain the spine in a horizontal and elevated position. The T2 spinal cord was exposed following a midline incision and dissection of the

intravertebral ligament; the dura was punctured and two 200 nl injections of cholera toxin B subunit (CTB; List Biological Laboratories, USA; .5 %) were made on each side at 0.75 mm lateral to the midline and 1 mm deep to the surface, co-ordinates that correspond to the interomediolateral column (IML) in the adult rat (Turner *et al.*, 2013). CTB was injected over a period of 5 min before the pipette was slowly retracted.

At the end of surgery, the exposed spinal cord was irrigated with sterile physiological saline, covered with oxidized cellulose haemostat, the wound closed and anaesthesia reversed. Post-operative care and monitoring were as describe above. Rats were perfused for histology 5 days after CTB injection.

Histology

Transcardial Perfusion

Animals were terminally anaesthetised with sodium pentobarbital (>100 mg/kg [Supplier]). When responses to hind-paw pinch were absent the chest cavity was opened and heart exposed. An 18 gauge needle was inserted into the ascending aorta via he left ventricle and clamped in position with a haemostat. The right atrium was then cut and 1 ml of heparin (1000 IU) injected into the aorta. The animal was perfused with 500 ml of ice-cold saline followed by 500 ml 4 % PFA. The brain and thoracic spinal cord were then removed and post-fixed overnight.

Tissue processing

The brains were blocked 2 mm rostral to the superior colliculus and caudal to the medullary-cervical junction. The brains and spinal cords were sectioned in the coronal plane using a Leica Vt1200S vibrating microtome at 50 µm thick and collected into 4 pots (section interval 200 µm per pot). Sections for immunohistochemistry were stored in 0.01 M Tris-phosphate buffered saline (TPBS). Sections not immediately used were stored in cryoprotectant solution (500 µM polyvinylpyrrolidone, 76.7 mM Na_2HPO_4, 26.6 mM NaH_2PO_4, 876 mM sucrose, 5mM ethylene glycol) at -20 ^{o}C.

Immunohistochemistry

Sections were washed in TPBS containing 0.2 % Triton-100 for 3 × 15 min and blocked for nonspecific binding in TPBS containing 2 % bovine serum albumin and 0.2 % Triton-100 for 1 h at room temperature. Sections were incubated in this solution with primary

antibodies for 12 h at 4°C, washed in TPBS containing 0.2 % Triton-100 for 3 × 15 min, and incubated with secondary antibodies in TPBS containing 2% bovine serum albumin and 0.2% Triton-100 overnight (refer to Table 4.1 for antibody information). Processed sections were washed again in TPBS 3 × 30 min before being mounted in serial order on glass slides with fluorescence mounting medium (Dako, North Sydney, Australia) and cover slipped.

Imaging

Fluorescence imaging was performed on a Zeiss Z2 (Carl Zeiss Pty Ltd, North Ryde, Australia) epifluorescence microscope and Leica TCS SP5X (Leica Microsystems Pty Ltd, North Ryde, NSW, Australia) confocal microscope. Image acquisition and processing were performed using Zen 2012 (Carl Zeiss Pty Ltd, North Ryde, Australia) and Leica Application Suite Advanced Fluorescence (LAS:AF) (Leica, Germany) software respectively. Low power epifluorescence mosaics (10x) were acquired to map the extent of vector injections and the general distribution of the tracer. High power (40x) confocal images were acquired to investigate axonal varicosities and putative synaptic contacts. Micrographs depicted in figures were taken from representative tracing experiments.

Table 4.1 Primary and Secondary antibodies

Application	Antigen	Species	Conjugate	Concentration	Clonality	Manufacturer	Code
1°	Tyrosine-Hydroxylase (TH)	Mouse	N/A	1:1000	Mono	Sigma	T1299
1°	Cholera Toxin B subunit (CTB)	Goat	N/A	1:1000	Poly	List Biological Laboratories	703
1°	Tryptophan-Hydroxylase (TPH)	Mouse	N/A	1:500	Mono	Sigma	T0678
1°	Neurokinin-1 Receptor (NK1R)	Rabbit	N/A	1:1000	Poly	Sigma	S8305
1°	CHX10	Sheep	N/A	1:500	Poly	Millipore	AB9016
2°	Rabbit IgG (H+L chain)	Donkey	Alexa Fluor® 647	1:500	Poly	Life Technologies	A31573
2°	Goat IgG (H+L chain)	Donkey	Alexa Fluor® 647	1:500	Poly	Life Technologies	A21447
2°	Mouse IgG (H+L chain)	Donkey	Alexa Fluor® 647	1:500	Poly	Life Technologies	A31571

Results

Injection sites

Vector injections were made in the colliculi of 14 animals targeted at the regions that most frequently recruited physiological responses to bicuculline or picrotoxin injection in our previous studies (Iigaya *et al.*, 2012). Four animals received additional CTB injections targeted at the T2 IML.

The collicular AAV injection sites constituted thousands of neurons forming a spheroid of reporter labelled soma and neuropil extending rostrocaudally between approximately

Bregma -7.08 to -8.28 mm, 1.2 to 3.4 mm mediolateral, and 3 to 6 mm dorsoventral. Injection boundaries were defined by the presence of reporter filled somata. Labelled soma often encompassed the entirety of the precuniform area and central nucleus of the inferior colliculus, the medial extent of the external cortex of the inferior colliculus, the lateral extent of the deep and intermediate layers of the superior collicular laminae and the lateral boundary of periaqueductal gray (PAG) (Figure 4.1).

The distribution of transduced cell bodies were mapped in the coronal plane onto the stereotaxic atlas of the rat brain (Paxinos & Watson, 2007) at 200 µm intervals. Using the densest region of labelled soma as a boundary guide, we determined that the injection sites of 8 animals were found to closely overlay the region(s) described in (Muller-Ribeiro *et al.*, 2014) without impingement on adjacent regions; data from these 8 animals were selected for detailed analysis. 2 of these animals had also received CTB injections. The T2 spinal segments of these animals were sectioned to confirm CTB injection site overlap with the IML

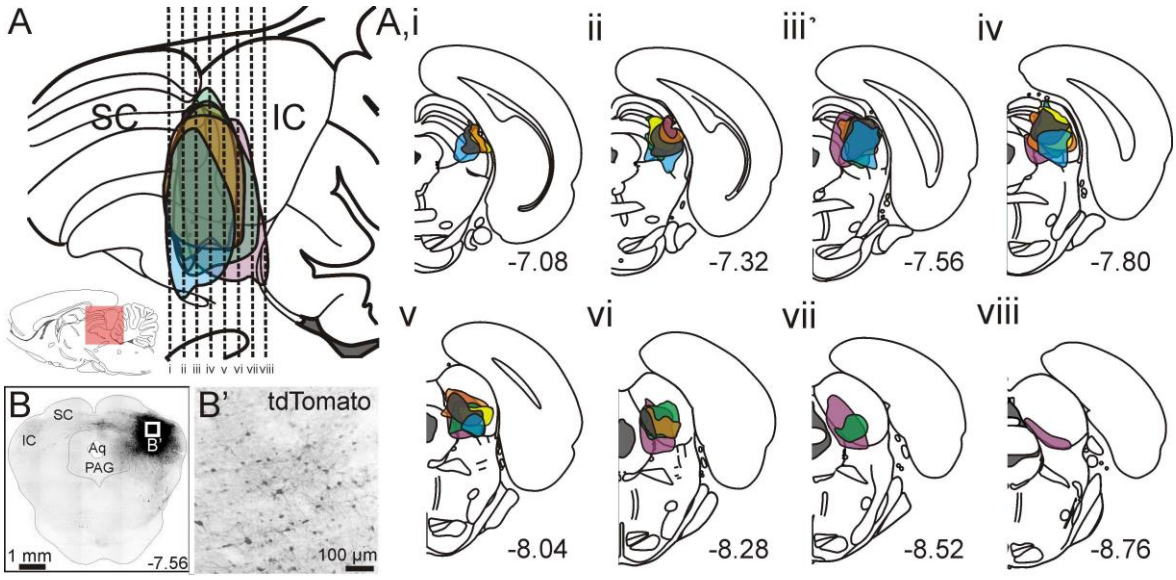

Figure 4.1 AAV injection sites. A. Parasagittal view depicting the extent of reporter expression from 8 animals following microinjection of AAV in the midbrain colliculi. The intersecting lines i-viii represent corresponding coronal planes (A,i - A,viii) mapped in accordance with Paxinos and Watson (2007). B. Coronal midbrain section with injection site with high power inset (B') demonstrating AAV-mediated tdTomato reporter expression. (IC: inferior colliculus; SC: superior colliculus; Aq: aqueduct; PAG: Periaqueductal Gray).

Efferent projections from the midbrain colliculi: general description

Transduced neurons were filled extensively with the tdTomato reporter, labelling the entire axonal and dendritic tree with sufficient definition to clearly trace axonal

trajectories and resolve terminal varicosities without amplification. Three tectofugal bundles emerged from the injection site, forming a clearly defined ascending projection to the thalamus and hypothalamus, a descending projection to the brainstem and a projection to the contralateral colliculi via the commissural nucleus of the inferior colliculus to innervate the contralateral SC and IC.

Ascending projections

Midbrain

Rostral to the injection site, transfected ascending fibres were concentrated primarily at the brachium of the inferior colliculus forming a dense wedge extending ventrolateral from the medial edge of the medial geniculate nucleus to an apex along the dorsal surface of the substantia nigra. The wedge of densely labelled fibres occupied the posterior thalamic nuclear group, sub-brachial area, posterior intralaminar thalamic nucleus the dorsal terminal nucleus of the accessory optic tract, the posterior limitans thalamic nucleus and the parabrachial pigmented nucleus of the ventral tegmental area. Fibres laterally adjacent to the wedge densely encapsulated and traversed the medial geniculate nucleus.

Dense patches of fibres were distributed throughout the optic nerve layer of the superior colliculus, particularly at the medial and lateral borders of the laminae. Fine fibres innervated the PAG and adjacent medial accessory oculomotor nucleus, Edinger-Westphal nucleus, oculomotor nucleus and magnocellular red nucleus.

Within the coronal plane encompassing the caudal emergence of the dorsal third ventricle and choroid plexus (-5.20 Bregma), ascending fibres encompassed and traversed the dorsal, ventral and medial geniculate nuclei, anterior pretectal nucleus, olivary pretectal nucleus and posterior pretectal nucleus, converging upon the lateral terminal nucleus of the accessory optic tract and the supraoptic decussation.

Hypothalamus

Ascending fibres were observed throughout the forebrain, present up to the rostral terminus of the third ventricle. The densest labelling was confined to the supraoptic decussation, forming a tract running along its entire rostral-caudal extent. Secondary to this tract, fibres were observed along the boundary of the posterior hypothalamus and

sub-thalamus, innervating the zona incerta, the posterior thalamic group, the ventral and dorsal posteromedial thalamic nuclei, the posterior hypothalamic nucleus and the reuniens thalamic nucleus. Sparser patches of fine fibres were scattered throughout the anterior hypothalamic area and medial forebrain bundle. We noted that fibres were present at the dorsal and lateral boundaries of the paraventricular hypothalamic nucleus, but never infiltrated the nucleus itself or formed close apposition with vasopressin- or CTB-immunoreactive neurons in the region (data not shown).

Thalamus

Fibres and terminals were distributed sparsely throughout the thalamus, overlaying the ventral anterior, ventrolateral, anteroventral, dorsomedial, anteroventral, ventrolateral, anterodorsal, laterodorsal and dorsomedial thalamic nuclei, and paraventricular thalamic nucleus, anterior part.

Descending projections

Fibres emerging from the injection site followed either a collicular-bulbar trajectory, via the lateral midbrain, or to the contralateral colliculi via the commissure of the inferior colliculus. The collicular-bulbar bundle split into two tracts, the more substantial of which (primary) emerged in the brainstem immediately lateral to the trapezoid nucleus (Figure 4.2A), and the lesser tract (secondary), immediately dorsal to the superior cerebellar peduncle (Figure 4.2B). The primary and secondary tracts are clearly apparent in figure 4.2C, indicated by blue and red asterisks respectively.

The primary descending branch occupied a column extending from the ventral surface to an apex at locus coeruleus (LC, Figure 4.2B). This branch was sparsely mirrored on the contralateral side of the brainstem. The rostral component of this branch was comprised of both large and fine calibre fibres and putative terminals. Caudal to the genu of the facial nerve, the primary branch was most densely concentrated dorsomedial to the pyramidal tract and inferior olive at the level of the caudal pole of the facial nucleus, and was composed predominantly of fine calibre fibres and putative terminals. Labelled fibres were infrequently caudal to the semicompact nucleus ambiguus and virtually absent caudal to the cervical-medullary junction. The spinal cords of 4 animals were retained and inspected for evidence of collicular projections; although we observed individual reporter-labelled axons they were infrequent.

The secondary tract followed a caudal trajectory lateral to the facial genu to the medulla. The fibres composing the secondary tract were often present throughout the rostrocaudal extent of the brainstem to a similar degree as the primary branch, however these fibres were of a considerably larger calibre. The secondary branch was located exclusively ipsilateral to the injection site and varied considerably in density and extent of caudal distribution between animals.

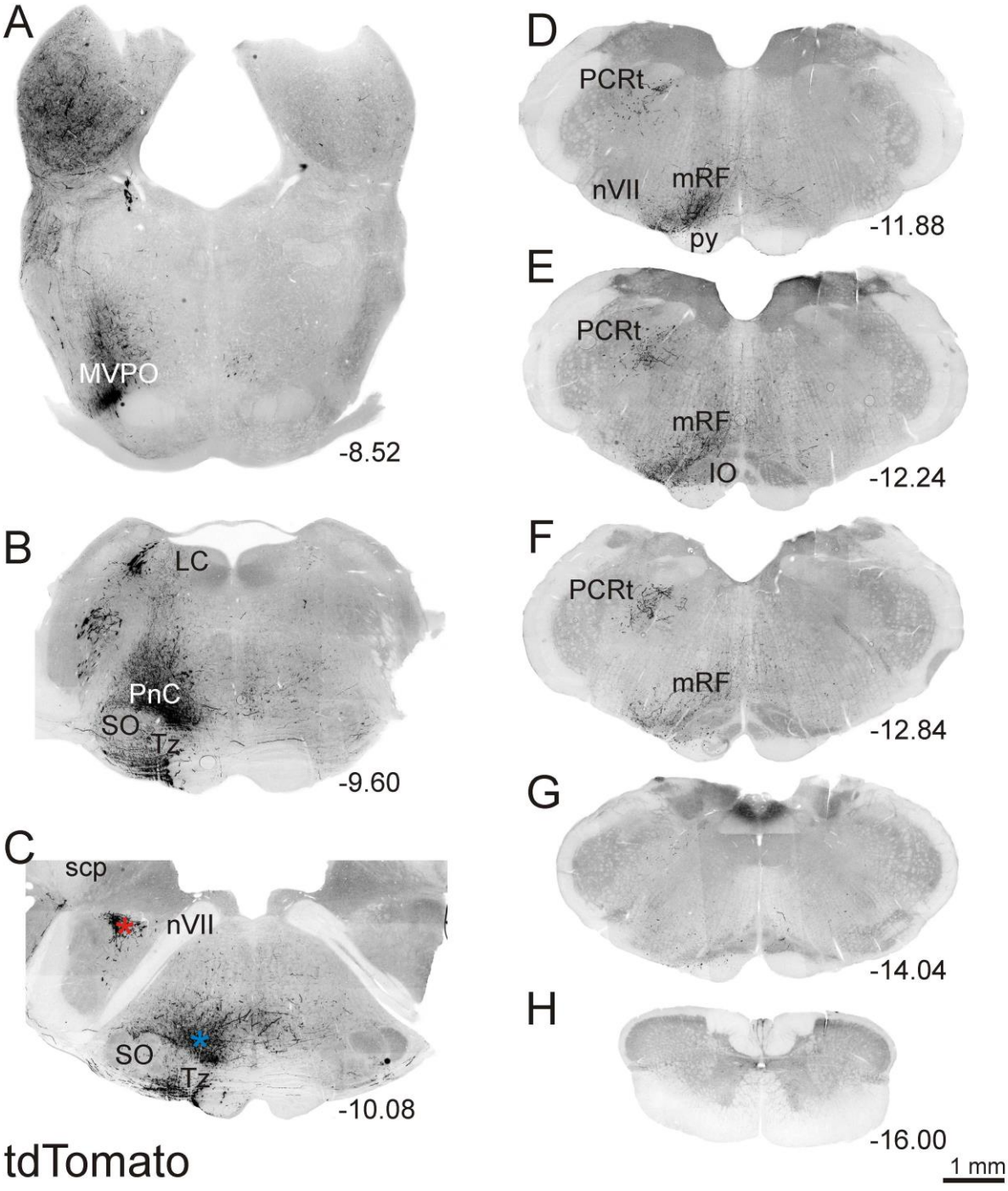

Figure 4.2 Neurons in the colliculus project to the brainstem but not the spinal cord. A-H: AAV-mediated reporter expression revealed descending projections that were observed from the pontine brainstem to the caudal medulla. Two distinct branches emerged: a primary ventromedial branch (C, blue asterisks) and a secondary dorsolateral branch (C, red asterisks). The ventromedial projection terminated primarily within a region of the medulla immediately dorsal to the pyramidal tract and inferior olive noted as the medullary reticular formation (mRF, D-F). The secondary branch terminated primarily within the parvicellular reticular nucleus (PCRt, D-F). Labelled fibres were sparse in the caudal medulla (G) and absent from the spinal cord (H). (MVPO: medioventral periolivary nucleus; SO: superior olive; PnC: pontine reticular nucleus; nVII: facial motor nucleus; IO: inferior olive; py: pyramidal tract; scp: superior cerebellar peduncle; LC: locus coeruleus; Tz: trapezoid body). Injection site for this animal displayed in Figure 4.1B.

Pontine Brainstem

Immediately caudal to the midbrain, transected fibres were primarily concentrated within the boundaries of the oral and caudal pontine recticular nuclei and along the ventral surface of the pons immediately lateral and ventral to the pontine nuclei and longitudinal fasciculus of the pons (Figure 4.2A). Caudal to the pontine nuclei, fibres occupied a wedge extending from the dorsal surface to a sparsely innervated apex at the locus coeruleus overlying the lateral tectospinal tract, the medial boundary of the sub coeruleus and coursing around the trapezoid and superior olivary nuclei (SO) and the lateral boundary of the pyramidal tract (Figure 4.2B).

Although large calibre fibres of passage constituted the densest labelling within the rostral brainstem, fine fibres and axonal varicosities were densely distributed throughout the pontine extent of the descending tract, particularly within the pontine reticular formation (Figure 4.2B).

Higher power investigation with a confocal microscope, revealed the presence of fine fibres and putative terminals throughout the A7 noradrenergic cell group (A7)(Figure 3), LC (Figure 4.4), subcoeruleus (not shown) and medial boundaries of the A5 noradrenergic cell group (A5, Figure 4.5), forming close apposition to CTB- and TH-immunoreactive neurons in these nuclei. Fine fibres and varicosities were also located with a region dorsolateral to A7 that overlapped the boundaries of the Kölliker-Fuse nucleus (KF, Figure 4.3B).

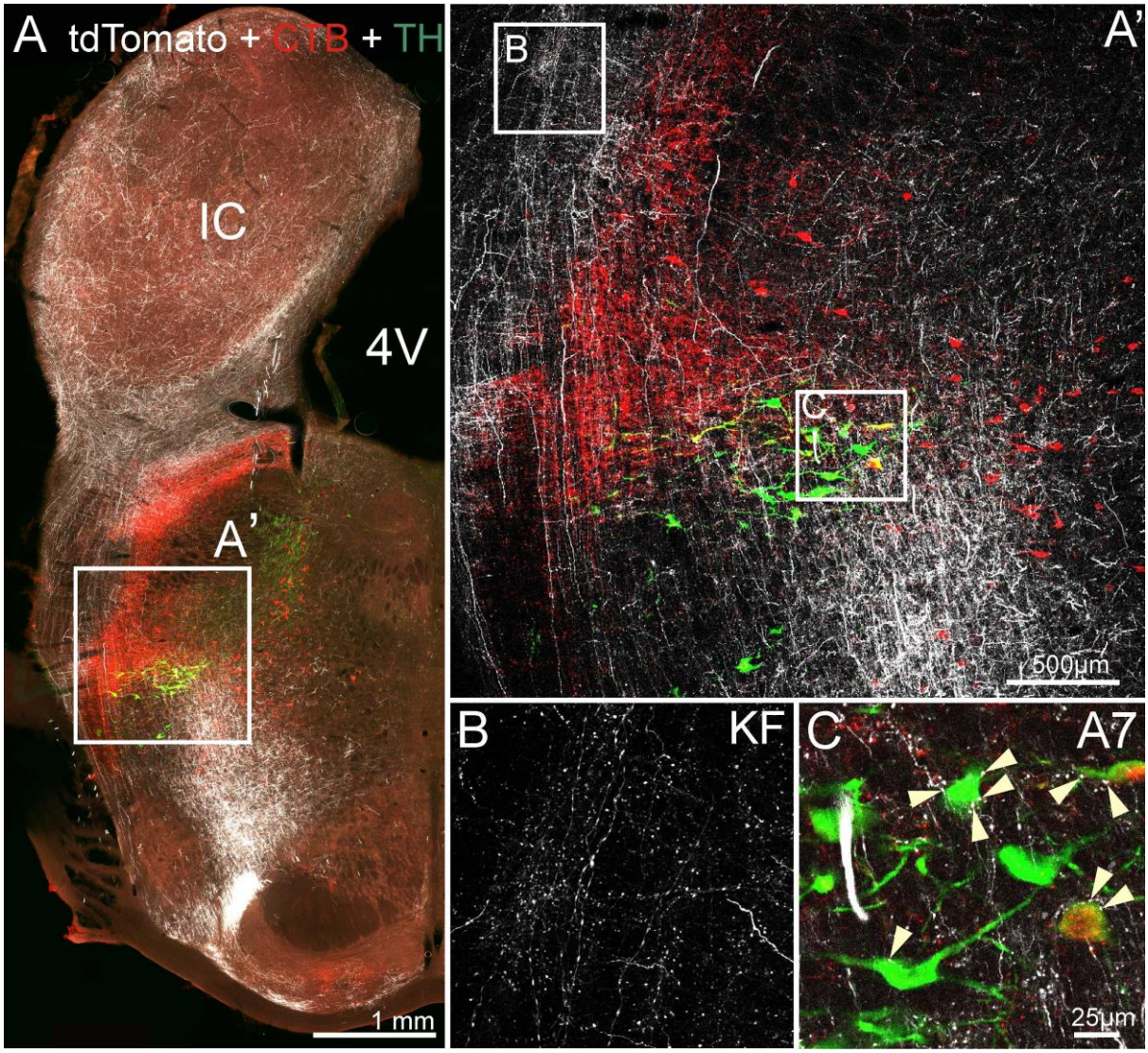

Figure 4.3 Collicular efferent neurons form close appositions with spinally projecting and tyrosine hydroxylase immunoreactive (TH) neurons in the A7 cell group. A: Epifluorescence micrograph at the level of the pontomedullary junction. Inset (A'), maximum projection of a confocal z-stack demonstrating labeled fibres (white) overlaying the Kölliker-Fuse (KF) nucleus and A7 cell group. Inset (B) shows a single optical plane image demonstrating fibers and putative terminals within the KF nucleus. Inset (C) shows single optical plane image demonstrating putative terminal apposition (indicated by arrowheads) with retrogradely labeled neurons immunoreactive for cholera toxin-B (CTB; red) and TH-positive neurons (green). (IC: inferior colliculus; 4V: fourth ventricle).

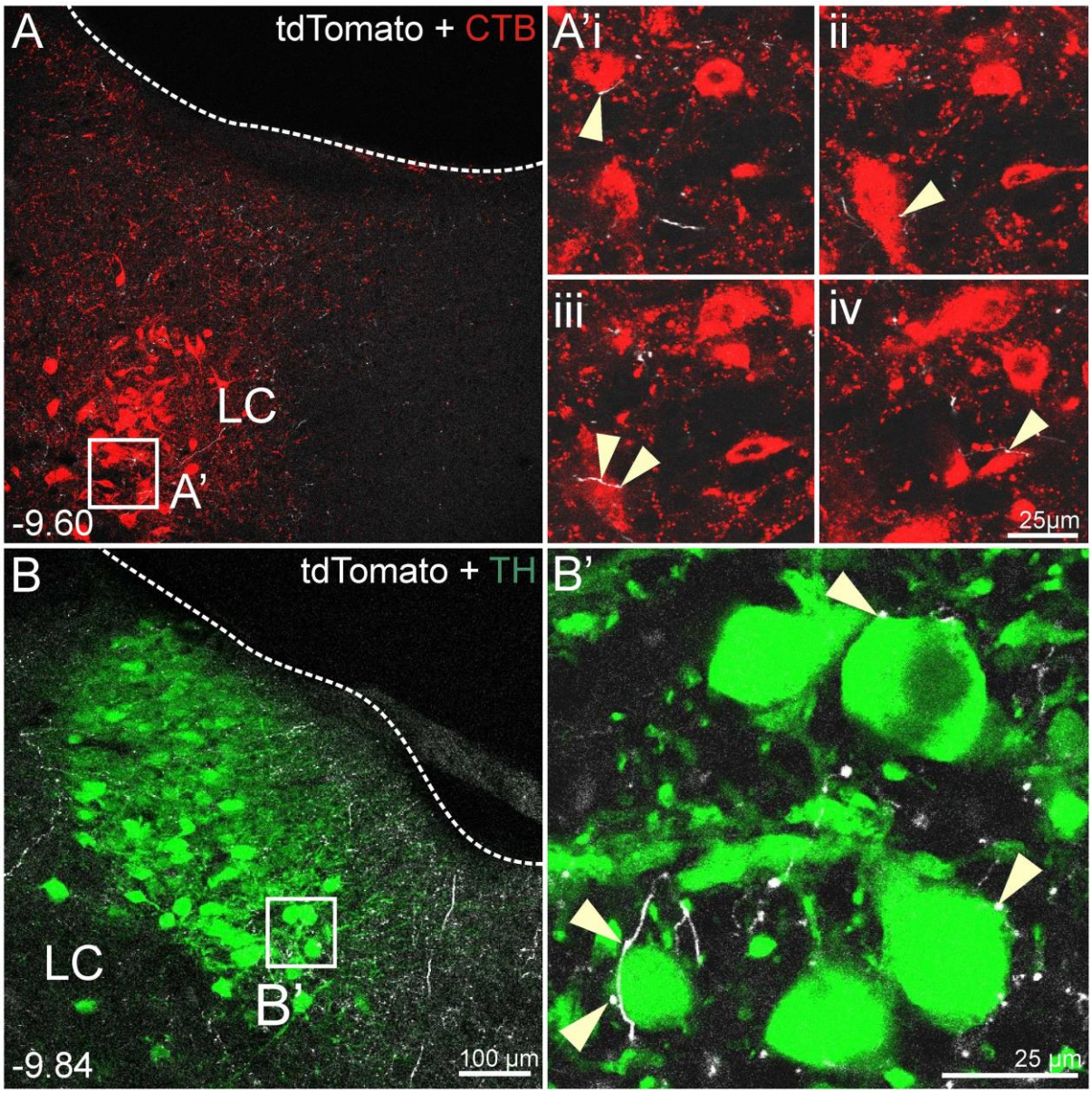

Figure 4.4: Collicular efferent neurons form close appositions with spinally projecting and TH-immunoreactive neurons in the locus coeruleus (LC). A, B: Single optical plane micrographs of AAV-mediated reporter expression (white), indicating terminal fields in the LC and putative terminals in close apposition to neurons immunoreactive for CTB (red) and TH (green). Inset in A' shows serial optical plane images of putative terminal appositions (arrowheads) with spinally projecting neurons. Inset in B' shows single optical plane image of putative terminal apposition with TH-immunoreactive neurons.

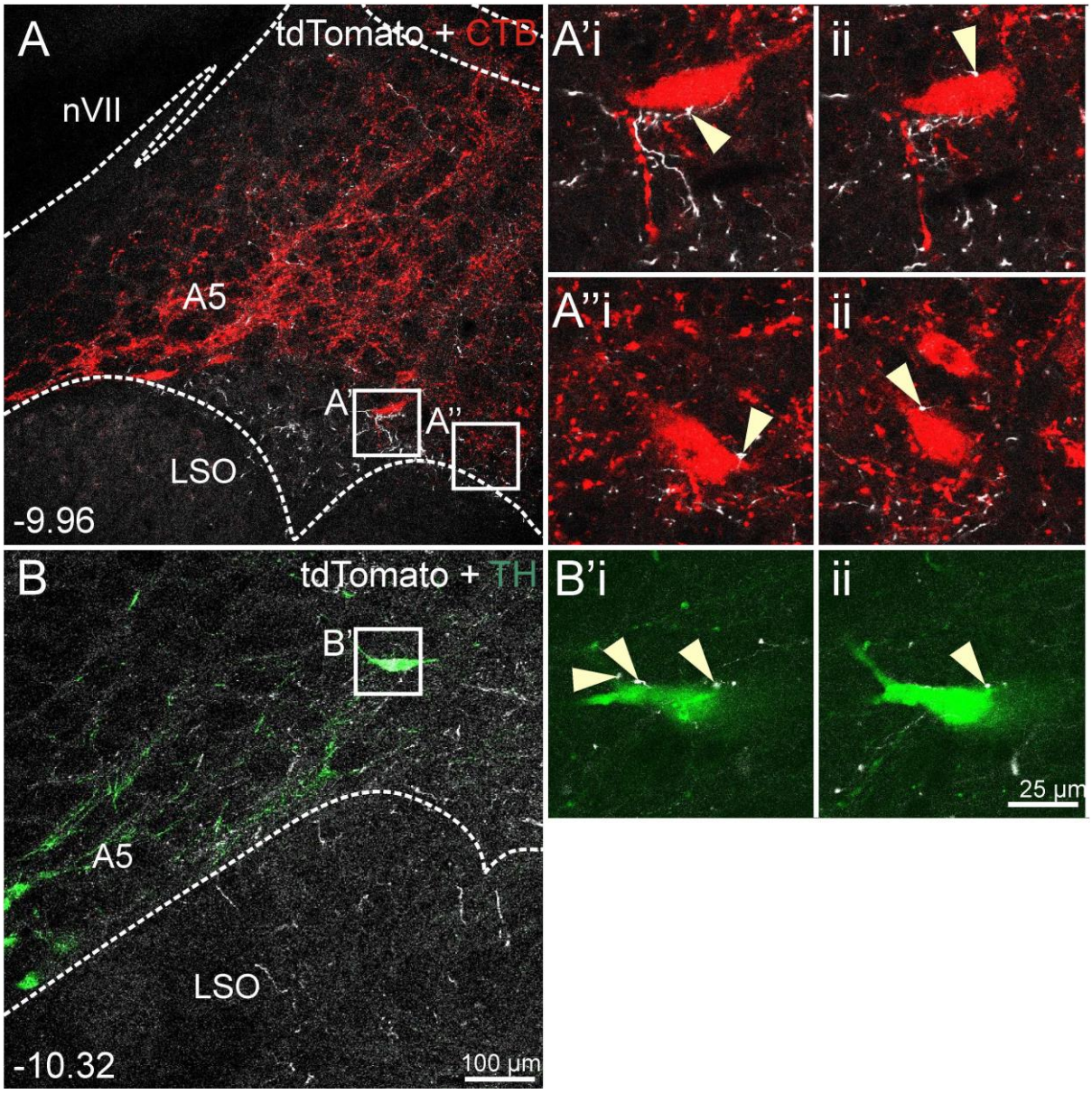

Figure 4.5 AAV-mediated reporter expression indicates close appositions between collicular efferent neurons and spinally projecting and TH-immunoreactive neurons in the caudal A5 cell group. A,B: Single optical plane micrographs of terminal fields in the A5 cell group immediately dorsal to the lateral superior olive (LSO). Insets show serial images from confocal z-stacks that demonstrate close apposition between reporter-labelled terminals (arrowheads) and spinally projecting (A' and A'') and TH-immunoreactive (B') neurons.

Medullary Brainstem

Within the medulla, the projection was concentrated immediately dorsal to the pyramidal tract and medial to the facial motor nucleus, forming a dense nexus of fibres and arborized varicosities that extended from the ventral surface immediately lateral to the pyramid, across the midline raphe and, at a greatly diminished density, to the equivalent region in the contralateral side. The terminal field spanned the caudal half of the facial nucleus and extended a further ~500 µm caudal to its pole. Fibre and axonal varicosities extended across the medullary reticular formation (mRF), a region that

corresponds to the rostral ventromedial medulla (RVMM) as described in Jansen *et al.* (1995), and includes the alpha and ventral aspects of the gigantocellular reticular nucleus (GiA, GiV); and lateral paragigantocellular nucleus (LPGi); and the obscurus (ROb), pallidus (RPa), and magnus (RMg) Raphe nuclei (Figure 4.2D-F). The most lateral fibres of this termination extended across the medial boundaries of the rostral ventrolateral medulla (RVLM) (Figure 2D-E).

The secondary tract of the collicular-bulbar projection terminated within the boundaries of the parvicellular reticular nucleus (PCRt), immediately ventrolateral of the nucleus of the solitary tract (NTS, Figure 4.2F-G). The projection was variable between experiments, and may reflect collicular input to pre-motor neurons of the orofacial motor nuclei (i.e. the motor trigeminal, facial, and hypoglossal nuclei (Holstege *et al.*, 1977; Terhorst *et al.*, 1991; Li *et al.*, 1993) or neurons involved in forelimb and hindlimb control (Esposito *et al.*, 2014). Retrograde and anterograde tracing studies indicate that this projection arises from neurons in the ventrolateral aspects of the SC (Yasui *et al.*, 1994; Tsumori & Yasui, 1997) which lie predominantly outside of the region circumscribed by (Muller-Ribeiro *et al.*, 2014). The ventrolateral boundaries of our injection sites often encroached upon this region of the SC, offering a possible explanation for the often variable distribution and density of this secondary descending branch.

A major projection site of descending collicular neurons is the medullar reticular formation (mRF) and Raphe

Reporter-labelled efferent fibres densely innervated a region of the mRF, concentrated immediately dorsal to the inferior olive (IO), ~200 μm rostral to the caudal pole of the facial nucleus (nVII) (Figure 4.2D). The distribution of collicular efferent terminals closely overlapped with the distribution of serotonergic neurons immunoreactive for tryptophan-hydroxylase (TPH) in the Raphe and RVMM (Figure 4.6A,B), but observation of terminal appositions TPH-ir neurons was infrequent (Figure 4.6A',A'' and B',B''). Thus TPH is a decent marker for the terminal field site in the mRF, but doesn't denote the actual target of those terminals.

In contrast, close appositions were frequently observed between axonal varicosities and CTB-immunoreactive neurons in the RMg (Figure 4.7C'i,ii), RPa (Figure 4.7C''i,ii), GiA

(Figure 4.7D'I,ii and GiV (Figure 4.7E'i,ii) including a subset of spinally projecting neurons that were immunoreactive for the transcription factor Chx10 (Figure 4.8B).

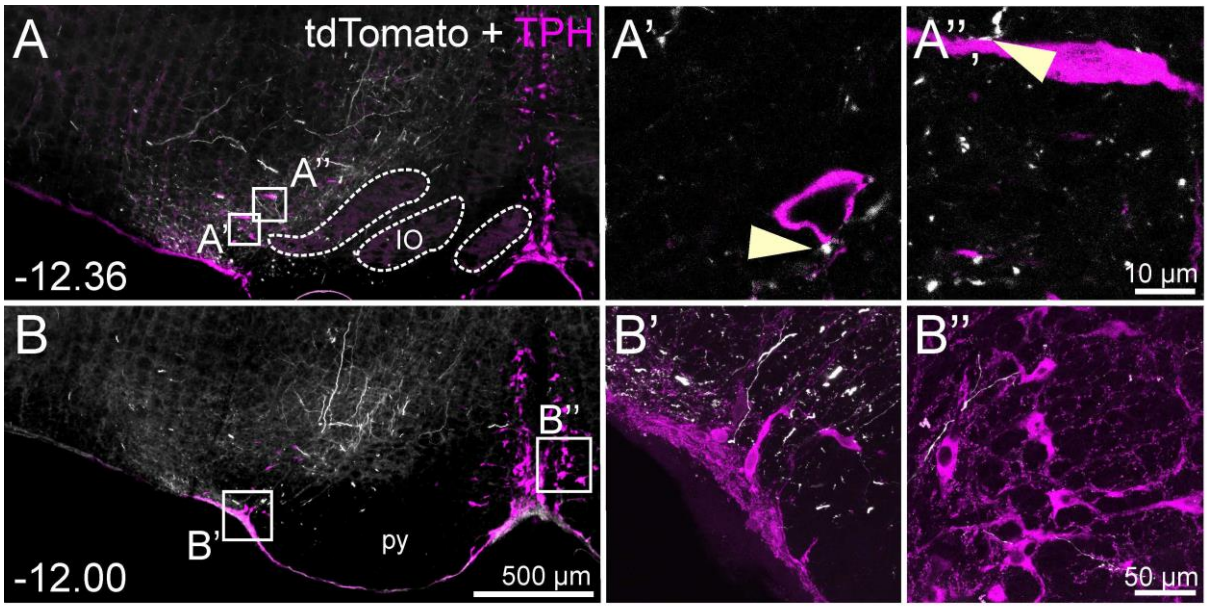

Figure 4.6 Collicular efferent neurons terminate in a region of the ventral medulla neurochemically defined by serotonergic neurons. A,B: reporter-labelled collicular fibres and putative terminals were often observed within the proximity of tryptophan-hydroxylase (TPH, purple) immunoreactive neurons of the RVMM and Raphe nuclei, but infrequently formed close appositions on serotonergic neurons. Insets shown in A' and A'' show single optical plane images that demonstrate rare terminal appositions (arrowheads) between collicular efferent neurons (white) and TPH-immunoreactive neurons within a region that corresponds to the RVMM. B: Maximum projection images demonstrates close proximity between fibres and serotonergic neurons in the ventral RVMM (B') but sparse innervation by labelled fibres in a region lateral of the Raphe Pallidus (B'').

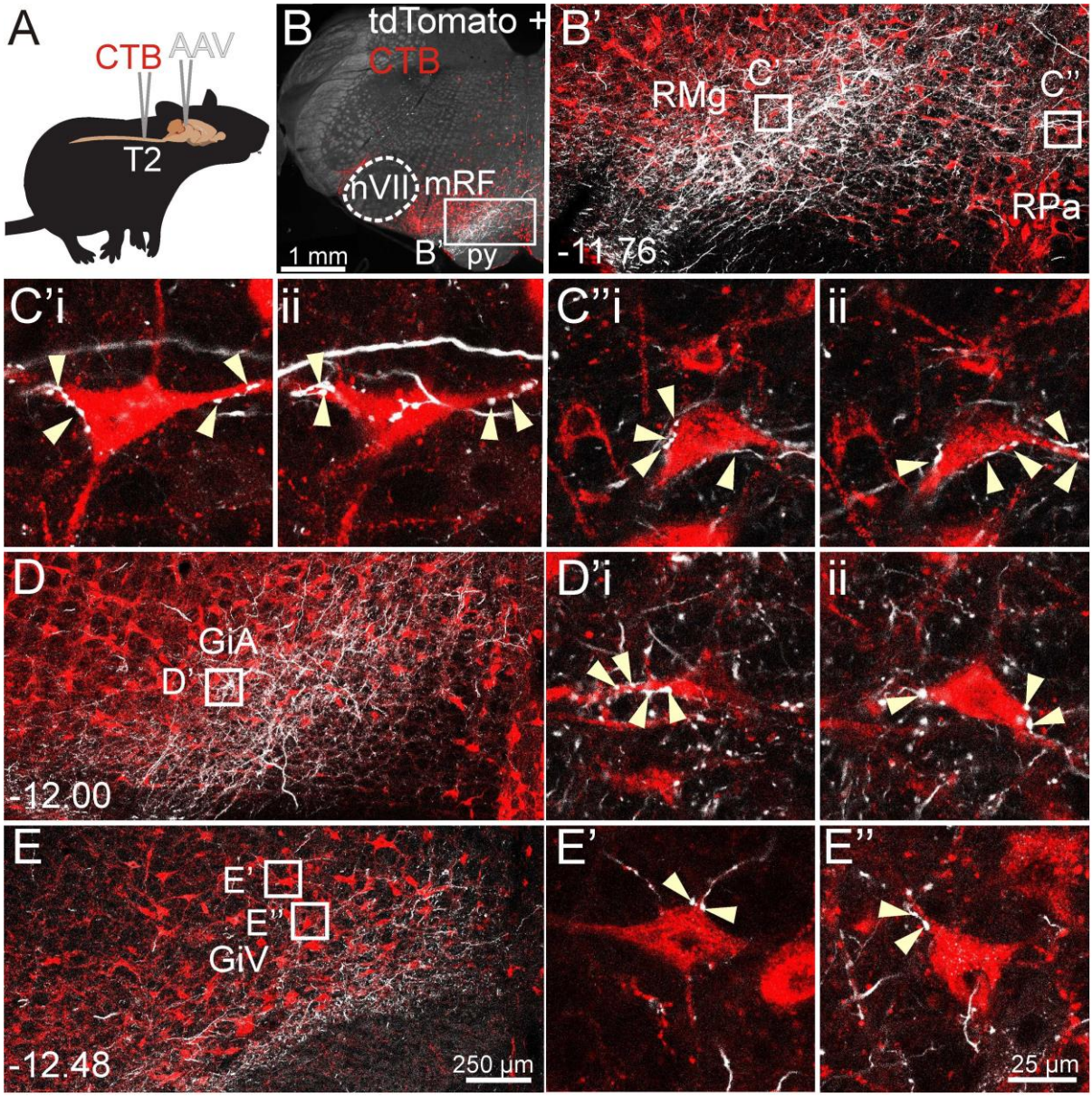

Figure 4.7 Putative terminals originating from the colliculus form close appositions with spinally projecting neurons in the medullary reticular formation (mRF). A: Schematic of combined retrograde tracing from the T2 spinal cord and anterograde tracing from the colliculi. Bii: coronal section of the T2 spinal cord demonstrating B: Micrograph of coronal medulla with tdTomato-labelled fibres (white) and spinally projecting neurons (red). Single optical plane micrographs of terminal field dorsal to pyramidal tract (py) at rostrocaudal levels -11.76 (B'), -12.00 (D'),-12.48 mm (E') from Bregma. Serial images of z-stack projection representing putative terminals forming close appositions (arrowheads) with spinally projecting neurons in the Raphe Magnus (RMg: C'i and C'ii), Raphe Palidus (RPa: C''i and C''ii), Gigantocellular reticular nucleus alpha (GiA: D'i and D'ii) and Gigantocellular reticular nucleus ventral (GiV: E' and E'').

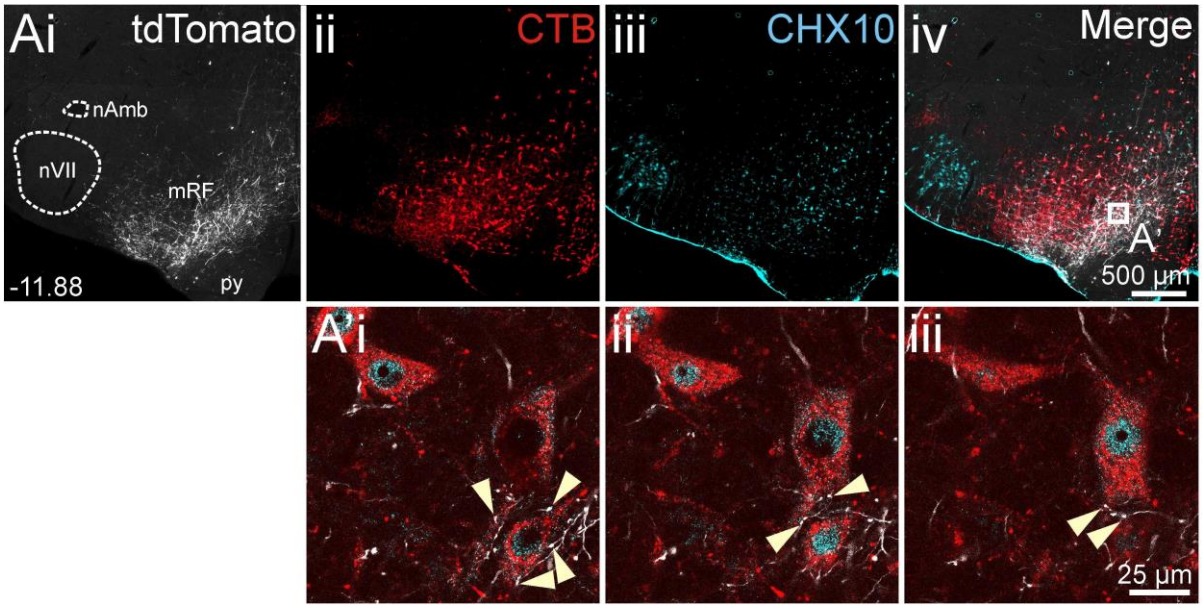

Figure 4.8 Collicular efferent projections terminate in the mRF and form close appositions with spinally projecting neurons that express the transcription factor CHX10. A: Micrograph of the coronal medulla with reporter-labelled fibres and putative terminals (Ai), retrogradely labelled neurons immunoreactive for CTB (Aii) and CHX10 (Aiii). Insets depict serial single optical plane images from a confocal z-stack that demonstrate terminal appositions (arrowheads) with three neurons that are immunoreactive for both CTB and CHX10 (A'i-iii). (nAmb: nucleus ambiguous; nVII: facial motor nucleus; mRF: medullary reticular formation).

The rostral ventrolateral medulla is not a substantial target of collicular efferent neurons

The lateral aspect of the medullary terminal field encroached upon the medial border of the RVLM C1 region, and under high magnification, sparse fine fibres and varicosities could be observed throughout the medial third of the RVLM. Given the key role played by the RVLM as a sympathoexcitatory relay, we closely examined C1 neurons for evidence of collicular terminal labelling. However, in contrast to the mRF/Raphe, we were unable to find evidence of terminal appositions (Figure 4.9A'). Similarly, spinally projecting RVLM neurons immunoreactive for CTB were substantially lateral of the terminal field and were not innervated (not shown). We conclude that the RVLM is not a major target of collicular efferents.

Collicular efferent neurons do not substantially target putative respiratory neurons in the pre-Bötzinger Complex

Our previous electrophysiological experiments found that colliculus disinhibition drove transient resetting of central respiratory rhythm with accompanying synchronised discharge in sympathetic and lumbar nerves. One obvious mechanism by which this could occur is by a direct innervation of the circuits that underlie the generation of

respiratory rhythm, which reside in anatomically, functionally, and neurochemically discrete compartments of the ventrolateral medulla. However, on the basis of the current study this scenario seems unlikely. First, we found no evidence of terminals immediately ventral to nucleus ambiguus in the region of the brainstem immediately caudal to the facial nucleus, corresponding to the region that contains most Bötzinger neurons.

Second, reporter labelling was largely absent at the level of the pre-Bötzinger Complex, and was not observed in more caudal areas associated with respiratory function (for example the rostral ventral respiratory group). Although fine fibres were occasionally encountered in more caudal sections corresponding to the region of the pre-Bötzinger complex, no evidence of appositions between putative axonal varicosities and neurons immunoreactive for the neurokinin-1 receptor (NK1R), considered a marker for putative inspiratory interneurons, were observed (Figure 4.9B').

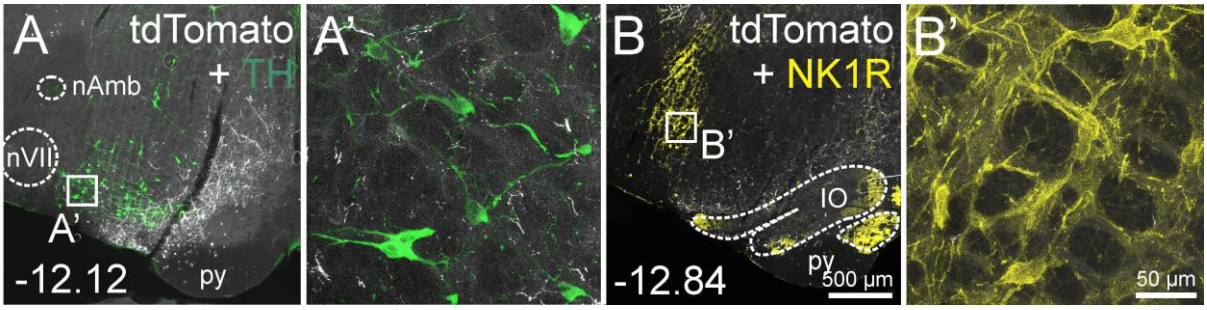

Figure 4.9 Labelled fibres were sparse in the rostral ventrolateral medulla (RVLM) and absent from the preBötzinger complex (PBC). Epifluorescence micrographs of the RVLM (A) and PBC (B) and accompanying maximum projections(A' and B') illustrate the absence of significant collicular terminals among TH- or neurokinin-1 receptor-immunoreactive neurons respectively. (nAmb: nucleus ambiguous; nVII: facial motor nucleus; py: pyramidal tract; IO: inferior olive).

Discussion

Collicular neurons play well-defined roles in the in the processing of sensory input and the coordination of motor commands (Dean *et al.*, 1989), thus the post-synaptic targets of this population have primarily been examined in the context of capacity for motor output. Recent functional evidence indicates that motor behaviour evoked via the colliculi also includes the parallel recruitment of sympathetic and respiratory outputs (Iigaya *et al.*, 2012; Muller-Ribeiro *et al.*, 2014). It would therefore be expected that the efferent termination of this population includes neural circuits associated with autonomic command.

The most direct potential pathway through which collicular efferents could mediate such effects would be innervation of the spinal neurons that control sympathetic, respiratory and motor activities (i.e. sympathetic preganglionic neurons and α-motoneurons respectively). However, in the current study anterograde tracing from regions of the colliculi previously demonstrated to drive synchronous bursts of splanchnic sympathetic, phrenic, and sciatic nerve activities revealed an extensive descending projection to the medulla that did not extend to the spinal cord

Following this observation, the next most plausible arrangement would be the innervation of pre-motor populations in the ventral medulla that control sympathetic, motor, and respiratory outputs. However, terminal labelling was conspicuously absent from two regions of the medulla frequently attributed with ordinant roles in transmission of sympathoexcitatory drive and generation of respiratory rhythm; the rostral ventrolateral medulla (RVLM) and ventral respiratory column respectively. The absence of collicular inputs on RVLM C1 neurons is consistent with the findings of Chapter 3; rabies labelled inputs to bulbospinal RVLM neurons included populations in the superior and inferior colliculus, but these were rostral to the region targeted in the current study. On the other hand, collicular terminals conspicuously innervated the medullary the adjacent medullary reticular formation (mRF). Neurons within this region serve integrative functions associated with both autonomic and motor command and ramify extensively throughout the brainstem and spinal cord.

It is logical to consider that autonomic and somatomotor functions are executed discretely due to the disparity in volitional control of these two systems. However, the

stimuli that activate the colliculus are distinct from the systems that govern volitional control of movement in everyday situations, and given that many behaviours (e.g. locomotion) require the simultaneous activation of both motor and autonomic effectors (Waldrop *et al.*, 2010), it would be expected that motor and autonomic outputs are driven simultaneously by a common pre-motor network. Interestingly, neurons that form integrated pre-motor output to sympathetic and somatomotor effectors (Allen & Cechetto, 1994; Kerman, 2008) and respiratory and somatomotor effectors (Billig *et al.*, 2000; Rice *et al.*, 2010) arise predominantly from the Raphe and mRF region in which we found the greatest collicular innervation. We posit this integrated relay underlies the synchronized responses we observed previously in response to stimulation of the colliculi (Iigaya *et al.*, 2012; Muller-Ribeiro *et al.*, 2014).

Technical limitations

In the current study we used AAV-driven reporter expression to visualise efferent projections from the colliculus. This approach has one major advantage compared to traditional anterograde tracers: AAV2 transduction is essentially restricted to neurons that reside within the injection site and therefore circumvents the non-selective uptake of conventional chemical tracers by fibres of passage (Glover *et al.*, 1986; Veenman *et al.*, 1992; Chen & Astonjones, 1995). Although some AAV subtypes have been associated with retrograde transduction profiles (Murlidharan *et al.*, 2014), we saw only a handful of retrogradely transduced somata lying in regions beyond the injection site, suggesting that the vast majority of reporter-filled axons and terminals originated from cell bodies within the colliculus.

AAV-mediated reporter expression was sufficient to resolve axonal varicosities, fine fibres and terminals, and was therefore considered appropriate for identification of major sites of synaptic termination. Identification of synaptic terminals was based on morphological observation alone and therefore potentially confounded by the presence of fibres of passage in the field of view – this confound was particularly problematic in reliably identifying terminals and varicosities in structures traversed by thick reporter-labelled axons en route to the brainstem, such as the KF. An attempt to resolve this shortcoming by quantifying the proportion of putative reporter-filled terminals that colocalised with synaptophysin immunoreactivity, a marker of synaptic terminals, was ultimately confounded by poor penetration of the anti-synaptophysin antibody (a

notorious limitation associated with staining for presynaptic proteins (Melone *et al.*, 2005)) and thus was subsequently abandoned. Recent developments in vector biology describe approaches that may circumvent this pitfall; (Esposito *et al.*, 2014) described an AAV vector that drives the expression of a synaptophysin-reporter fusion protein, limiting reporter expression to the synaptic terminals of transduced neurons, eliminating potential for false-positive identification of synaptic terminals. Similarly, Kim *et al.* (2012) describe a non-fluorescent cleaved GFP that becomes fluorescent when both subunits are in close physical proximity to one another. In this system, terminal-specific GFP recombination can be achieved by expression of one subunit in the pre-synaptic neuron and the other in the post-synaptic cell.

Notwithstanding the shortcomings discussed above, vector-mediated cytosolic reporter expression has been widely used as a reliable approach for anterograde tracing (Card *et al.*, 2006a; Abbott *et al.*, 2009a; Tan *et al.*, 2010). Given the prominence of the descending bundle in the level of the ponto-medullary junction, where thousands of intensely labelled fibre bundles split around the rostral margin of the facial nucleus, and the absence of labelling in the caudal medulla, it stands to reason that the fields observed in the ventromedial medulla represent the synaptic termination of the projection.

However, the identification of close appositions on histologically labelled post-synaptic neurons also comes with its own pitfalls. Previous studies note that putative synaptic contacts identified under light microscopy are not always in concordance with corresponding ultrastructural data. Murphy *et al.* (1995) found that physical synapses confirmed using "gold standard" electron microscopy approaches only constituted 50% of what would be considered synaptic contact under light microscopy. In a similar vein, it is important to note that not all axonal boutons even establish synaptic contact (Descarries & Mechawar, 2000). In the context of this study we concede that identification of close appositions, while suggestive of synaptic contacts, are not considered definitive.

Although these injections sites were determined to closely overlay the circumscribed region, previously characterised by (Muller-Ribeiro *et al.*, 2014) to generate an autonomic and somatomotor response, using the present tracing approach it is

impossible to determine if the labelled soma and projections we identified serve possess the same functional characteristics. An alternative approach compatible with injection site validation, would utilize an AAV variant that drives the expression of ChR2, thus transfected neurons from which tracing data would be acquired, could be functionally validated by assessment of autonomic and motor output to optogenetic stimulation of the injection site. Similarly, it is difficult to rule out the possibility of false positive, anterograde labelling that may have occurred due to "overspill" of the viral vector in adjacent brain regions during brain regions, despite efforts to only use tracing data from animals in which the bulk of virally labelled soma were restricted within the intended locality. A potential concern that would confound interpretation is labelling arising from neurons in the immediately adjacent PAG that have well described descending projections to autonomic nuclei in the ventral medulla (Carrive, 1993; Lovick, 1993; Hudson & Lumb, 1996).

Finally, the most extensive terminal field identified was in a region that encompassed subnuclei of the mRF/Raphe that has been previously associated with roles in the regulation of cardiovascular (Minson *et al.*, 1987; Cox & Brody, 1989; Varner *et al.*, 1992; Babic & Ciriello, 2004), respiratory (Fukuda *et al.*, 1993; Miura *et al.*, 1996; Morris *et al.*, 1996; Cao *et al.*, 2006; Depuy *et al.*, 2011) and somatomotor (Bretzner & Brownstone, 2013; Esposito *et al.*, 2014; Bouvier *et al.*, 2015) functions. However, the association between functional properties and neurochemical phenotype in this area is poor (with the exception of Chx10; see below). As a consequence, the discovery of putative boutons in close apposition to neurons that project to the thoracic spinal cord, although encouraging, is by no means sufficient to reliably infer function. Experiments addressing that question are ongoing, but do not form part of the current thesis.

Medullary targets of collicular output neurons

Reporter-labelled efferent fibre bundles projected rostrally to the midbrain, thalamus, and hypothalamus, and caudally, where terminal fields were identified in the pons and medulla. Rostral targets included brain regions with previously reported roles in the control of respiratory and sympathetic activities, such as the PVN. However, our previous experiments demonstrated that multimodal burst responses to disinhibition of the colliculi were persistent after pre-collicular decerebration, which included removal of the prefrontal cortex, amygdala, auditory cortex, and the dorsomedial, perifornical,

and lateral hypothalamus (Muller-Ribeiro *et al.*, 2014), which would have eliminated the rostral projection described here, so consideration of our results will be restricted to the descending fibre bundle.

AAV-mediated reporter expression revealed a dominant projection from the colliculi to the ventral medulla. Interestingly, this projection was absent or sparse in experiments where injection sites failed to encompass the region of the colliculi circumscribed by Muller-Ribeiro *et al.* (2014), suggesting that projections to the ventral medulla arise exclusively from neurons that lie within this particular region of the colliculi. Consultation with the "Allen Mouse Brain Connectivity Atlas" (Oh *et al.*, 2014) reaffirms this observation; an experiment described in the atlas, with a similar injection site to those attained in the present study (experiment 113072328), exhibited a robust projection to the ventral medulla. Conversely, experiments described in the atlas in which the injection sites prominently fell within adjacent, dorsal (experiment 100142706) or lateral (experiment 100145841) regions of the SC lacked projections to the brainstem altogether.

A predicted outcome of the present study was a projection to the spinal cord, an observation previously described in studies that used traditional anterograde tracers (e.g. WGA-HRP) (Huerta & Harting, 1982; Redgrave *et al.*, 1987). We found no evidence of a direct spinal projection: the prominent descending track had become sparse by the time it reached the caudal medulla and virtually absent from the spinal cord, which is in concordance with the observations of early axonal degeneration studies from the region (Nyberg-Hansen, 1964, 1966; Petras, 1967). We suspect that these differences may reflect uptake of WGA by spinally projecting collicular neurons that lie rostral and dorsal of the injection sites in the current study, either as a result of direct injection or uptake by fibres of passage that traversed the injection site (Murray & Coulter, 1982). Viral based anterograde studies described in the Allen Mouse Brain Connectivity Atlas that map projections from injection sites in rostral regions of the SC, adjacent to the injection sites described in the current study (experiments 100142302 and 100143833) produced a distinct projection to the spinal cord that was compact and concentrated exclusively to the midline of the caudal medulla. These observations suggest that spinal projections from the colliculus are most likely restricted to exclusively pre-motor

regions of the rostral SC, which lie outside of the active region we described previously (Muller-Ribeiro *et al.*, 2014).

The mRF/Raphe terminal field contains neurons that regulate sympathetic, respiratory, and somatomotor output

The densest medullary innervation encompassed a region of the mRF, which overlaid the RVMM, RMg, RPa and GiA, the ventral aspects of the GiV and ROb and the lateral most aspects of the LPGi, LPGiE. Delineating structure function relationships from this region is notoriously difficult due the functional heterogeneity of overlapping populations and lack of anatomically discrete nuclei. For ease of diction this termination site will be henceforth referred to collectively as the mRF.

Our focused examination of the mRF identified putative terminal appositions on neurons retrogradely labelled with CTB. Ideally these neurons would be representative of sympathetic pre-motor neurons as the injection was focused to the IML within the T2 spinal segment, a region that contains the majority of SPN which contribute to vasomotor output (Strack *et al.*, 1988), however as described above it is difficult to determine the post-synaptic targets of these neurons.

The neurons in the mRF, primarily the Raphe and RVMM, form a major source of the pre-motor input to sympathetic nerves, as determined by retrograde transynaptic tracing from sympathetic paravertebral ganglia, the kidney, the adrenal gland and the vascular beds of skeletal muscle (Strack *et al.*, 1989a; Schramm *et al.*, 1993; Jansen *et al.*, 1995; Farkas *et al.*, 1998; Lee *et al.*, 2007). Retrograde tracing with conventional tracers demonstrates a projection to the IML at all levels of the spinal cord and anterograde tracing from the mRF also demonstrates projections to the IML and cardioinhibitory parasympathetic motor neuron populations in the medulla, including the nucleus of the solitary tract, nucleus ambiguus and dostral motor nucleus of the vagus (Hermann *et al.*, 2003; Babic & Ciriello, 2004). Retrograde tracing from the medial mRF in the cat (Wang & Wessendorf, 2002), sparsely labels neurons distributed in a region of the external cortex of the inferior colliculus similar to that described by (Muller-Ribeiro *et al.*, 2014).

Functional data also support sympathoexcitatory roles for the RVMM neurons: The RVMM terminal site overlays a well-established pressor region (Willette *et al.*, 1983a; Minson *et al.*, 1987; Cox & Brody, 1989; Varner *et al.*, 1992; Babic & Ciriello, 2004),

contains neurons that differentially express c-fos after baroreceptor unloading (Minson *et al.*, 1996) and are silenced by baroreceptor loading (Pilowsky *et al.*, 1995).The RVMM contains neurons that contribute to basal vasomotor tone in the arterial (Cox & Brody, 1989; Varner *et al.*, 1989) and cutaneous circulation (Blessing, 2005; Shafton & McAllen, 2013) as well as neurons that innervate parasympathetic sites (Thurston & Randich, 1995) and mediate the activation of non-vasomotor effectors including brown adipose tissue (BAT) and the urogenital tract and perineal muscles (Johnson & Hubscher, 1998, 2000).

Neurons within the mRF, primarily the Raphe, also contribute to the regulation of respiratory output: stimulation of the ROb and RMg, drives both increases (Depuy *et al.*, 2011) and decreases in respiratory frequency (Cao *et al.*, 2006) Focal cooling or lesion of the parapyramidal RVMM elicits a reduction in respiratory frequency (Fukuda *et al.*, 1993) and abolishes normal hyperpneic and tachypneic responses to hypercapnia (Miura *et al.*, 1996). These respiratory effects are potentially mediated via efferent projections to respiratory pre-motor neurons of the ventral and dorsal respiratory groups (Smith *et al.*, 1989a; Ellenberger & Feldman, 1990), direct projections to phrenic motor neurons (Dobbins & Feldman, 1994; Yates *et al.*, 1999; Lois *et al.*, 2009; Depuy *et al.*, 2011) and accessory respiratory muscles (Shintani *et al.*, 2003), and via vagal pre-ganglionic neurons that innervate the upper airways (Hadziefendic & Haxhiu, 1999).

The mRF also forms a substantial component of the descending motor pathway, relaying command from higher order centres to the motor neurons in the brainstem and spinal cord (Drew *et al.*, 2004; Lemon, 2008). The single unit activity of these neurons correlate with motor behaviours (reviewed Siegel (1979) and stimulation of the mRF has been demonstrated to drive the activity of lumbar axial muscles (Femano *et al.*, 1984).

Anterograde tracing from the mRF/Raphe has extensively defined termination on motor neurons in the spinal cord (Holstege & Kuypers, 1987; Rubelowski *et al.*, 2013; Liang *et al.*, 2015) and recent studies using monosynaptically restricted viral tracing strategy (SADΔG rabies) have unambiguously identified sub-populations within the mRF that contribute to the pre-motor networks that control limb movement (Stepien *et al.*, 2010; Esposito *et al.*, 2014).

In the present study we observed collicular innervation of a subpopulation of neurons in the mRF that express CHX10, a transcription factor that denotes V2a neurons, a subset of excitatory interneurons distributed along the spinal cord and hindbrain that arise from the p2 progenitor domain population during development (inter alia: Cepeda-Nieto *et al.*, 2005). These neurons are considered to primarily serve in the coordination of motor behaviours (Bretzner & Brownstone, 2013) and have been implicated as critical to respiratory function. Crone *et al.* (2012) demonstrated that CHX10 neurons provide excitatory input to the VRC including putative inspiratory neurons in the PBC. Transgenic mice with a depleted CHX10 population exhibit reduced breathing frequency and gasping, which is ultimately fatal. Further experiments by Crone *et al.* (2012) demonstrated that inspiratory deficit in these mice was persistent in a reduced preparation of the central respiratory pattern generator, suggesting that the influence of CHX10 neurons in the mRF over respiration is mediated via direct projections of these neurons to the Pre-Bötzinger Complex. CHX10 neurons are also implicated in somatomotor control; they are activated during locomotor activity (Bretzner & Brownstone, 2013), and their selective inhibition evokes cessation of locomotion (Bouvier *et al.*, 2015).

The diverse functional attributes of this region and the dense innervation received from the colliculus, lead us to consider the rMF as the most feasible candidate for the relay of descending collicular command.

Other targets of significance

Although the main efferent output from the colliculus seemed to terminate in the mRF, we also observed evidence of substantial input to the A5, A6 (locus coeruleus) and A7 noradrenergic cell groups of the rostral brainstem. We observed putative terminal appositions on TH- and CTB-immunoreactive neurons in all 3 nuclei, although appositions in A5 were substantially less frequent than A6 or A7. From a functional standpoint, A5 and A6 are implicated in respiratory command (Hilaire *et al.*, 2004) and, similar to the mRF, all three provide input to sympathetic and somatomotor targets (Kerman, 2008). Thus it is plausible that the A5, A6 and A7 may contribute to synchronous autonomic and motor output driven by the colliculi. We also examined the KF, which is a well-established source of input to respiratory nuclei in the medulla (Dutschmann *et al.*, 2004; Ezure & Tanaka, 2006). Although we were able establish the

presence of fibres and putative terminals in the KF, the input was relatively minor, and detailed investigation was hampered by the lack of a well-established functional marker in this region.

Functional significance

The directive of this study was to identify pathways responsible for the previously demonstrated collicular command of respiratory, sympathetic or somatomotor command in response to disinhibition. An ideal first step would be to directly test the consequences of selective activation of the pathway that links the colliculus to the rMF *in vivo*; indeed, initial experiments based on an optogenetic strategy were attempted, but failed due to poor vector performance. In the absence of functional data, it is important to temper inference of our results with acknowledgement of the limitations of purely structural data. Simply put, studying the components of a circuit in isolation is insufficient to determine its role in mediating behaviour. Ultimately, the function(s) served by a circuit remain unknown until the outcomes of perturbing its components are realised. In this case, we at best demonstrate the set of pathways by which the colliculi exerts its influence, and these include nuclei that mediate sympathetic, respiratory and somatomotor activity *inter alia*. Nonetheless, the anatomical data presented here suggest clear hypotheses that can be tested.

CHAPTER 5: Synthesis and Future Directions

Inhibition or stimulation of the RVLM drives profound effects on baseline sympathetic nerve activity and blood pressure, and its lesion inhibits a wide variety of adaptive vasomotor reflexes, suggesting it as a key site of homeostatic control and reflex integration. Single unit recordings from neurons identified as bulbospinal and barosensitive, widely accepted as criteria for putative sympathetic premotor neurons, indicate that convergence of diverse inputs occurs at a single-cell level. However, the organization of the network of neurons that regulates sympathetic nerve activity, via convergent synaptic drive to sympathetic premotor neurons, is poorly resolved due to the limitations of conventional tracing approaches. Mapping the organization of this network was the central goal of the current thesis; the results of which will serve as a platform for the generation of new hypotheses and the testing of existing theories regarding the origins of vasomotor command, a key outcome of which is to determine the neurogenic contributors to hypertensive pathology.

Ultimately, my goal was to selectively label the brain wide set of neurons that form direct input to RVLM sympathetic pre-motor neurons. The key hurdle for this tracing project was to devise an approach that permitted the expression of transgenes complementary to the SADΔG tracing paradigm (the TVA receptor and rabies glycoprotein) in RVLM sympathetic premotor neurons. Initially we focused on establishing a method by which transgene expression could be targeted to single neurons based on functional criteria, as this would provide a powerful means to resolve the structure of a circuit within the functional context of its summative output. Previous investigations had demonstrated that single cell delivery via a patch pipette or electroporation was an effective means by which to trace the circuits of a functionally defined target (Rancz *et al.*, 2011; Velez-Fort *et al.*, 2014; Wertz *et al.*, 2015).

This trajectory of investigation led us to integrate single unit recording approaches with single cell electroporation (SCE) as a means by which to achieve transfection of single neurons in deeper brain structures. This innovation required the modification of a standard single unit recording kit to deliver electrical pulses that evoked dielectric breakdown of the cell membrane. In our hands, this approach worked very well *in vitro* but was difficult to perform reliably *in vivo*, where transfection was only possible following rigorous adherence to a number of electrophysiological criteria. This approach

may prove an effective means of optical guidance free gene delivery to more superficial targets, where pipette blockage is less frequent..

The technique we developed rivals the current gold-standard single-cell dye labeling technique in terms of ease of application and the level of morphological detail that can be achieved: we have recently demonstrated the practicality of our approach, in lieu of the juxtacellular technique, for the labelling of medullary respiratory neurons *in vivo* (Le *et al.*, 2015). However, despite its initial promise, we ultimately decided that the throughput was likely to be too low to make this strategy feasible within the available time, in particular when considering the foreseeable compounding difficulties incumbent with functionally validating recorded units (e.g. antidromic stimulation). We instead decided to pursue the same goal using a vector-based approach to target putative sympathetic premotor neurons.

Although many studies have focused on the expression of catecholamine-biosynthetic enzymes as a genetic access point (Card *et al.*, 2006a; Abbott *et al.*, 2013) to RVLM sympathetic premotor neurons, we instead opted to use their axonal projection to the thoracic spinal cord as the basis for our transduction strategy. This was based on the significant proportion of RVLM C1 neurons that do not project to the spinal cord (~2/3), the high proportion of functionally identified sympathetic premotor neurons that are not C1 (~1/2), and the functional diversity of the C1 population. Although the retrograde vectors used in this study transduced a band of spinally projecting neurons that included neurons throughout the brain including other nearby cell groups (RVMM and Raphe), careful targeting of the epicenter of the bulbospinal TH group with our rabies injections led to a restricted seeding of neurons within the anatomical boundaries of the RVLM and included a combination of C1 and non-C1 neurons. The major drawback of this approach is the ambiguity of the RVLM seed population with regard to their postsynaptic target in the spinal cord. Although HSV injections were targeted to the IML, the injections were massive (2x~500nL), generating lesions that encompassing an area approximately 400μm in diameter that included the IML at its centre, much of the IV, V, VI and VII laminae and surrounding white matter. Thus, the seed population probably includes amongst IML terminating sympathetic pre-motor neurons, neurons that form input to somatomotor pathways (and others). Therefore at best we have mapped the input network of spinally projecting RVLM neurons.

Overall the distribution of the RVLM connectome is consistent with generally accepted pre-autonomic circuit models (reviewed by Dampney, 1994b; Guyenet, 2006). We identified prominent inputs from well-established neurohumoral and viscero-sympathetic actuators such as the area postrema and NTS, and inputs that spanned medullary autonomic (A5, RVLM, ventromedial medulla, CVLM, nucleus ambiguus) and supramedullary autonomic nuclei (ventrolateral PAG, colliculi and pontine parabrachial nuclei). Importantly, our study identified a direct connection between nuclei constituting the respiratory pattern generator nuclei (Bötzinger, pre-Bötzinger Complex, rostral ventral respiratory group) and the RVLM, providing a potential anatomical basis for the well documented observation of respiratory modulation of sympathetic outflow, a process that is enhanced in models of neurogenic hypertension (Zoccal *et al.*, 2008; Simms *et al.*, 2009; Oliveira-Sales *et al.*, 2016). A notable deviation from the standard model is the discovery of a numerically significant input from the region of the prepositus hypoglossi, a brainstem nucleus conventionally associated with vestibulo-occulomotor integration (McCrea, 1988). This region has been previously shown to drive pressor responses to glutamate microinjection (Talman & Robertson, 1991) but is not labelled by conventional retrograde tracers, suggesting that synaptic contact may occur on the distal dendrites of RVLM sympathetic pre-motor neurons, that lie outside of the RVLM.

However, the most striking feature of the connectome is its diffuse distribution (rather than the highly nodal schemes often used to conceptualize it: Dampney, 1994a; Pilowsky & Goodchild, 2002; Guyenet, 2006) and its strong weighting towards local inputs, with around 14% of input neurons residing within the boundary of the RVLM region and 50% of inputs lying within 3 mm of the RVLM epicenter. In contrast, the dataset includes a relatively low number of inputs from the forebrain and midbrain, and a virtual absence of inputs from locus coeruleus, the amygdala, cortex and subfornical organ and median preoptic nucleus, despite compelling prior evidence for both functional and neuroanatomical connectivity (Dampney *et al.*, 1987; Gelsema *et al.*, 1989; Verberne, 1996; Saha, 2005; Card *et al.*, 2011; Bou-Farah *et al.*, 2015). This unexpected finding is unlikely to represent a limitation of SADΔG(EnvA), as distance is not thought to impair its labelling efficiency (Callaway & Luo, 2015; Schwarz *et al.*, 2015). The most parsimonious explanation is that input from these sources are routed via a polysynaptic relay involving RVLM interneurons.

In addition, we demonstrated the suitability of volumetric brain atlases for connectomic analysis. Using a relatively primitive workflow we were able to render >300 Gb of imaging data to <100 kb of Cartesian coordinates that are immediately amenable to statistical analysis. The approach allows the quantification, standardization and sharing of complete neuroanatomical datasets, and therefore provides a platform by which researchers may independently visualize, analyze and compare each other's data. Bioinformatics at a single-cell resolution may allow researchers to move beyond the ball-and-stick diagrams often used to conceptualize the organization of spatially diffuse real-world neuronal networks (Rockland, 2015) and realize the full potential of novel connectomic technologies.

Experiments conducted previously in our lab indicated that a defined region of the SC and IC was capable of driving patterned motor ouput, which included a significant sympathetic component (Muller-Ribeiro *et al.*, 2014). We hypothesized that the RVLM was a likely target of this sympathetic command to mediate this response. The observations of Chapter 3 indicated a sparse source of input from the inferior colliculus, however these inputs were not from the region previously demonstrated to drive synchronous output. The examination of anterograde tracing from the colliculi confirmed this, termination within the RVLM was sparse. We determined that a dense termination within the adjacent mRF was the likely site of sympathetic recruitment (among others). We lacked a neurochemical phenotype after failing to observed close apposition with serotonergic neurons in this region. However retrograde tracing from the spinal cord revealed that collicular afferents formed putative synaptic contacts with spinally projecting mRF neurons, including a population that expressed the transcription factor CHX10, a phenotype previously implicated in respiratory and motor command.

We are left in the overt position to begin investigation of the pathways we identified in Chapters 3 and 4 to determine their functional contribution to behavior. In combination with viral vectors, optogentic tools present an opportunity to examine the action of a particular neuron population, pathway or termination with rapid temporal control, through excitation and inhibition with light (Packer *et al.*, 2013). This now widely adopted technique has made the manipulation of defined circuits accessible in the behaving animal, acute anaesthetized preparation and the brain slice. We have begun to

investigate the mRF relay using an anterograde vector (similar to the AAV described in Chapter 3) to anterogradely express channel rhodopsin 2 within collicular terminals. These experiments will allow us to determine whether the mRF serves as the critical juncture from collicular driven autonomic command (as demonstrated in past physiology experiments). The pathways defined in the Chapter 4 may be investigated in a similar manner. Anterograde terminal stimulation may be an appropriate approach to examine inputs from well delineated sources (i.e. the nucleus prepositus), however more embedded sources would require a more finessed approach, in particular those arising from respiratory nuceli in proximity to the RVLM and CVLM.

Final thoughts

The promise of the connectomic approach is reflected by its widespread adoption and the continued refinement of viral vectors for transynaptic tracing (Osakada *et al.*, 2011; Mitra, 2014; McGovern *et al.*, 2015; Kim *et al.*, 2016). In combination with functional genetic technologies, the emergence of restricted, transynaptic tracers have fostered a "seek and destroy" approach to intersectional neuroscience that is rapidly characterizing long sought after connectivity schemes throughout the brain (e.g.(Weber *et al.*, 2015; Wei *et al.*, 2015; Roseberry *et al.*, 2016). As these technologies are further improved and inevitably find their place as a standard laboratory tool for neuroscientists everywhere, many of the questions that remain, regarding circuit structure and function may soon be resolved.

“Ever tried. Ever failed. No matter. Try Again. Fail again. Fail better”

- Samuel Beckett.

REFERENCES

Abbott SB, DePuy SD, Nguyen T, Coates MB, Stornetta RL & Guyenet PG. (2013). Selective optogenetic activation of rostral ventrolateral medullary catecholaminergic neurons produces cardiorespiratory stimulation in conscious mice. *The Journal of neuroscience : the official journal of the Society for Neuroscience* **33,** 3164-3177.

Abbott SB & Pilowsky PM. (2009). Galanin microinjection into rostral ventrolateral medulla of the rat is hypotensive and attenuates sympathetic chemoreflex. *Am J Physiol Regul Integr Comp Physiol* **296,** R1019-1026.

Abbott SB, Stornetta RL, Fortuna MG, Depuy SD, West GH, Harris TE & Guyenet PG. (2009a). Photostimulation of retrotrapezoid nucleus phox2b-expressing neurons in vivo produces long-lasting activation of breathing in rats. *The Journal of neuroscience : the official journal of the Society for Neuroscience* **29,** 5806-5819.

Abbott SB, Stornetta RL, Socolovsky CS, West GH & Guyenet PG. (2009b). Photostimulation of channelrhodopsin-2 expressing ventrolateral medullary neurons increases sympathetic nerve activity and blood pressure in rats. *J Physiol* **587,** 5613-5631.

Adams DB, Baccelli G, Mancia G & Zanchetti A. (1971). Relation of cardiovascular changes in fighting to emotion and exercise. *J Physiol* **212,** 321-335.

Adrian ED, Bronk DW & Phillips G. (1932). Discharges in mammalian sympathetic nerves. *J Physiol* **74,** 115-133.

Affleck VS, Coote JH & Pyner S. (2012). The projection and synaptic organisation of NTS afferent connections with presympathetic neurons, GABA and nNOS neurons in the paraventricular nucleus of the hypothalamus. *Neuroscience* **219,** 48-61.

Agarwal SK & Calaresu FR. (1991). Monosynaptic connection from caudal to rostral ventrolateral medulla in the baroreceptor reflex pathway. *Brain Res* **555,** 70-74.

Agassandian K, Shan Z, Raizada M, Sved AF & Card JP. (2012). C1 catecholamine neurons form local circuit synaptic connections within the rostroventrolateral medulla of rat. *Neuroscience* **227,** 247-259.

Aicher SA, Saravay RH, Cravo S, Jeske I, Morrison SF, Reis DJ & Milner TA. (1996). Monosynaptic projections from the nucleus tractus solitarii to C1 adrenergic neurons in the rostral ventrolateral medulla: comparison with input from the caudal ventrolateral medulla. *J Comp Neurol* **373,** 62-75.

Alexander RS. (1946). Tonic and reflex functions of medullary sympathetic cardiovascular centers. *Journal of neurophysiology* **9,** 205-217.

Allen AM & Guyenet PG. (1993). Alpha 2-adrenoceptor-mediated inhibition of bulbospinal barosensitive cells of rat rostral medulla. *Am J Physiol* **265,** R1065-1075.

Allen GV & Cechetto DF. (1994). Serotoninergic and nonserotoninergic neurons in the medullary raphe system have axon collateral projections to autonomic and somatic cell groups in the medulla and spinal cord. *The Journal of comparative neurology* **350,** 357-366.

Amendt K, Czachurski J, Dembowsky K & Seller H. (1979). Bulbospinal projections to the intermediolateral cell column: a neuroanatomical study. *J Auton Nerv Syst* **1,** 103-107.

Andresen MC & Yang M. (1995). Dynamics of sensory afferent synaptic transmission in aortic baroreceptor regions on nucleus tractus solitarius. *Journal of neurophysiology* **74,** 1518-1528.

Appel NM & Elde RP. (1988). The intermediolateral cell column of the thoracic spinal cord is comprised of target-specific subnuclei: evidence from retrograde transport studies and immunohistochemistry. *The Journal of neuroscience : the official journal of the Society for Neuroscience* **8,** 1767-1775.

Apps R & Ruigrok TJ. (2007). A fluorescence-based double retrograde tracer strategy for charting central neuronal connections. *Nat Protoc* **2,** 1862-1868.

Araujo GC, Lopes OU & Campos RR. (1999). Importance of glycinergic and glutamatergic synapses within the rostral ventrolateral medulla for blood pressure regulation in conscious rats. *Hypertension* **34,** 752-755.

Aston-Jones G & Card JP. (2000). Use of pseudorabies virus to delineate multisynaptic circuits in brain: opportunities and limitations. *Journal of neuroscience methods* **103,** 51-61.

Azevedo FA, Carvalho LR, Grinberg LT, Farfel JM, Ferretti RE, Leite RE, Jacob Filho W, Lent R & Herculano-Houzel S. (2009). Equal numbers of neuronal and nonneuronal cells make the human brain an isometrically scaled-up primate brain. *The Journal of comparative neurology* **513,** 532-541.

Babic T & Ciriello J. (2004). Medullary and spinal cord projections from cardiovascular responsive sites in the rostral ventromedial medulla. *The Journal of comparative neurology* **469,** 391-412.

Badoer E. (2001). Hypothalamic paraventricular nucleus and cardiovascular regulation. *Clin Exp Pharmacol Physiol* **28,** 95-99.

Badoer E & Merolli J. (1998). Neurons in the hypothalamic paraventricular nucleus that project to the rostral ventrolateral medulla are activated by haemorrhage. *Brain research* **791,** 317-320.

Bailey TW, Hermes SM, Andresen MC & Aicher SA. (2006). Cranial visceral afferent pathways through the nucleus of the solitary tract to caudal ventrolateral medulla or paraventricular hypothalamus: target-specific synaptic reliability and convergence patterns. *The Journal of neuroscience : the official journal of the Society for Neuroscience* **26,** 11893-11902.

Barman SM & Gebber GL. (1987). Lateral tegmental field neurons of cat medulla: a source of basal activity of ventrolateral medullospinal sympathoexcitatory neurons. *J Neurophysiol* **57,** 1410-1424.

Barman SM & Gebber GL. (1989). Basis for the naturally occurring activity of rostral ventrolateral medullary sympathoexcitatory neurons. *Prog Brain Res* **81,** 117-129.

Barman SM & Gebber GL. (1992). Rostral ventrolateral medullary and caudal medullary raphe neurons with activity correlated to the 10-Hz rhythm in sympathetic nerve discharge. *J Neurophysiol* **68,** 1535-1547.

Barman SM, Gebber GL & Orer HS. (2000). Medullary lateral tegmental field: an important source of basal sympathetic nerve discharge in the cat. *American Journal of Physiology-Regulatory Integrative and Comparative Physiology* **278,** R995-R1004.

Barnett EM, Evans GD, Sun N, Perlman S & Cassell MD. (1995). Anterograde tracing of trigeminal afferent pathways from the murine tooth pulp to cortex using herpes simplex virus type 1. *The Journal of neuroscience : the official journal of the Society for Neuroscience* **15,** 2972-2984.

Beacham WS & Perl ER. (1964). Background and Reflex Discharge of Sympathetic Preganglionic Neurones in the Spinal Cat. *J Physiol* **172,** 400-416.

Beckert A, Geue L, Vos A, Neubert A, Freuling C & Muller T. (2009). Genetic stability (in vivo) of the attenuated oral rabies virus vaccine SAD B19. *Microbiology and immunology* **53,** 16-21.

Bestman JE, Ewald RC, Chiu S-L & Cline HT. (2006). In vivo single-cell electroporation for transfer of DNA and macromolecules. *Nat Protocols* **1,** 1267-1272.

Betley JN & Sternson SM. (2011). Adeno-Associated Viral Vectors for Mapping, Monitoring, and Manipulating Neural Circuits. *Human Gene Therapy* **22,** 669-677.

Bevan MD. (1998). Selective innervation of neostriatal interneurons by a subclass of neuron in the globus pallidus of the rat. *Journal of Neuroscience* **18,** 9438-9452.

Billig I, Foris JM, Enquist LW, Card JP & Yates BJ. (2000). Definition of neuronal circuitry controlling the activity of phrenic and abdominal motoneurons in the ferret using recombinant strains of pseudorabies virus. *J Neurosci* **20,** 7446-7454.

Blessing WW. (1988). Depressor neurons in rabbit caudal medulla act via GABA receptors in rostral medulla. *Am J Physiol* **254,** H686-692.

Blessing WW. (2005). BAT control shows the way: medullary raphe/parapyramidal neurons and sympathetic regulation of brown adipose tissue. *American journal of physiology Regulatory, integrative and comparative physiology* **288,** R557-560.

Blessing WW, Goodchild AK, Dampney RA & Chalmers JP. (1981). Cell groups in the lower brain stem of the rabbit projecting to the spinal cord, with special reference to catecholamine-containing neurons. *Brain Res* **221,** 35-55.

Blessing WW & Nalivaiko E. (2000). Regional blood flow and nociceptive stimuli in rabbits: patterning by medullary raphe, not ventrolateral medulla. *J Physiol-London* **524,** 279-292.

Bou-Farah L, Bowman BR, Bokiniec P, Karim S, Le S, Goodchild AK & McMullan S. (2015). Somatostatin in the rat rostral ventrolateral medulla: Origins and mechanism of action. *J Comp Neurol* **In Press**.

Boucetta S, Cisse Y, Mainville L, Morales M & Jones BE. (2014). Discharge profiles across the sleep-waking cycle of identified cholinergic, GABAergic, and glutamatergic neurons in the pontomesencephalic tegmentum of the rat. *J Neurosci* **34,** 4708-4727.

Bouvier J, Caggiano V, Leiras R, Caldeira V, Bellardita C, Balueva K, Fuchs A & Kiehn O. (2015). Descending Command Neurons in the Brainstem that Halt Locomotion. *Cell* **163,** 1191-1203.

Bowman BR, Kumar NN, Hassan SF, McMullan S & Goodchild AK. (2013). Brain sources of inhibitory input to the rat rostral ventrolateral medulla. *J Comp Neurol* **521,** 213-232.

Braeken D, Jans D, Huys R, Stassen A, Collaert N, Hoffman L, Eberle W, Peumans P & Callewaert G. (2012). Open-cell recording of action potentials using active electrode arrays. *Lab on a Chip - Miniaturisation for Chemistry and Biology* **12,** 4397-4402.

Branco T & Staras K. (2009). The probability of neurotransmitter release: variability and feedback control at single synapses. *Nature reviews Neuroscience* **10,** 373-383.

Brandao ML, Tomaz C, Borges PCL, Coimbra NC & Bagri A. (1988). Defense Reaction Induced by Microinjections of Bicuculline into the Inferior Colliculus. *Physiol Behav* **44,** 361-365.

Brennand KJ, Simone A, Jou J, Gelboin-Burkhart C, Tran N, Sangar S, Li Y, Mu Y, Chen G, Yu D, McCarthy S, Sebat J & Gage FH. (2011). Modelling schizophrenia using human induced pluripotent stem cells. *Nature* **473,** 221-225.

Bretzner F & Brownstone RM. (2013). Lhx3-Chx10 reticulospinal neurons in locomotor circuits. *The Journal of neuroscience : the official journal of the Society for Neuroscience* **33,** 14681-14692.

Briggman KL, Helmstaedter M & Denk W. (2011). Wiring specificity in the direction-selectivity circuit of the retina. *Nature* **471,** 183-188.

Brown DL & Guyenet PG. (1984). Cardiovascular neurons of brain stem with projections to spinal cord. *The American journal of physiology* **247,** R1009-1016.

Brown DL & Guyenet PG. (1985). Electrophysiological Study of Cardiovascular Neurons in the Rostral Ventrolateral Medulla in Rats. *Circulation research* **56,** 359-369.

Bryant TH, Yoshida S, de Castro D & Lipski J. (1993). Expiratory neurons of the Botzinger Complex in the rat: a morphological study following intracellular labeling with biocytin. *J Comp Neurol* **335,** 267-282.

Burke PG, Abbott SB, Coates MB, Viar KE, Stornetta RL & Guyenet PG. (2014). Optogenetic stimulation of adrenergic C1 neurons causes sleep state-dependent cardiorespiratory stimulation and arousal with sighs in rats. *Am J Respir Crit Care Med* **190,** 1301-1310.

Burke PG, Neale J, Korim WS, McMullan S & Goodchild AK. (2011). Patterning of somatosympathetic reflexes reveals nonuniform organization of presympathetic drive from C1 and non-C1 RVLM neurons. *Am J Physiol Regul Integr Comp Physiol* **301,** R1112-1122.

Callaway EM. (2005). A molecular and genetic arsenal for systems neuroscience. *Trends in neurosciences* **28,** 196-201.

Callaway EM. (2008). Transneuronal circuit tracing with neurotropic viruses. *Curr Opin Neurobiol* **18,** 617-623.

Callaway EM & Luo L. (2015). Monosynaptic Circuit Tracing with Glycoprotein-Deleted Rabies Viruses. *J Neurosci* **35,** 8979-8985.

Campos RR & McAllen RM. (1999). Tonic drive to sympathetic premotor neurons of rostral ventrolateral medulla from caudal pressor area neurons. *Am J Physiol* **276,** R1209-1213.

Cao Y, Matsuyama K, Fujito Y & Aoki M. (2006). Involvement of medullary GABAergic and serotonergic raphe neurons in respiratory control: electrophysiological and immunohistochemical studies in rats. *Neuroscience research* **56,** 322-331.

Carandini M. (2012). From circuits to behavior: A bridge too far? *Nature Neuroscience* **15,** 507-509.

Card JP & Enquist LW. (1995). Neurovirulence of pseudorabies virus. *Critical reviews in neurobiology* **9,** 137-162.

Card JP, Kobiler O, McCambridge J, Ebdlahad S, Shan Z, Raizada MK, Sved AF & Enquist LW. (2011). Microdissection of neural networks by conditional reporter expression from a Brainbow herpesvirus. *Proceedings of the National Academy of Sciences of the United States of America* **108,** 3377-3382.

Card JP, Sved JC, Craig B, Raizada M, Vazquez J & Sved AF. (2006a). Efferent projections of rat rostroventrolateral medulla C1 catecholamine neurons: Implications for the central control of cardiovascular regulation. *The Journal of comparative neurology* **499,** 840-859.

Card JP, Sved JC, Craig B, Raizada M, Vazquez J & Sved AF. (2006b). Efferent projections of rat rostroventrolateral medulla C1 catecholamine neurons: Implications for the central control of cardiovascular regulation. *The Journal of Comparative Neurology* **499,** 840-859.

Cardoso SH, Coimbra NC & Brandao ML. (1994). Defensive reactions evoked by activation of NMDA receptors in distinct sites of the inferior colliculus. *Behavioural brain research* **63,** 17-24.

Carey CL & Webster DB. (1971). Ascending and descending projections of the inferior colliculus in the Kangaroo rat (Dipodomys merriami). *Brain, behavior and evolution* **4,** 401-412.

Carrive P. (1993). The periaqueductal gray and defensive behavior: functional representation and neuronal organization. *Behav Brain Res* **58,** 27-47.

Carrive P. (2013). Orexin, orexin receptor antagonists and central cardiovascular control. *Frontiers in neuroscience* **7,** 257.

Carrive P & Bandler R. (1991). Viscerotopic organization of neurons subserving hypotensive reactions within the midbrain periaqueductal grey: a correlative functional and anatomical study. *Brain research* **541,** 206-215.

Carrive P, Bandler R & Dampney RA. (1988). Anatomical evidence that hypertension associated with the defence reaction in the cat is mediated by a direct projection from a restricted portion of the midbrain periaqueductal grey to the subretrofacial nucleus of the medulla. *Brain Res* **460,** 339-345.

Carrive P, Bandler R & Dampney RA. (1989). Viscerotopic control of regional vascular beds by discrete groups of neurons within the midbrain periaqueductal gray. *Brain Res* **493,** 385-390.

Casseday JH & Covey E. (1996). A neuroethological theory of the operation of the inferior colliculus. *Brain Behav Evolut* **47,** 311-336.

Cepeda-Nieto AC, Pfaff SL & Varela-Echavarria A. (2005). Homeodomain transcription factors in the development of subsets of hindbrain reticulospinal neurons. *Molecular and cellular neurosciences* **28,** 30-41.

Chalasani SH, Chronis N, Tsunozaki M, Gray JM, Ramot D, Goodman MB & Bargmann CI. (2007). Dissecting a circuit for olfactory behaviour in Caenorhabditis elegans. *Nature* **450,** 63-70.

Chalfie M, Sulston JE, White JG, Southgate E, Thomson JN & Brenner S. (1985). The neural circuit for touch sensitivity in Caenorhabditis elegans. *The Journal of neuroscience : the official journal of the Society for Neuroscience* **5,** 956-964.

Chan RK & Sawchenko PE. (1998). Organization and transmitter specificity of medullary neurons activated by sustained hypertension: implications for understanding baroreceptor reflex circuitry. *The Journal of neuroscience : the official journal of the Society for Neuroscience* **18,** 371-387.

Chen QH & Toney GM. (2010). In vivo discharge properties of hypothalamic paraventricular nucleus neurons with axonal projections to the rostral ventrolateral medulla. *J Neurophysiol* **103,** 4-15.

Chen S & Astonjones G. (1995). Evidence That Cholera-Toxin-B Subunit (Ctb) Can Be Avidly Taken up and Transported by Fibers of Passage. *Brain research* **674,** 107-111.

Chung K, Wallace J, Kim SY, Kalyanasundaram S, Andalman AS, Davidson TJ, Mirzabekov JJ, Zalocusky KA, Mattis J, Denisin AK, Pak S, Bernstein H, Ramakrishnan C, Grosenick L, Gradinaru V & Deisseroth K. (2013). Structural and molecular interrogation of intact biological systems. *Nature* **497,** 332-337.

Cohen L, Koffman N, Meiri H, Yarom Y, Lampl I & Mizrahi A. (2013). Time-lapse electrical recordings of single neurons from the mouse neocortex. *Proc Natl Acad Sci U S A* **110,** 5665-5670.

Coote JH. (2007). Landmarks in understanding the central nervous control of the cardiovascular system. *Exp Physiol* **92,** 3-18.

Cowan WM, Gottlieb DI, Hendrickson AE, Price JL & Woolsey TA. (1972). The autoradiographic demonstration of axonal connections in the central nervous system. *Brain research* **37,** 21-51.

Cox BF & Brody MJ. (1989). Subregions of rostral ventral medulla control arterial pressure and regional hemodynamics. *Am J Physiol* **257,** R635-640.

Cravo SL, Morrison SF & Reis DJ. (1991). Differentiation of 2 Cardiovascular Regions within Caudal Ventrolateral Medulla. *American Journal of Physiology* **261,** R985-R994.

Crone SA, Viemari JC, Droho S, Mrejeru A, Ramirez JM & Sharma K. (2012). Irregular Breathing in Mice following Genetic Ablation of V2a Neurons. *The Journal of neuroscience : the official journal of the Society for Neuroscience* **32,** 7895-7906.

Cruz JC, Bonagamba LG, Machado BH, Biancardi VC & Stern JE. (2008). Intermittent activation of peripheral chemoreceptors in awake rats induces Fos expression in rostral ventrolateral medulla-projecting neurons in the paraventricular nucleus of the hypothalamus. *Neuroscience* **157,** 463-472.

Csucs G & Bjaalie JG. (2015). CutNII for Waxholm Space atlas of the Sprague Dawley rat brain. INCF Software Center.

Dampney RA. (1994a). Functional organization of central pathways regulating the cardiovascular system. *Physiological Reviews* **74,** 323-364.

Dampney RA. (1994b). The subretrofacial vasomotor nucleus: anatomical, chemical and pharmacological properties and role in cardiovascular regulation. *Prog Neurobiol* **42,** 197-227.

Dampney RA, Blessing WW & Tan E. (1988). Origin of tonic GABAergic inputs to vasopressor neurons in the subretrofacial nucleus of the rabbit. *J Auton Nerv Syst* **24,** 227-239.

Dampney RA, Czachurski J, Dembowsky K, Goodchild AK & Seller H. (1987). Afferent connections and spinal projections of the pressor region in the rostral ventrolateral medulla of the cat. *J Auton Nerv Syst* **20,** 73-86.

Dampney RA, Goodchild AK, Robertson LG & Montgomery W. (1982). Role of ventrolateral medulla in vasomotor regulation: a correlative anatomical and physiological study. *Brain Res* **249,** 223-235.

Dampney RA, Horiuchi J, Tagawa T, Fontes MA, Potts PD & Polson JW. (2003). Medullary and supramedullary mechanisms regulating sympathetic vasomotor tone. *Acta Physiol Scand* **177,** 209-218.

Dampney RA & Moon EA. (1980). Role of ventrolateral medulla in vasomotor response to cerebral ischemia. *Am J Physiol* **239,** H349-358.

Dampney RA, Tagawa T, Horiuchi J, Potts PD, Fontes M & Polson JW. (2000). What drives the tonic activity of presympathetic neurons in the rostral ventrolateral medulla? *Clinical and experimental pharmacology & physiology* **27,** 1049-1053.

Daniel J, Polder HR, Lessmann V & Brigadski T. (2013). Single-cell juxtacellular transfection and recording technique. *Pflugers Arch* **465,** 1637-1649.

De Simoni A & Yu LM. (2006). Preparation of organotypic hippocampal slice cultures: interface method. *Nature protocols* **1,** 1439-1445.

Dean P & Redgrave P. (1984). The superior colliculus and visual neglect in rat and hamster. I. Behavioural evidence. *Brain research* **320,** 129-141.

Dean P, Redgrave P & Westby GW. (1989). Event or emergency? Two response systems in the mammalian superior colliculus. *Trends in neurosciences* **12,** 137-147.

DeBruin KA & Krassowska W. (1999). Modeling electroporation in a single cell. I. Effects Of field strength and rest potential. *Biophys J* **77,** 1213-1224.

DeFalco J, Tomishima M, Liu H, Zhao C, Cai X, Marth JD, Enquist L & Friedman JM. (2001). Virus-assisted mapping of neural inputs to a feeding center in the hypothalamus. *Science* **291,** 2608-2613.

Dembowsky K, Czachurski J & Seller H. (1985). An intracellular study of the synaptic input to sympathetic preganglionic neurones of the third thoracic segment of the cat. *J Auton Nerv Syst* **13,** 201-244.

Dempsey B, Turner AJ, Le S, Sun QJ, Bou Farah L, Allen AM, Goodchild AK & McMullan S. (2015). Recording, labeling, and transfection of single neurons in deep brain structures. *Physiological reports* **3**.

Denk W, Briggman KL & Helmstaedter M. (2012). Structural neurobiology: Missing link to a mechanistic understanding of neural computation. *Nature Reviews Neuroscience* **13,** 351-358.

Depuy SD, Kanbar R, Coates MB, Stornetta RL & Guyenet PG. (2011). Control of breathing by raphe obscurus serotonergic neurons in mice. *The Journal of neuroscience : the official journal of the Society for Neuroscience* **31,** 1981-1990.

Descarries L & Mechawar N. (2000). Ultrastructural evidence for diffuse transmission by monoamine and acetylcholine neurons of the cetral nervous system. *Progress in brain research* **125,** 27-47.

DesJardin JT, Holmes AL, Forcelli PA, Cole CE, Gale JT, Wellman LL, Gale K & Malkova L. (2013). Defense-like behaviors evoked by pharmacological disinhibition of the superior colliculus in the primate. *The Journal of neuroscience : the official journal of the Society for Neuroscience* **33,** 150-155.

Deuchars SA, Morrison SF & Gilbey MP. (1995). Medullary-evoked EPSPs in neonatal rat sympathetic preganglionic neurones in vitro. *J Physiol* **487 (Pt 2),** 453-463.

Development B. (2013). Spots split into surface objects. In *Bitplane XTensions*, pp. To run this XTension the user has to create a Spots and a Surface component.

For each Surface object located in the same Surpass group as the Spots object, this XTension creates a new subset of Spots that contains only the Spots that lie inside the Surface. Oxford Instruments.

Dobbins EG & Feldman JL. (1994). Brainstem network controlling descending drive to phrenic motoneurons in rat. *J Comp Neurol* **347,** 64-86.

Dorward PK, Burke SL, Janig W & Cassell J. (1987). Reflex responses to baroreceptor, chemoreceptor and nociceptor inputs in single renal sympathetic neurones in the rabbit and the effects of anaesthesia on them. *J Auton Nerv Syst* **18,** 39-54.

Drew T, Prentice S & Schepens B. (2004). Cortical and brainstem control of locomotion. *Progress in brain research* **143,** 251-261.

Dutschmann M, Morschel M, Kron M & Herbert H. (2004). Development of adaptive behaviour of the respiratory network: implications for the pontine Kolliker-Fuse nucleus. *Respir Physiol Neurobiol* **143,** 155-165.

Edwards FA, Konnerth A, Sakmann B & Takahashi T. (1989). A thin slice preparation for patch clamp recordings from neurones of the mammalian central nervous system. *Pflügers Archiv European Journal of Physiology* **414,** 600-612.

Ekstrand MI, Enquist LW & Pomeranz LE. (2008). The alpha-herpesviruses: molecular pathfinders in nervous system circuits. *Trends in molecular medicine* **14,** 134-140.

Ellenberger HH & Feldman JL. (1990). Brainstem connections of the rostral ventral respiratory group of the rat. *Brain Res* **513,** 35-42.

Esposito MS, Capelli P & Arber S. (2014). Brainstem nucleus MdV mediates skilled forelimb motor tasks. *Nature* **508,** 351-356.

Etessami R, Conzelmann KK, Fadai-Ghotbi B, Natelson B, Tsiang H & Ceccaldi PE. (2000). Spread and pathogenic characteristics of a G-deficient rabies virus recombinant: an in vitro and in vivo study. *J Gen Virol* **81,** 2147-2153.

Ezure K & Tanaka I. (2006). Distribution and medullary projection of respiratory neurons in the dorsolateral pons of the rat. *Neuroscience* **141,** 1011-1023.

Ezure K, Tanaka I & Kondo M. (2003). Glycine is used as a transmitter by decrementing expiratory neurons of the ventrolateral medulla in the rat. *J Neurosci* **23,** 8941-8948.

Farkas E, Jansen AS & Loewy AD. (1998). Periaqueductal gray matter input to cardiac-related sympathetic premotor neurons. *Brain research* **792,** 179-192.

Farnham MM & Pilowsky PM. (2009). Local anaesthetics for acute reversible blockade of the sympathetic baroreceptor reflex in the rat. *Journal of neuroscience methods* **179,** 58-62.

Feinberg EH, Vanhoven MK, Bendesky A, Wang G, Fetter RD, Shen K & Bargmann CI. (2008). GFP Reconstitution Across Synaptic Partners (GRASP) defines cell contacts and synapses in living nervous systems. *Neuron* **57,** 353-363.

Feldberg W & Guertzenstein PG. (1976). Vasodepressor effects obtained by drugs acting on the ventral surface of the brain stem. *The Journal of physiology* **258,** 337-355.

Feldman JL, Del Negro CA & Gray PA. (2013). Understanding the rhythm of breathing: So near, yet so far. In *Annual Review of Physiology*, pp. 423-452.

Femano PA, Schwartz-Giblin S & Pfaff DW. (1984). Brain stem reticular influences on lumbar axial muscle activity. II. Temporal aspects. *The American journal of physiology* **246,** R396-401.

Fenno LE, Mattis J, Ramakrishnan C, Hyun M, Lee SY, He M, Tucciarone J, Selimbeyoglu A, Berndt A, Grosenick L, Zalocusky KA, Bernstein H, Swanson H, Perry C, Diester I, Boyce FM, Bass CE, Neve R, Huang ZJ & Deisseroth K. (2014). Targeting cells with single vectors using multiple-feature Boolean logic. *Nat Methods* **11,** 763-772.

Fink RP & Heimer L. (1967). Two methods for selective silver impregnation of degenerating axons and their synaptic endings in the central nervous system. *Brain research* **4,** 369-374.

Fukuda Y, Tojima H, Tanaka K & Chiba T. (1993). Respiratory suppression by focal cooling of ventral medullary surface in anesthetized rats; functional and neuroanatomical correlate. *Neuroscience letters* **153,** 177-180.

Furlong TM, McDowall LM, Horiuchi J, Polson JW & Dampney RA. (2014). The effect of air puff stress on c-Fos expression in rat hypothalamus and brainstem: central circuitry mediating sympathoexcitation and baroreflex resetting. *Eur J Neurosci* **39,** 1429-1438.

Gaytan SP, Calero F, Nunez-Abades PA, Morillo AM & Pasaro R. (1997). Pontomedullary efferent projections of the ventral respiratory neuronal subsets of the rat. *Brain Res Bull* **42,** 323-334.

Gebber GL & Barman SM. (1988). Studies on the origin and generation of sympathetic nerve activity. *ClinExpHypertensA* **10 Suppl 1:33-44.,** 33-44.

Gelsema AJ, Agarwal SK & Calaresu FR. (1989). Cardiovascular responses and changes in neural activity in the rostral ventrolateral medulla elicited by electrical stimulation of the amygdala of the rat. *J Auton Nerv Syst* **27,** 91-100.

Gerfen CR & Sawchenko PE. (1984). An anterograde neuroanatomical tracing method that shows the detailed morphology of neurons, their axons and terminals: immunohistochemical localization of an axonally transported plant lectin, Phaseolus vulgaris leucoagglutinin (PHA-L). *Brain research* **290,** 219-238.

Gieroba ZJ, Li YW & Blessing WW. (1992). Characteristics of caudal ventrolateral medullary neurons antidromically activated from rostral ventrolateral medulla in the rabbit. *Brain Res* **582,** 196-207.

Gilbey MP. (2007). Sympathetic rhythms and nervous integration. *Clin Exp Pharmacol Physiol* **34,** 356-361.

Gilbey MP, Numao Y & Spyer KM. (1986). Discharge patterns of cervical sympathetic preganglionic neurones related to central respiratory drive in the rat. *The Journal of physiology* **378,** 253-265.

Glees P. (1946). Terminal degeneration within the central nervous system as studied by a new silver method. *J Neuropathol Exp Neurol* **5,** 54-59.

Glover JC, Petursdottir G & Jansen JK. (1986). Fluorescent dextran-amines used as axonal tracers in the nervous system of the chicken embryo. *Journal of neuroscience methods* **18,** 243-254.

Gofflot F, Wendling O, Chartoire N, Birling MC, Warot X & Auwerx J. (2011). Characterization and Validation of Cre-Driver Mouse Lines. *Current protocols in mouse biology* **1,** 1-15.

Golanov EV, Christensen JR & Reis DJ. (2001). Neurons of a limited subthalamic area mediate elevations in cortical cerebral blood flow evoked by hypoxia and excitation of neurons of the rostral ventrolateral medulla. *The Journal of neuroscience : the official journal of the Society for Neuroscience* **21,** 4032-4041.

Golanov EV & Reis DJ. (1996). Contribution of oxygen-sensitive neurons of the rostral ventrolateral medulla to hypoxic cerebral vasodilatation in the rat. *The Journal of physiology* **495 (Pt 1),** 201-216.

Gomez RE, Cannata MA, Milner TA, Anwar M, Reis DJ & Ruggiero DA. (1993). Vasopressinergic mechanisms in the nucleus reticularis lateralis in blood pressure control. *Brain Res* **604,** 90-105.

Goodchild AK, Dampney RA & Bandler R. (1982). A method for evoking physiological responses by stimulation of cell bodies, but not axons of passage, within localized regions of the central nervous system. *J Neurosci Methods* **6,** 351-363.

Goodchild AK & Moon EA. (2009). Maps of cardiovascular and respiratory regions of rat ventral medulla: focus on the caudal medulla. *J Chem Neuroanat* **38,** 209-221.

Goodchild AK, Moon EA, Dampney RA & Howe PR. (1984). Evidence that adrenaline neurons in the rostral ventrolateral medulla have a vasopressor function. *Neurosci Lett* **45,** 267-272.

Goodchild AK, Phillips JK, Lipski J & Pilowsky PM. (2001). Differential expression of catecholamine synthetic enzymes in the caudal ventral pons. *Journal of Comparative Neurology* **438,** 457-467.

Gowen MF, Ogburn SW, Suzuki T, Sugiyama Y, Cotter LA & Yates BJ. (2012). Collateralization of projections from the rostral ventrolateral medulla to the rostral and caudal thoracic spinal cord in felines. *Exp Brain Res* **220,** 121-133.

Grafstein B. (1967). Transport of protein by goldfish optic nerve fibers. *Science* **157,** 196-198.

Granata AR & Chang HT. (1994). Relationship of calbindin D-28k with afferent neurons to the rostral ventrolateral medulla in the rat. *Brain Res* **645,** 265-277.

Granata AR, Ruggiero DA, Park DH, Joh TH & Reis DJ. (1985). Brain stem area with C1 epinephrine neurons mediates baroreflex vasodepressor responses. *The American journal of physiology* **248,** H547-567.

Gray JM, Hill JJ & Bargmann CI. (2005). A circuit for navigation in Caenorhabditis elegans. *Proceedings of the National Academy of Sciences of the United States of America* **102,** 3184-3191.

Gray PA, Rekling JC, Bocchiaro CM & Feldman JL. (1999). Modulation of respiratory frequency by peptidergic input to rhythmogenic neurons in the preBotzinger complex. *Science* **286,** 1566-1568.

Guertzenstein PG & Silver A. (1974). Fall in blood pressure produced from discrete regions of the ventral surface of the medulla by glycine and lesions. *The Journal of physiology* **242,** 489-503.

Guyenet PG. (2000). Neural structures that mediate sympathoexcitation during hypoxia. *Resp Physiol* **121,** 147-162.

Guyenet PG. (2006). The sympathetic control of blood pressure. *Nat Rev Neurosci* **7,** 335-346.

Guyenet PG, Filtz TM & Donaldson SR. (1987). Role of excitatory amino acids in rat vagal and sympathetic baroreflexes. *Brain research* **407,** 272-284.

Guyenet PG, Stornetta RL, Bochorishvili G, Depuy SD, Burke PG & Abbott SB. (2013). C1 neurons: the body's EMTs. *American journal of physiology Regulatory, integrative and comparative physiology* **305,** R187-204.

Guyenet PG & Wang H. (2001). Pre-Botzinger neurons with preinspiratory discharges "in vivo" express NK1 receptors in the rat. *J Neurophysiol* **86,** 438-446.

Guyer S. (2013). CreateSpotsFromFile. In *Bitplane XTensions*, pp. This python XTension reads the content of a text file and creates a Spots component from it. The text file format is very simple, basically a list of XYZ positions. Time indices and Spot radii can also be set.

This XTension is useful if you quickly want to visualize some positions in an image. Oxford Instruments, Imaris XT.

Haas K, Sin WC, Javaherian A, Li Z & Cline HT. (2001). Single-cell electroporation for gene transfer in vivo. *Neuron* **29,** 583-591.

Habler HJ, Janig W & Michaelis M. (1994). Respiratory modulation in the activity of sympathetic neurones. *Prog Neurobiol* **43,** 567-606.

Hadziefendic S & Haxhiu MA. (1999). CNS innervation of vagal preganglionic neurons controlling peripheral airways: a transneuronal labeling study using pseudorabies virus. *Journal of the autonomic nervous system* **76,** 135-145.

Hancock MB. (1988). Evidence for direct projections from the nucleus of the solitary tract onto medullary adrenaline cells. *The Journal of comparative neurology* **276,** 460-467.

Hardy SG. (2001). Hypothalamic projections to cardiovascular centers of the medulla. *Brain Res* **894,** 233-240.

Haselton JR & Guyenet PG. (1989). Central respiratory modulation of medullary sympathoexcitatory neurons in rat. *Am J Physiol* **256,** R739-750.

Haselton JR & Guyenet PG. (1990). ASCENDING COLLATERALS OF MEDULLARY BAROSENSITIVE NEURONS AND C1 CELLS IN RATS. *American Journal of Physiology* **258,** R1051-R1063.

Hayakawa T, Zheng JQ & Seki M. (1999). Direct parabrachial nuclear projections to the pharyngeal motoneurons in the rat: an anterograde and retrograde double-labeling study. *Brain Res* **816,** 364-374.

Hayes K, Calaresu FR & Weaver LC. (1994). PONTINE RETICULAR NEURONS PROVIDE TONIC EXCITATION TO NEURONS IN ROSTRAL VENTROLATERAL MEDULLA IN RATS. *American Journal of Physiology* **266,** R237-R244.

Hellenbrand DJ, Kaeppler KE, Hwang E, Ehlers ME, Toigo RD, Giesler JD, Vassar-Olsen ER & Hanna A. (2013). Basic techniques for long distance axon tracing in the spinal cord. *Microsc Res Tech* **76,** 1240-1249.

Helmstaedter M, Briggman KL, Turaga SC, Jain V, Seung HS & Denk W. (2013). Connectomic reconstruction of the inner plexiform layer in the mouse retina. *Nature* **500,** 168-174.

Herculano-Houzel S. (2009). The human brain in numbers: a linearly scaled-up primate brain. *Frontiers in human neuroscience* **3,** 31.

Herculano-Houzel S & Lent R. (2005). Isotropic fractionator: a simple, rapid method for the quantification of total cell and neuron numbers in the brain. *The Journal of neuroscience : the official journal of the Society for Neuroscience* **25,** 2518-2521.

Hermann GE, Holmes GM, Rogers RC, Beattie MS & Bresnahan JC. (2003). Descending spinal projections from the rostral gigantocellular reticular nuclei complex. *The Journal of comparative neurology* **455,** 210-221.

Hilaire G, Viemari JC, Coulon P, Simonneau M & Bevengut M. (2004). Modulation of the respiratory rhythm generator by the pontine noradrenergic A5 and A6 groups in rodents. *Respiratory physiology & neurobiology* **143,** 187-197.

Hilbert M & Lopez P. (2011). The world's technological capacity to store, communicate, and compute information. *Science* **332,** 60-65.

Hilton SM, Marshall JM & Timms RJ. (1983). Ventral medullary relay neurones in the pathway from the defence areas of the cat and their effect on blood pressure. *The Journal of physiology* **345,** 149-166.

Hilton SM & Redfern WS. (1986). A search for brain stem cell groups integrating the defence reaction in the rat. *JPhysiol* **378,** 213.

Hoff EC. (1932). Central Nerve Terminals in the Mammalian Spinal Cord and their Examination by Experimental Degeneration. *Proceedings of the Royal Society of London Series B, Containing Papers of a Biological Character* **111,** 175-188.

Hokfelt T, Fuxe K, Goldstein M & Johansson O. (1973). Evidence for adrenaline neurons in the rat brain. *Acta Physiol Scand* **89,** 286-288.

Holstege G, Kuypers HG & Dekker JJ. (1977). The organization of the bulbar fibre connections to the trigeminal, facial and hypoglossal motor nuclei. II. An autoradiographic tracing study in cat. *Brain : a journal of neurology* **100,** 264-286.

Holstege JC & Kuypers HG. (1987). Brainstem projections to spinal motoneurons: an update. *Neuroscience* **23,** 809-821.

Holstein GR, Martinelli GP & Friedrich VL. (2011). Anatomical observations of the caudal vestibulo-sympathetic pathway. *Journal of vestibular research : equilibrium & orientation* **21,** 49-62.

Hoover WB & Vertes RP. (2011). Projections of the medial orbital and ventral orbital cortex in the rat. *The Journal of comparative neurology* **519,** 3766-3801.

Horikawa K & Armstrong WE. (1988). A versatile means of intracellular labeling: injection of biocytin and its detection with avidin conjugates. *J Neurosci Methods* **25,** 1-11.

Horiuchi J & Dampney RA. (2002). Evidence for tonic disinhibition of RVLM sympathoexcitatory neurons from the caudal pressor area. *Auton Neurosci* **99,** 102-110.

Horiuchi J, Killinger S & Dampney RA. (2004). Contribution to sympathetic vasomotor tone of tonic glutamatergic inputs to neurons in the RVLM. *American journal of physiology Regulatory, integrative and comparative physiology* **287,** R1335-1343.

Hudson PM & Lumb BM. (1996). Neurones in the midbrain periaqueductal grey send collateral projections to nucleus raphe magnus and the rostral ventrolateral medulla in the rat. *Brain Res* **733,** 138-141.

Huerta MF & Harting JK. (1982). Projections of the superior colliculus to the supraspinal nucleus and the cervical spinal cord gray of the cat. *Brain research* **242,** 326-331.

Huerta MF & Harting JK. (1984). Connectional Organization of the Superior Colliculus. *Trends in neurosciences* **7,** 286-289.

Iceman KE & Harris MB. (2014). A group of non-serotonergic cells is CO2-stimulated in the medullary raphe. *Neuroscience* **259,** 203-213.

Iigaya K, Muller-Ribeiro FC, Horiuchi J, McDowall LM, Nalivaiko E, Fontes MA & Dampney RA. (2012). Synchronized activation of sympathetic vasomotor, cardiac, and respiratory outputs by neurons in the midbrain colliculi. *Am J Physiol Regul Integr Comp Physiol* **303,** R599-610.

Ilch CP & Golanov EV. (2004). Cerebrovasodilation evoked by stimulation of subthalamic vasodilator area and hypoxia depends upon the integrity of cortical neurons in the rat. *Neuroscience letters* **368,** 92-95.

Ito S & Sved AF. (1997). Tonic glutamate-mediated control of rostral ventrolateral medulla and sympathetic vasomotor tone. *Am J Physiol* **273,** R487-494.

Janig W. (1988). Pre- and postganglionic vasoconstrictor neurons: differentiation, types, and discharge properties. *Annual review of physiology* **50,** 525-539.

Jansen AS, Wessendorf MW & Loewy AD. (1995). Transneuronal labeling of CNS neuropeptide and monoamine neurons after pseudorabies virus injections into the stellate ganglion. *Brain research* **683,** 1-24.

Jeske I, Reis DJ & Milner TA. (1995). Neurons in the barosensory area of the caudal ventrolateral medulla project monosynaptically on to sympathoexcitatory bulbospinal neurons in the rostral ventrolateral medulla. *Neuroscience* **65,** 343-353.

Jiang X, Wang G, Lee AJ, Stornetta RL & Zhu JJ. (2013). The organization of two new cortical interneuronal circuits. *Nature Neuroscience* **16,** 210-218.

Johnson RD & Hubscher CH. (1998). Brainstem microstimulation differentially inhibits pudendal motoneuron reflex inputs. *Neuroreport* **9,** 341-345.

Johnson RD & Hubscher CH. (2000). Brainstem microstimulation activates sympathetic fibers in pudendal nerve motor branch. *Neuroreport* **11,** 379-382.

Jones EG. (2007). Neuroanatomy: Cajal and after Cajal. *Brain research reviews* **55,** 248-255.

Judkewitz B, Rizzi M, Kitamura K & Hausser M. (2009). Targeted single-cell electroporation of mammalian neurons in vivo. *Nature protocols* **4,** 862-869.

Kanbar R, Depuy SD, West GH, Stornetta RL & Guyenet PG. (2011). Regulation of visceral sympathetic tone by A5 noradrenergic neurons in rodents. *J Physiol* **589,** 903-917.

Kangrga IM & Loewy AD. (1995). Whole-cell recordings from visualized C1 adrenergic bulbospinal neurons: ionic mechanisms underlying vasomotor tone. *Brain research* **670,** 215-232.

Kanjhan R, Lipski J, Kruszewska B & Rong W. (1995). A comparative study of pre-sympathetic and Botzinger neurons in the rostral ventrolateral medulla (RVLM) of the rat. *Brain Res* **699,** 19-32.

Kasthuri N, Hayworth KJ, Berger DR, Schalek RL, Conchello JA, Knowles-Barley S, Lee D, Vazquez-Reina A, Kaynig V, Jones TR, Roberts M, Morgan JL, Tapia JC, Seung HS, Roncal WG,

Vogelstein JT, Burns R, Sussman DL, Priebe CE, Pfister H & Lichtman JW. (2015). Saturated Reconstruction of a Volume of Neocortex. *Cell* **162,** 648-661.

Keay KA, Dean P & Redgrave P. (1990). N-Methyl D-Aspartate (Nmda) Evoked Changes in Blood-Pressure and Heart-Rate from the Rat Superior Colliculus. *Exp Brain Res* **80,** 148-156.

Keay KA, Redgrave P & Dean P. (1988). Cardiovascular and Respiratory Changes Elicited by Stimulation of Rat Superior Colliculus. *Brain Res Bull* **20,** 13-26.

Kelly RM & Strick PL. (2000). Rabies as a transneuronal tracer of circuits in the central nervous system. *J Neurosci Methods* **103,** 63-71.

Kelly RM & Strick PL. (2003). Cerebellar loops with motor cortex and prefrontal cortex of a nonhuman primate. *The Journal of neuroscience : the official journal of the Society for Neuroscience* **23,** 8432-8444.

Kemp PJ. (2006). Detecting acute changes in oxygen: will the real sensor please stand up? *Experimental physiology* **91,** 829-834.

Kerman IA. (2008). Organization of brain somatomotor-sympathetic circuits. *Exp Brain Res* **187,** 1-16.

Kiely JM & Gordon FJ. (1994). Role of rostral ventrolateral medulla in centrally mediated pressor responses. *Am J Physiol* **267,** H1549-1556.

Kim EJ, Jacobs MW, Ito-Cole T & Callaway EM. (2016). Improved Monosynaptic Neural Circuit Tracing Using Engineered Rabies Virus Glycoproteins. *Cell Rep*.

Kim J, Zhao T, Petralia RS, Yu Y, Peng H, Myers E & Magee JC. (2012). mGRASP enables mapping mammalian synaptic connectivity with light microscopy. *Nature methods* **9,** 96-102.

Kitamura K, Judkewitz B, Kano M, Denk W & Hausser M. (2008). Targeted patch-clamp recordings and single-cell electroporation of unlabeled neurons in vivo. *Nat Methods* **5,** 61-67.

Kline DD, King TL, Austgen JR, Heesch CM & Hasser EM. (2010). Sensory afferent and hypoxia-mediated activation of nucleus tractus solitarius neurons that project to the rostral ventrolateral medulla. *Neuroscience* **167,** 510-527.

Kobbert C, Apps R, Bechmann I, Lanciego JL, Mey J & Thanos S. (2000). Current concepts in neuroanatomical tracing. *Progress in neurobiology* **62,** 327-351.

Koganezawa T & Paton JF. (2014). Intrinsic chemosensitivity of rostral ventrolateral medullary sympathetic premotor neurons in the in situ arterially perfused preparation of rats. *Experimental physiology* **99,** 1453-1466.

Koganezawa T, Shimomura Y & Terui N. (2010). The viscerosympathetic response in rabbits is mediated by GABAergic and glutamatergic inputs into the sympathetic premotor neurons of the rostral ventrolateral medulla. *Experimental physiology* **95,** 1061-1070.

Koganezawa T & Terui N. (2007). Differential responsiveness of RVLM sympathetic premotor neurons to hypoxia in rabbits. *American journal of physiology Heart and circulatory physiology* **292,** H408-414.

Koizumi H, Koshiya N, Chia JX, Cao F, Nugent J, Zhang R & Smith JC. (2013). Structural-functional properties of identified excitatory and inhibitory interneurons within pre-Botzinger complex respiratory microcircuits. *J Neurosci* **33,** 2994-3009.

Kollai M, Koizumi K & Brooks CM. (1978). Nature of differential sympathetic discharges in chemoreceptor reflexes. *Proceedings of the National Academy of Sciences of the United States of America* **75,** 5239-5243.

Koshiya N & Guyenet PG. (1996). NTS neurons with carotid chemoreceptor inputs arborize in the rostral ventrolateral medulla. *The American journal of physiology* **270,** R1273-1278.

Koshiya N, Huangfu D & Guyenet PG. (1993). Ventrolateral medulla and sympathetic chemoreflex in the rat. *Brain Res* **609,** 174-184.

Krassioukov AV & Weaver LC. (1993). Connections between the Pontine Reticular-Formation and Rostral Ventrolateral Medulla. *American Journal of Physiology* **265,** H1386-H1392.

Krieger EM & Marseillan RF. (1963). Aortic Depressor Fibers in the Rat: An Electrophysiological Study. *The American journal of physiology* **205,** 771-774.

Kristensson K & Olsson Y. (1971). Retrograde axonal transport of protein. *Brain research* **29,** 363-365.

Kubin L, Trzebski A & Lipski J. (1985). Split medulla preparation in the cat: arterial chemoreceptor reflex and respiratory modulation of the renal sympathetic nerve activity. *J Auton Nerv Syst* **12,** 211-225.

Kumar P & Prabhakar NR. (2012). Peripheral chemoreceptors: function and plasticity of the carotid body. *Compr Physiol* **2,** 141-219.

Kupfermann IaW, K. R. (1978). The command neuron concept. *Behavioral and Brain Sciences* **1,** 3-10.

Kuypers HG, Bentivoglio M, van der Kooy D & Catsman-Berrevoets CE. (1979). Retrograde transport of bisbenzimide and propidium iodide through axons to their parent cell bodies. *Neuroscience letters* **12,** 1-7.

Lafon M. (2005). Rabies virus receptors. *Journal of neurovirology* **11,** 82-87.

Lanciego JL & Wouterlood FG. (2011). A half century of experimental neuroanatomical tracing. *Journal of chemical neuroanatomy* **42,** 157-183.

Le S, Turner AJ, Parker LM, Burke PG, Kumar NN, Goodchild AK & McMullan S. (2015). Somatostatin 2A receptors are not expressed on functionally identified respiratory neurons in the ventral respiratory column of the rat. *J Comp Neurol*.

Lee TK, Lois JH, Troupe JH, Wilson TD & Yates BJ. (2007). Transneuronal tracing of neural pathways that regulate hindlimb muscle blood flow. *American Journal of Physiology-Regulatory Integrative and Comparative Physiology* **292,** R1532-R1541.

Lein ES, Hawrylycz MJ, Ao N, Ayres M, Bensinger A, Bernard A, Boe AF, Boguski MS, Brockway KS, Byrnes EJ, Chen L, Chen L, Chen TM, Chin MC, Chong J, Crook BE, Czaplinska A, Dang CN, Datta S, Dee NR, Desaki AL, Desta T, Diep E, Dolbeare TA, Donelan MJ, Dong HW, Dougherty JG, Duncan BJ, Ebbert AJ, Eichele G, Estin LK, Faber C, Facer BA, Fields R, Fischer SR, Fliss TP, Frensley C, Gates SN, Glattfelder KJ, Halverson KR, Hart MR, Hohmann JG, Howell MP, Jeung DP, Johnson RA, Karr PT, Kawal R, Kidney JM, Knapik RH, Kuan CL, Lake JH, Laramee AR, Larsen KD, Lau C, Lemon TA, Liang AJ, Liu Y, Luong LT, Michaels J, Morgan JJ, Morgan RJ, Mortrud MT, Mosqueda NF, Ng LL, Ng R, Orta GJ, Overly CC, Pak TH, Parry SE, Pathak SD, Pearson OC, Puchalski RB, Riley ZL, Rockett HR, Rowland SA, Royall JJ, Ruiz MJ, Sarno NR, Schaffnit K, Shapovalova NV, Sivisay T, Slaughterbeck CR, Smith SC, Smith KA, Smith BI, Sodt AJ, Stewart NN, Stumpf KR, Sunkin SM, Sutram M, Tam A, Teemer CD, Thaller C, Thompson CL, Varnam LR, Visel A, Whitlock RM, Wohnoutka PE, Wolkey CK, Wong VY, Wood M, Yaylaoglu MB, Young RC, Youngstrom BL, Yuan XF, Zhang B, Zwingman TA & Jones AR. (2007). Genome-wide atlas of gene expression in the adult mouse brain. *Nature* **445,** 168-176.

Lemon RN. (2008). Descending pathways in motor control. *Annual review of neuroscience* **31,** 195-218.

Li Y, Stam FJ, Aimone JB, Goulding M, Callaway EM & Gage FH. (2013). Molecular layer perforant path-associated cells contribute to feed-forward inhibition in the adult dentate gyrus. *Proceedings of the National Academy of Sciences of the United States of America* **110,** 9106-9111.

Li YQ, Takada M & Mizuno N. (1993). Identification of Premotor Interneurons Which Project Bilaterally to the Trigeminal Motor, Facial or Hypoglossal Nuclei - a Fluorescent Retrograde Double-Labeling Study in the Rat. *Brain research* **611,** 160-164.

Li YW, Bayliss DA & Guyenet PG. (1995). C1 neurons of neonatal rats: intrinsic beating properties and alpha 2-adrenergic receptors. *Am J Physiol* **269,** R1356-1369.

Li YW, Wesselingh SL & Blessing WW. (1992). Projections from rabbit caudal medulla to C1 and A5 sympathetic premotor neurons, demonstrated with phaseolus leucoagglutinin and herpes simplex virus. *J Comp Neurol* **317,** 379-395.

Liang H, Watson C & Paxinos G. (2015). Terminations of reticulospinal fibers originating from the gigantocellular reticular formation in the mouse spinal cord. *Brain structure & function*.

Lichtman JW & Denk W. (2011). The big and the small: challenges of imaging the brain's circuits. *Science* **334,** 618-623.

Lim F & Neve RL. (2001). Generation of high-titer defective HSV-1 vectors. *Current protocols in neuroscience / editorial board, Jacqueline N Crawley [et al]* **Chapter 4,** Unit 4.13.

Lipski J, Kanjhan R, Kruszewska B & Rong W. (1996). Properties of presympathetic neurones in the rostral ventrolateral medulla in the rat: an intracellular study "in vivo'. *J Physiol* **490,** 729-744.

Lipski J, Kanjhan R, Kruszewska B & Smith M. (1995). Barosensitive neurons in the rostral ventrolateral medulla of the rat in vivo: morphological properties and relationship to C1 adrenergic neurons. *Neuroscience* **69,** 601-618.

Liu Y-J, Ehrengruber Markus U, Negwer M, Shao H-J, Cetin Ali H & Lyon David C. (2013). Tracing Inputs to Inhibitory or Excitatory Neurons of Mouse and Cat Visual Cortex with a Targeted Rabies Virus. *Current Biology* **23,** 1746-1755.

Livet J, Weissman TA, Kang H, Draft RW, Lu J, Bennis RA, Sanes JR & Lichtman JW. (2007). Transgenic strategies for combinatorial expression of fluorescent proteins in the nervous system. *Nature* **450,** 56-62.

Llewellyn-Smith IJ, Arnolda LF, Pilowsky PM, Chalmers JP & Minson JB. (1998). GABA- and glutamate-immunoreactive synapses on sympathetic preganglionic neurons projecting to the superior cervical ganglion. *Journal of the autonomic nervous system* **71,** 96-110.

Llinas RR. (2003). The contribution of Santiago Ramon y Cajal to functional neuroscience. *Nature reviews Neuroscience* **4,** 77-80.

Lois JH, Rice CD & Yates BJ. (2009). Neural circuits controlling diaphragm function in the cat revealed by transneuronal tracing. *Journal of applied physiology* **106,** 138-152.

Lovick TA. (1985). Projections from the diencephalon and mesencephalon to nucleus paragigantocellularis lateralis in the cat. *Neuroscience* **14,** 853-861.

Lovick TA. (1986). Projections from brainstem nuclei to the nucleus paragigantocellularis lateralis in the cat. *J Auton Nerv Syst* **16,** 1-11.

Lovick TA. (1993). The periaqueductal gray-rostral medulla connection in the defence reaction: efferent pathways and descending control mechanisms. *Behav Brain Res* **58,** 19-25.

Luo L, Callaway EM & Svoboda K. (2008). Genetic dissection of neural circuits. *Neuron* **57,** 634-660.

Madden CJ, Ito S, Rinaman L, Wiley RG & Sved AF. (1999). Lesions of the C1 catecholaminergic neurons of the ventrolateral medulla in rats using anti-DbetaH-saporin. *Am J Physiol* **277,** R1063-1075.

Madden CJ, Stocker SD & Sved AF. (2006). Attenuation of homeostatic responses to hypotension and glucoprivation after destruction of catecholaminergic rostral ventrolateral medulla neurons. *American journal of physiology Regulatory, integrative and comparative physiology* **291,** R751-759.

Madden CJ & Sved AF. (2003). Cardiovascular regulation after destruction of the C1 cell group of the rostral ventrolateral medulla in rats. *Am J Physiol Heart Circ Physiol* **285,** H2734-2748.

Maior RS, Hori E, Barros M, Teixeira DS, Tavares MC, Ono T, Nishijo H & Tomaz C. (2011). Superior colliculus lesions impair threat responsiveness in infant capuchin monkeys. *Neuroscience letters* **504,** 257-260.

Mandel DA & Schreihofer AM. (2006). Central respiratory modulation of barosensitive neurones in rat caudal ventrolateral medulla. *J Physiol* **572,** 881-896.

Margrie TW, Brecht M & Sakmann B. (2002). In vivo, low-resistance, whole-cell recordings from neurons in the anaesthetized and awake mammalian brain. *Pflugers Arch* **444,** 491-498.

Marshall JM. (1994). Peripheral Chemoreceptors and Cardiovascular Regulation. *Physiological reviews* **74,** 543-594.

Marshel JH, Mori T, Nielsen KJ & Callaway EM. (2010). Targeting Single Neuronal Networks for Gene Expression and Cell Labeling In Vivo. *Neuron* **67,** 562-574.

Mayorov DN & Head GA. (2002). Ionotropic glutamate receptors in the rostral ventrolateral medulla mediate sympathetic responses to acute stress in conscious rabbits. *Autonomic neuroscience : basic & clinical* **98,** 20-23.

McAllen RM. (1986). Identification and properties of sub-retrofacial bulbospinal neurones: a descending cardiovascular pathway in the cat. *J Auton Nerv Syst* **17,** 151-164.

McAllen RM. (1987). Central respiratory modulation of subretrofacial bulbospinal neurones in the cat. *J Physiol* **388,** 533-545.

McAllen RM. (1992). Actions of carotid chemoreceptors on subretrofacial bulbospinal neurons in the cat. *J Auton Nerv Syst* **40,** 181-188.

McAllen RM, Habler HJ, Michaelis M, Peters O & Janig W. (1994). Monosynaptic excitation of preganglionic vasomotor neurons by subretrofacial neurons of the rostral ventrolateral medulla. *Brain Res* **634,** 227-234.

McAllen RM & May CN. (1994). Effects of preoptic warming on subretrofacial and cutaneous vasoconstrictor neurons in anaesthetized cats. *The Journal of physiology* **481 (Pt 3),** 719-730.

McAllister RM. (1998). Adaptations in control of blood flow with training: splanchnic and renal blood flows. *Medicine and science in sports and exercise* **30,** 375-381.

McCarthy KM, Tank DW & Enquist LW. (2009). Pseudorabies virus infection alters neuronal activity and connectivity in vitro. *PLoS Pathog* **5,** e1000640.

McCrea RA. (1988). Neuroanatomy of the oculomotor system. The nucleus prepositus. *Rev Oculomot Res* **2,** 203-223.

McCrea RA & Baker R. (1985a). Anatomical connections of the nucleus prepositus of the cat. *The Journal of comparative neurology* **237,** 377-407.

McCrea RA & Baker R. (1985b). Cytology and intrinsic organization of the perihypoglossal nuclei in the cat. *The Journal of comparative neurology* **237,** 360-376.

McCulloch PF & Panneton WM. (2003). Activation of brainstem catecholaminergic neurons during voluntary diving in rats. *Brain research* **984,** 42-53.

McGeoch DJ, Dalrymple MA, Davison AJ, Dolan A, Frame MC, McNab D, Perry LJ, Scott JE & Taylor P. (1988). The complete DNA sequence of the long unique region in the genome of herpes simplex virus type 1. *The Journal of general virology* **69 (Pt 7),** 1531-1574.

McGovern AE, Davis-Poynter N, Farrell MJ & Mazzone SB. (2012a). Transneuronal tracing of airways-related sensory circuitry using herpes simplex virus 1, strain H129. *Neuroscience* **207,** 148-166.

McGovern AE, Davis-Poynter N, Rakoczy J, Phipps S, Simmons DG & Mazzone SB. (2012b). Anterograde neuronal circuit tracing using a genetically modified herpes simplex virus expressing EGFP. *Journal of neuroscience methods* **209,** 158-167.

McGovern AE, Driessen AK, Simmons DG, Powell J, Davis-Poynter N, Farrell MJ & Mazzone SB. (2015). Distinct brainstem and forebrain circuits receiving tracheal sensory neuron inputs revealed using a novel conditional anterograde transsynaptic viral tracing system. *The Journal of neuroscience : the official journal of the Society for Neuroscience* **35,** 7041-7055.

McHaffie JG, Kao CQ & Stein BE. (1989). Nociceptive neurons in rat superior colliculus: response properties, topography, and functional implications. *Journal of neurophysiology* **62,** 510-525.

McMullan S, Pathmanandavel K, Pilowsky PM & Goodchild AK. (2008). Somatic nerve stimulation evokes qualitatively different somatosympathetic responses in the cervical and splanchnic sympathetic nerves in the rat. *Brain Res* **1217,** 139-147.

McMullan S & Pilowsky PM. (2012). Sympathetic premotor neurones project to and are influenced by neurones in the contralateral rostral ventrolateral medulla of the rat in vivo. *Brain Res* **1439,** 34-43.

Meckler RL & Weaver LC. (1984). Comparison of the distributions of renal and splenic neurons in sympathetic ganglia. *Journal of the autonomic nervous system* **11,** 189-200.

Melone M, Burette A & Weinberg RJ. (2005). Light microscopic identification and immunocytochemical characterization of glutamatergic synapses in brain sections. *J Comp Neurol* **492,** 495-509.

Meredith MA & Stein BE. (1986). Visual, auditory, and somatosensory convergence on cells in superior colliculus results in multisensory integration. *Journal of neurophysiology* **56,** 640-662.

Meredith MA, Wallace MT & Stein BE. (1992). Visual, auditory and somatosensory convergence in output neurons of the cat superior colliculus: multisensory properties of the tecto-reticulo-spinal projection. *Exp Brain Res* **88,** 181-186.

Mifflin SW. (1992). Arterial chemoreceptor input to nucleus tractus solitarius. *The American journal of physiology* **263,** R368-375.

Mileykovskiy BY, Kiyashchenko LI & Siegel JM. (2005). Behavioral correlates of activity in identified hypocretin/orexin neurons. *Neuron* **46,** 787-798.

Milner TA, Reis DJ & Giuliano R. (1996). Afferent sources of substance P in the C1 area of the rat rostral ventrolateral medulla. *Neuroscience letters* **205,** 37-40.

Minson J, Arnolda L, Llewellyn-Smith I, Pilowsky P & Chalmers J. (1996). Altered c-fos in rostral medulla and spinal cord of spontaneously hypertensive rats. *Hypertension* **27,** 433-441.

Minson JB, Chalmers JP, Caon AC & Renaud B. (1987). Separate areas of rat medulla oblongata with populations of serotonin- and adrenaline-containing neurons alter blood pressure after L-glutamate stimulation. *Journal of the autonomic nervous system* **19,** 39-50.

Minson JB, Llewellyn-Smith IJ, Chalmers JP, Pilowsky PM & Arnolda LF. (1997). c-fos identifies GABA-synthesizing barosensitive neurons in caudal ventrolateral medulla. *NeuroReport* **8,** 3015-3021.

Mitra PP. (2014). The circuit architecture of whole brains at the mesoscopic scale. *Neuron* **83,** 1273-1283.

Miura M, Okada J & Takayama K. (1996). Parapyramidal rostroventromedial medulla as a respiratory rhythm modulator. *Neuroscience letters* **203,** 41-44.

Miyawaki T, Minson J, Arnolda L, Llewellyn-Smith I, Chalmers J & Pilowsky P. (1996). AMPA/kainate receptors mediate sympathetic chemoreceptor reflex in the rostral ventrolateral medulla. *Brain Res* **726,** 64-68.

Miyawaki T, Pilowsky P, Sun QJ, Minson J, Suzuki S, Arnolda L, Llewellyn-Smith I & Chalmers J. (1995). Central inspiration increases barosensitivity of neurons in rat rostral ventrolateral medulla. *The American journal of physiology* **268,** R909-918.

Moraes DJ, da Silva MP, Bonagamba LG, Mecawi AS, Zoccal DB, Antunes-Rodrigues J, Varanda WA & Machado BH. (2013). Electrophysiological properties of rostral ventrolateral medulla presympathetic neurons modulated by the respiratory network in rats. *The Journal of neuroscience : the official journal of the Society for Neuroscience* **33,** 19223-19237.

Morris KF, Arata A, Shannon R & Lindsey BG. (1996). Long-term facilitation of phrenic nerve activity in cats: responses and short time scale correlations of medullary neurones. *The Journal of physiology* **490 (Pt 2),** 463-480.

Morrison SF. (2001). Differential control of sympathetic outflow. *American journal of physiology Regulatory, integrative and comparative physiology* **281,** R683-698.

Morrison SF. (2003). Glutamate transmission in the rostral ventrolateral medullary sympathetic premotor pathway. *Cell Mol Neurobiol* **23,** 761-772.

Morrison SF, Milner TA & Reis DJ. (1988). Reticulospinal vasomotor neurons of the rat rostral ventrolateral medulla: relationship to sympathetic nerve activity and the C1 adrenergic cell group. *J Neurosci* **8,** 1286-1301.

Morrison SF & Reis DJ. (1989). Reticulospinal vasomotor neurons in the RVL mediate the somatosympathetic reflex. *Am J Physiol* **256,** R1084-1097.

Muller-Ribeiro FC, Dampney RA, McMullan S, Fontes MA & Goodchild AK. (2014). Disinhibition of the midbrain colliculi unmasks coordinated autonomic, respiratory, and somatomotor responses to auditory and visual stimuli. *Am J Physiol Regul Integr Comp Physiol* **307,** R1025-1035.

Munoz DP, Guitton D & Pelisson D. (1991). Control of orienting gaze shifts by the tectoreticulospinal system in the head-free cat. III. Spatiotemporal characteristics of phasic motor discharges. *Journal of neurophysiology* **66,** 1642-1666.

Murlidharan G, Samulski RJ & Asokan A. (2014). Biology of adeno-associated viral vectors in the central nervous system. *Frontiers in molecular neuroscience* **7,** 76.

Murphy SM, Pilowsky PM, Sun QJ & Llewellyn-Smith IJ. (1995). Thyrotropin-releasing hormone-immunoreactive varicosities synapse on rat phrenic motoneurons. *The Journal of comparative neurology* **359,** 310-322.

Murray EA & Coulter JD. (1982). Organization of tectospinal neurons in the cat and rat superior colliculus. *Brain research* **243,** 201-214.

Nassi JJ, Cepko CL, Born RT & Beier KT. (2015). Neuroanatomy goes viral! *Frontiers in neuroanatomy* **9,** 80.

Nauta WJ. (1952). Selective silver impregnation of degenerating axons in the central nervous system. *Stain Technol* **27,** 175-179.

Nicholas AP & Hancock MB. (1991). Projections from the rostral ventrolateral medulla to brainstem monoamine neurons in the rat. *Neurosci Lett* **122,** 91-95.

Nimchinsky EA, Sabatini BL & Svoboda K. (2002). Structure and function of dendritic spines. *Annual review of physiology* **64,** 313-353.

Noseda R, Kainz V, Jakubowski M, Gooley JJ, Saper CB, Digre K & Burstein R. (2010). A neural mechanism for exacerbation of headache by light. *Nat Neurosci* **13,** 239-245.

Nyberg-Hansen R. (1964). The Location and Termination of Tectospinal Fibers in the Cat. *Experimental neurology* **9,** 212-227.

Nyberg-Hansen R. (1966). Functional organization of descending supraspinal fibre systems to the spinalcord. Anatomical observations and physiological correlations. *Ergebnisse der Anatomie und Entwicklungsgeschichte* **39,** 3-48.

Oh SW, Harris JA, Ng L, Winslow B, Cain N, Mihalas S, Wang Q, Lau C, Kuan L, Henry AM, Mortrud MT, Ouellette B, Nguyen TN, Sorensen SA, Slaughterbeck CR, Wakeman W, Li Y,

Feng D, Ho A, Nicholas E, Hirokawa KE, Bohn P, Joines KM, Peng H, Hawrylycz MJ, Phillips JW, Hohmann JG, Wohnoutka P, Gerfen CR, Koch C, Bernard A, Dang C, Jones AR & Zeng H. (2014). A mesoscale connectome of the mouse brain. *Nature* **508,** 207-214.

Oliveira-Sales EB, Colombari E, Abdala AP, Campos RR & Paton JF. (2016). Sympathetic overactivity occurs before hypertension in the two-kidney, one-clip model. *Exp Physiol* **101,** 67-80.

Onimaru H & Homma I. (2007). Spontaneous oscillatory burst activity in the piriform-amygdala region and its relation to in vitro respiratory activity in newborn rats. *Neuroscience* **144,** 387-394.

Osakada F & Callaway EM. (2013). Design and generation of recombinant rabies virus vectors. *Nat Protoc* **8,** 1583-1601.

Osakada F, Mori T, Cetin AH, Marshel JH, Virgen B & Callaway EM. (2011). New rabies virus variants for monitoring and manipulating activity and gene expression in defined neural circuits. *Neuron* **71,** 617-631.

Oshima N, Kumagai H, Onimaru H, Kawai A, Pilowsky PM, Iigaya K, Takimoto C, Hayashi K, Saruta T & Itoh H. (2008). Monosynaptic excitatory connection from the rostral ventrolateral medulla to sympathetic preganglionic neurons revealed by simultaneous recordings. *Hypertension research : official journal of the Japanese Society of Hypertension* **31,** 1445-1454.

Oshima N, McMullan S, Goodchild AK & Pilowsky PM. (2006). A monosynaptic connection between baroinhibited neurons in the RVLM and IML in Sprague-Dawley rats. *Brain Res* **1089,** 153-161.

Osten P & Margrie TW. (2013). Mapping brain circuitry with a light microscope. *Nature methods* **10,** 515-523.

Oyama K, Ohara S, Sato S, Karube F, Fujiyama F, Isomura Y, Mushiake H, Iijima T & Tsutsui K. (2013). Long-lasting single-neuron labeling by in vivo electroporation without microscopic guidance. *Journal of neuroscience methods* **218,** 139-147.

Packer AM, Roska B & Hausser M. (2013). Targeting neurons and photons for optogenetics. *Nature neuroscience* **16,** 805-815.

Papp EA, Csucs G & Bjaalie JG. (2015). Sprague Dawley Atlas v2 bundle. In *Waxholm Space atlas of the Sprague Dawley rat brain*. The International Neuroinformatics Coordinating Facility, INCF Software Center.

Papp EA, Leergaard TB, Calabrese E, Johnson GA & Bjaalie JG. (2014). Waxholm Space atlas of the Sprague Dawley rat brain. *Neuroimage* **97,** 374-386.

Pasternak JF & Woolsey TA. (1975). On the "selectivity" of the Golgi-Cox method. *The Journal of comparative neurology* **160,** 307-312.

Paton JF. (1996). A working heart-brainstem preparation of the mouse. *J Neurosci Methods* **65,** 63-68.

Paxinos G & Watson C. (2005). *The rat brain in stereotaxic coordinates*. Elsevier Academic Press, Amsterdam ; Boston.

Paxinos G & Watson C. (2006). *The Rat Brain in Stereotaxic Coordinates*. Academic Press.

Paxinos G & Watson C. (2007). *The rat brain in stereotaxic coordinates*. Academic Press/Elsevier, Amsterdam ; Boston ;.

Petras JM. (1967). Cortical, tectal and tegmental fiber connections in the spinal cord of the cat. *Brain research* **6,** 275-324.

Petrov T, Krukoff TL & Jhamandas JH. (1993). Branching projections of catecholaminergic brainstem neurons to the paraventricular hypothalamic nucleus and the central nucleus of the amygdala in the rat. *Brain Res* **609,** 81-92.

Phillips JK, Goodchild AK, Dubey R, Sesiashvili E, Takeda M, Chalmers J, Pilowsky PM & Lipski J. (2001). Differential expression of catecholamine biosynthetic enzymes in the rat ventrolateral medulla. *J Comp Neurol* **432,** 20-34.

Pickering AE, Spanswick D & Logan SD. (1991). Whole-cell recordings from sympathetic preganglionic neurons in rat spinal cord slices. *Neurosci Lett* **130,** 237-242.

Pilowsky P, West M & Chalmers J. (1985). Renal sympathetic nerve responses to stimulation, inhibition and destruction of the ventrolateral medulla in the rabbit. *Neuroscience letters* **60,** 51-55.

Pilowsky PM & Goodchild AK. (2002). Baroreceptor reflex pathways and neurotransmitters: 10 years on. *J Hypertens* **20,** 1675-1688.

Pilowsky PM, Miyawaki T, Minson JB, Sun QJ, Arnolda LF, Llewellyn-Smith IJ & Chalmers JP. (1995). Bulbospinal sympatho-excitatory neurons in the rat caudal raphe. *Journal of hypertension* **13,** 1618-1623.

Pinault D. (1996). A novel single-cell staining procedure performed in vivo under electrophysiological control: morpho-functional features of juxtacellularly labeled thalamic cells and other central neurons with biocytin or Neurobiotin. *J Neurosci Methods* **65,** 113-136.

Pinault D. (2011). The juxtacellular recording-labeling technique. In *Electrophysiological Recording Techniques*, ed. Vertes RP & Stackman RW, pp. 41-75. Springer Science+Business Media, LLC.

Pinol RA, Bateman R & Mendelowitz D. (2012). Optogenetic approaches to characterize the long-range synaptic pathways from the hypothalamus to brain stem autonomic nuclei. *Journal of neuroscience methods* **210,** 238-246.

Potts JT & Mitchell JH. (1998). Rapid resetting of carotid baroreceptor reflex by afferent input from skeletal muscle receptors. *The American journal of physiology* **275,** H2000-2008.

Powell EW & Hatton JB. (1969). Projections of the inferior colliculus in cat. *The Journal of comparative neurology* **136,** 183-192.

Pyner S & Coote JH. (1994a). A comparison between the adult rat and neonate rat of the architecture of sympathetic preganglionic neurones projecting to the superior cervical ganglion, stellate ganglion and adrenal medulla. *Journal of the autonomic nervous system* **48,** 153-166.

Pyner S & Coote JH. (1994b). Evidence that sympathetic preganglionic neurones are arranged in target-specific columns in the thoracic spinal cord of the rat. *The Journal of comparative neurology* **342,** 15-22.

Pyner S & Coote JH. (1998). Rostroventrolateral medulla neurons preferentially project to target-specified sympathetic preganglionic neurons. *Neuroscience* **83,** 617-631.

Rae JL & Levis RA. (2002). Single-cell electroporation. *Pflugers Arch* **443,** 664-670.

Rancz EA, Franks KM, Schwarz MK, Pichler B, Schaefer AT & Margrie TW. (2011). Transfection via whole-cell recording in vivo: bridging single-cell physiology, genetics and connectomics. *Nature neuroscience* **14,** 527-532.

Rathenberg J, Nevian T & Witzemann V. (2003). High-efficiency transfection of individual neurons using modified electrophysiology techniques. *Journal of Neuroscience Methods* **126,** 91-98.

Reardon TR, Murray AJ, Turi GF, Wirblich C, Croce KR, Schnell MJ, Jessell TM & Losonczy A. (2016). Rabies Virus CVS-N2c Strain Enhances Retrograde Synaptic Transfer and Neuronal Viability. *Neuron*.

Redgrave P, Mitchell IJ & Dean P. (1987). Descending projections from the superior colliculus in rat: a study using orthograde transport of wheatgerm-agglutinin conjugated horseradish peroxidase. *Exp Brain Res* **68,** 147-167.

Reiner A, Veenman CL, Medina L, Jiao Y, Del Mar N & Honig MG. (2000). Pathway tracing using biotinylated dextran amines. *Journal of neuroscience methods* **103,** 23-37.

Reis DJ, Golanov EV, Galea E & Feinstein DL. (1997). Central neurogenic neuroprotection: central neural systems that protect the brain from hypoxia and ischemia. *Ann N Y Acad Sci* **835,** 168-186.

Reis DJ, Morrison S & Ruggiero DA. (1988). The C1 area of the brainstem in tonic and reflex control of blood pressure. State of the art lecture. *Hypertension* **11,** I8-13.

Rhoades RW, Mooney RD, Klein BG, Jacquin MF, Szczepanik AM & Chiaia NL. (1987). The structural and functional characteristics of tectospinal neurons in the golden hamster. *The Journal of comparative neurology* **255,** 451-465.

Rice CD, Weber SA, Waggoner AL, Jessell ME & Yates BJ. (2010). Mapping of neural pathways that influence diaphragm activity and project to the lumbar spinal cord in cats. *Exp Brain Res* **203,** 205-211.

Rinaman L & Schwartz G. (2004). Anterograde transneuronal viral tracing of central viscerosensory pathways in rats. *The Journal of neuroscience : the official journal of the Society for Neuroscience* **24,** 2782-2786.

Ritter S, Bugarith K & Dinh TT. (2001). Immunotoxic destruction of distinct catecholamine subgroups produces selective impairment of glucoregulatory responses and neuronal activation. *The Journal of comparative neurology* **432,** 197-216.

Rockland KS. (2015). About connections. *Front Neuroanat* **9,** 61.

Roseberry TK, Lee AM, Lalive AL, Wilbrecht L, Bonci A & Kreitzer AC. (2016). Cell-Type-Specific Control of Brainstem Locomotor Circuits by Basal Ganglia. *Cell* **164,** 526-537.

Rosin DL, Chang DA & Guyenet PG. (2006). Afferent and efferent connections of the rat retrotrapezoid nucleus. *The Journal of comparative neurology* **499,** 64-89.

Ross CA, Armstrong DM, Ruggiero DA, Pickel VM, Joh TH & Reis DJ. (1981). Adrenaline neurons in the rostral ventrolateral medulla innervate thoracic spinal cord: a combined immunocytochemical and retrograde transport demonstration. *Neurosci Lett* **25,** 257-262.

Ross CA, Ruggiero DA, Park DH, Joh TH, Sved AF, Fernandez-Pardal J, Saavedra JM & Reis DJ. (1984). Tonic vasomotor control by the rostral ventrolateral medulla: effect of electrical or chemical stimulation of the area containing C1 adrenaline neurons on arterial pressure, heart rate, and plasma catecholamines and vasopressin. *J Neurosci* **4,** 474-494.

Ross CA, Ruggiero DA & Reis DJ. (1985). Projections from the nucleus tractus solitarii to the rostral ventrolateral medulla. *J Comp Neurol* **242,** 511-534.

Rowell LB. (1974). Human cardiovascular adjustments to exercise and thermal stress. *Physiological reviews* **54,** 75-159.

Rubelowski JM, Menge M, Distler C, Rothermel M & Hoffmann KP. (2013). Connections of the superior colliculus to shoulder muscles of the rat: a dual tracing study. *Frontiers in neuroanatomy* **7,** 17.

Saha S. (2005). Role of the central nucleus of the amygdala in the control of blood pressure: descending pathways to medullary cardiovascular nuclei. *Clin Exp Pharmacol Physiol* **32,** 450-456.

Sahibzada N, Dean P & Redgrave P. (1986). Movements resembling orientation or avoidance elicited by electrical stimulation of the superior colliculus in rats. *The Journal of neuroscience : the official journal of the Society for Neuroscience* **6,** 723-733.

Santos SF, Luz LL, Szucs P, Lima D, Derkach VA & Safronov BV. (2009). Transmission efficacy and plasticity in glutamatergic synapses formed by excitatory interneurons of the substantia gelatinosa in the rat spinal cord. *PLoS One* **4,** e8047.

Santos SF, Rebelo S, Derkach VA & Safronov BV. (2007). Excitatory interneurons dominate sensory processing in the spinal substantia gelatinosa of rat. *J Physiol* **581,** 241-254.

Sartor DM & Verberne AJ. (2003). Phenotypic identification of rat rostroventrolateral medullary presympathetic vasomotor neurons inhibited by exogenous cholecystokinin. *The Journal of comparative neurology* **465,** 467-479.

Sato A. (1973). Spinal and medullary reflex components of the somatosympathetic reflex discharges evoked by stimulation of the group IV somatic afferents. *Brain research* **51,** 307-318.

Saunders A, Johnson CA & Sabatini BL. (2012). Novel recombinant adeno-associated viruses for Cre activated and inactivated transgene expression in neurons. *Front Neural Circuits* **6,** 47.

Sawchenko PE & Swanson LW. (1982). The organization of noradrenergic pathways from the brainstem to the paraventricular and supraoptic nuclei in the rat. *Brain Res* **257,** 275-325.

Schmued LC & Fallon JH. (1986). Fluoro-Gold: a new fluorescent retrograde axonal tracer with numerous unique properties. *Brain research* **377,** 147-154.

Schnutgen F, Doerflinger N, Calleja C, Wendling O, Chambon P & Ghyselinck NB. (2003). A directional strategy for monitoring Cre-mediated recombination at the cellular level in the mouse. *Nat Biotechnol* **21,** 562-565.

Schramm AE, Marinazzo D, Gener T & Graham LJ. (2014). The touch and zap method for in vivo whole-cell patch recording of intrinsic and visual responses of cortical neurons and glial cells. *PLoS One* **9,** e97310.

Schramm LP, Strack AM, Platt KB & Loewy AD. (1993). Peripheral and central pathways regulating the kidney: a study using pseudorabies virus. *Brain research* **616,** 251-262.

Schreihofer AM & Guyenet PG. (1997). Identification of C1 presympathetic neurons in rat rostral ventrolateral medulla by juxtacellular labeling in vivo. *J Comp Neurol* **387,** 524-536.

Schreihofer AM & Guyenet PG. (2000). Sympathetic reflexes after depletion of bulbospinal catecholaminergic neurons with anti-DbetaH-saporin. *Am J Physiol Regul Integr Comp Physiol* **279,** R729-742.

Schreihofer AM & Guyenet PG. (2002). The baroreflex and beyond: control of sympathetic vasomotor tone by GABAergic neurons in the ventrolateral medulla. *Clin Exp Pharmacol Physiol* **29,** 514-521.

Schreihofer AM & Guyenet PG. (2003). Baro-activated neurons with pulse-modulated activity in the rat caudal ventrolateral medulla express GAD67 mRNA. *J Neurophysiol* **89,** 1265-1277.

Schreihofer AM, Stornetta RL & Guyenet PG. (1999). Evidence for glycinergic respiratory neurons: Botzinger neurons express mRNA for glycinergic transporter 2. *Journal of Comparative Neurology* **407,** 583-597.

Schwarz LA, Miyamichi K, Gao XJ, Beier KT, Weissbourd B, DeLoach KE, Ren J, Ibanes S, Malenka RC, Kremer EJ & Luo L. (2015). Viral-genetic tracing of the input-output organization of a central noradrenaline circuit. *Nature* **524,** 88-92.

Sevigny CP, Bassi J, Teschemacher AG, Kim KS, Williams DA, Anderson CR & Allen AM. (2008). C1 neurons in the rat rostral ventrolateral medulla differentially express vesicular monoamine transporter 2 in soma and axonal compartments. *European Journal of Neuroscience* **28,** 1536-1544.

Shafton AD & McAllen RM. (2013). Location of cat brain stem neurons that drive sweating. *Am J Physiol-Reg I* **304,** R804-R809.

Shafton AD, Ryan A & Badoer E. (1998). Neurons in the hypothalamic paraventricular nucleus send collaterals to the spinal cord and to the rostral ventrolateral medulla in the rat. *Brain Res* **801,** 239-243.

Shintani T, Anker AR, Billig I, Card JP & Yates BJ. (2003). Transneuronal tracing of neural pathways influencing both diaphragm and genioglossal muscle activity in the ferret. *Journal of applied physiology* **95,** 1453-1459.

Siegel JM. (1979). Behavioral functions of the reticular formation. *Brain research* **180,** 69-105.

Simms AE, Paton JF, Pickering AE & Allen AM. (2009). Amplified respiratory-sympathetic coupling in the spontaneously hypertensive rat: does it contribute to hypertension? *J Physiol* **587,** 597-610.

Smith JC, Abdala AP, Borgmann A, Rybak IA & Paton JF. (2013). Brainstem respiratory networks: building blocks and microcircuits. *Trends Neurosci* **36,** 152-162.

Smith JC, Abdala AP, Rybak IA & Paton JF. (2009). Structural and functional architecture of respiratory networks in the mammalian brainstem. *Philos Trans R Soc Lond B Biol Sci* **364,** 2577-2587.

Smith JC, Ellenberger HH, Ballanyi K, Richter DW & Feldman JL. (1991). Pre-Botzinger complex: A brainstem region that may generate respiratory rhythm in mammals. *Science* **254,** 726-729.

Smith JC, Morrison DE, Ellenberger HH, Otto MR & Feldman JL. (1989a). Brainstem projections to the major respiratory neuron populations in the medulla of the cat. *The Journal of comparative neurology* **281,** 69-96.

Smith JC, Morrison DE, Ellenberger HH, Otto MR & Feldman JL. (1989b). Brainstem projections to the major respiratory neuron populations in the medulla of the cat. *J Comp Neurol* **281,** 69-96.

Song CK, Schwartz GJ & Bartness TJ. (2009). Anterograde transneuronal viral tract tracing reveals central sensory circuits from white adipose tissue. *American journal of physiology Regulatory, integrative and comparative physiology* **296,** R501-511.

Sparks DL. (1988). Neural cartography: sensory and motor maps in the superior colliculus. *Brain, behavior and evolution* **31,** 49-56.

Spira ME & Hai A. (2013). Multi-electrode array technologies for neuroscience and cardiology. *Nat Nanotechnol* **8,** 83-94.

Sporns O, Tononi G & Kotter R. (2005). The human connectome: A structural description of the human brain. *PLoS Comput Biol* **1,** e42.

Stein BE, Wallace MT & Meredith MA. (1995). Neural mechanisms mediating attention and orientation to multisensory cues. In *The cognitive neurosciences*, pp. 683-702. The MIT Press, Cambridge, MA, US.

Steinbacher BC, Jr. & Yates BJ. (1996). Brainstem interneurons necessary for vestibular influences on sympathetic outflow. *Brain Res* **720,** 204-210.

Steinmeyer JD & Yanik MF. (2012). High-throughput single-cell manipulation in brain tissue. *PLoS One* **7,** e35603.

Stepien AE, Tripodi M & Arber S. (2010). Monosynaptic rabies virus reveals premotor network organization and synaptic specificity of cholinergic partition cells. *Neuron* **68,** 456-472.

Stocker SD, Osborn JL & Carmichael SP. (2008). Forebrain osmotic regulation of the sympathetic nervous system. *Clinical and experimental pharmacology & physiology* **35,** 695-700.

Stoeckel K, Schwab M & Thoenen H. (1977). Role of gangliosides in the uptake and retrograde axonal transport of cholera and tetanus toxin as compared to nerve growth factor and wheat germ agglutinin. *Brain research* **132,** 273-285.

Stornetta RL & Guyenet PG. (1999). Distribution of glutamic acid decarboxylase mRNA-containing neurons in rat medulla projecting to thoracic spinal cord in relation to monoaminergic brainstem neurons. *The Journal of comparative neurology* **407,** 367-380.

Stornetta RL, Inglis MA, Viar KE & Guyenet PG. (2015). Afferent and efferent connections of C1 cells with spinal cord or hypothalamic projections in mice. *Brain structure & function*.

Stornetta RL, McQuiston TJ & Guyenet PG. (2004). GABAergic and glycinergic presympathetic neurons of rat medulla oblongata identified by retrograde transport of pseudorabies virus and in situ hybridization. *The Journal of comparative neurology* **479,** 257-270.

Stornetta RL, Sevigny CP, Schreihofer AM, Rosin DL & Guyenet PG. (2002). Vesicular glutamate transporter DNPI/VGLUT2 is expressed by both C1 adrenergic and nonaminergic presympathetic vasomotor neurons of the rat medulla. *J Comp Neurol* **444,** 207-220.

Strack AM, Sawyer WB, Hughes JH, Platt KB & Loewy AD. (1989a). A general pattern of CNS innervation of the sympathetic outflow demonstrated by transneuronal pseudorabies viral infections. *Brain research* **491,** 156-162.

Strack AM, Sawyer WB, Marubio LM & Loewy AD. (1988). Spinal origin of sympathetic preganglionic neurons in the rat. *Brain research* **455,** 187-191.

Strack AM, Sawyer WB, Platt KB & Loewy AD. (1989b). CNS cell groups regulating the sympathetic outflow to adrenal gland as revealed by transneuronal cell body labeling with pseudorabies virus. *Brain Res* **491,** 274-296.

Stretton AO & Kravitz EA. (1968). Neuronal geometry: determination with a technique of intracellular dye injection. *Science* **162,** 132-134.

Sugiyama Y, Suzuki T & Yates BJ. (2011). Role of the rostral ventrolateral medulla (RVLM) in the patterning of vestibular system influences on sympathetic nervous system outflow to the upper and lower body. *Exp Brain Res* **210,** 515-527.

Sun MK & Guyenet PG. (1985). GABA-mediated baroreceptor inhibition of reticulospinal neurons. *AmJPhysiol* **249,** R672.

Sun MK & Guyenet PG. (1986). Hypothalamic glutamatergic input to medullary sympathoexcitatory neurons in rats. *Am J Physiol* **251,** R798-810.

Sun MK, Jeske IT & Reis DJ. (1992). Cyanide excites medullary sympathoexcitatory neurons in rats. *Am J Physiol* **262,** R182-189.

Sun MK, Young BS, Hackett JT & Guyenet PG. (1988). Reticulospinal pacemaker neurons of the rat rostral ventrolateral medulla with putative sympathoexcitatory function: an intracellular study in vitro. *Brain Res* **442,** 229-239.

Sun QJ, Minson J, Llewellyn-Smith IJ, Arnolda L, Chalmers J & Pilowsky P. (1997). Botzinger neurons project towards bulbospinal neurons in the rostral ventrolateral medulla of the rat. *Journal of Comparative Neurology* **388,** 23-31.

Takatoh J, Nelson A, Zhou X, Bolton MM, Ehlers MD, Arenkiel BR, Mooney R & Wang F. (2013). New modules are added to vibrissal premotor circuitry with the emergence of exploratory whisking. *Neuron* **77,** 346-360.

Talman WT & Robertson SC. (1991). Nucleus prepositus hypoglossi. A medullary pressor region. *Hypertension* **17,** 1173-1176.

Tan W, Pagliardini S, Yang P, Janczewski WA & Feldman JL. (2010). Projections of preBotzinger complex neurons in adult rats. *J Comp Neurol* **518,** 1862-1878.

Tanaka M, Nagashima K, McAllen RM & Kanosue K. (2002). Role of the medullary raphe in thermoregulatory vasomotor control in rats. *The Journal of physiology* **540,** 657-664.

Terhorst GJ, Copray JCVM, Liem RSB & Vanwilligen JD. (1991). Projections from the Rostral Parvocellular Reticular-Formation to Pontine and Medullary Nuclei in the Rat - Involvement in Autonomic Regulation and Orofacial Motor Control. *Neuroscience* **40,** 735-758.

Thurston CL & Randich A. (1995). Responses of on and off cells in the rostral ventral medulla to stimulation of vagal afferents and changes in mean arterial blood pressure in intact and cardiopulmonary deafferented rats. *Pain* **62,** 19-38.

Tomer R, Ye L, Hsueh B & Deisseroth K. (2014). Advanced CLARITY for rapid and high-resolution imaging of intact tissues. *Nature protocols* **9,** 1682-1697.

Tsumori T & Yasui Y. (1997). Organization of the nigro-tecto-bulbar pathway to the parvicellular reticular formation: a light- and electron-microscopic study in the rat. *Exp Brain Res* **116,** 341-350.

Tucker DC, Saper CB, Ruggiero DA & Reis DJ. (1987). Organization of central adrenergic pathways: I. Relationships of ventrolateral medullary projections to the hypothalamus and spinal cord. *J Comp Neurol* **259,** 591-603.

Turner A, Kumar N, Farnham M, Lung M, Pilowsky P & McMullan S. (2013). Rostroventrolateral medulla neurons with commissural projections provide input to sympathetic premotor neurons: anatomical and functional evidence. *Eur J Neurosci* **38,** 2504-2515.

Turner DL. (1991). Cardiovascular and respiratory control mechanisms during exercise: an integrated view. *The Journal of experimental biology* **160,** 309-340.

Ugolini G. (1995). Specificity of rabies virus as a transneuronal tracer of motor networks: transfer from hypoglossal motoneurons to connected second-order and higher order central nervous system cell groups. *J Comp Neurol* **356,** 457-480.

Ugolini G. (2008). Use of rabies virus as a transneuronal tracer of neuronal connections: implications for the understanding of rabies pathogenesis. *Dev Biol (Basel)* **131,** 493-506.

Ugolini G. (2010a). Advances in viral transneuronal tracing. *Journal of Neuroscience Methods* **194,** 2-20.

Ugolini G. (2010b). Advances in viral transneuronal tracing. *Journal of neuroscience methods* **194,** 2-20.

Ugolini G. (2011). Rabies Virus as a Transneuronal Tracer of Neuronal Connections. *Adv Virus Res* **79,** 165-202.

Umeda T, Ebihara T & Okabe S. (2005). Simultaneous observation of stably associated presynaptic varicosities and postsynaptic spines: morphological alterations of CA3-CA1 synapses in hippocampal slice cultures. *Mol Cell Neurosci* **28,** 264-274.

Van Bockstaele EJ, Pieribone VA & Aston-Jones G. (1989). Diverse afferents converge on the nucleus paragigantocellularis in the rat ventrolateral medulla: retrograde and anterograde tracing studies. *The Journal of comparative neurology* **290,** 561-584.

Varner KJ, Grosskreutz CL, Cox BF & Brody MJ. (1989). Differential regulation of sympathetic nerve activity by lateral and medial subregions of the rostral ventral medulla. *Progress in brain research* **81,** 99-103.

Varner KJ, Rutherford DS, Vasquez EC & Brody MJ. (1992). Identification of cardiovascular neurons in the rostral ventromedial medulla in anesthetized rats. *Hypertension* **19,** II193-197.

Varner KJ, Vasquez EC & Brody MJ. (1994). Lesions in rostral ventromedial or rostral ventrolateral medulla block neurogenic hypertension. *Hypertension* **24,** 91-96.

Vaughan CH & Bartness TJ. (2012). Anterograde transneuronal viral tract tracing reveals central sensory circuits from brown fat and sensory denervation alters its thermogenic responses. *American journal of physiology Regulatory, integrative and comparative physiology* **302,** R1049-1058.

Veenman CL, Reiner A & Honig MG. (1992). Biotinylated Dextran Amine as an Anterograde Tracer for Single-Labeling and Double-Labeling Studies. *Journal of neuroscience methods* **41,** 239-254.

Velez-Fort M, Rousseau CV, Niedworok CJ, Wickersham IR, Rancz EA, Brown AP, Strom M & Margrie TW. (2014). The stimulus selectivity and connectivity of layer six principal cells reveals cortical microcircuits underlying visual processing. *Neuron* **83,** 1431-1443.

Verberne AJ. (1996). Medullary sympathoexcitatory neurons are inhibited by activation of the medial prefrontal cortex in the rat. *Am J Physiol* **270,** R713-719.

Verberne AJ & Sartor DM. (2010). Rostroventrolateral medullary neurons modulate glucose homeostasis in the rat. *Am J Physiol Endocrinol Metab* **299,** E802-807.

Verberne AJ, Stornetta RL & Guyenet PG. (1999a). Properties of C1 and other ventrolateral medullary neurones with hypothalamic projections in the rat. *The Journal of physiology* **517 (Pt 2),** 477-494.

Verberne AJ, Stornetta RL & Guyenet PG. (1999b). Properties of C1 and other ventrolateral medullary neurones with hypothalamic projections in the rat. *Journal of Physiology* **517 (Pt 2),** 477-494.

Vivar C & van Praag H. (2013). Functional circuits of new neurons in the dentate gyrus. *Front Neural Circuits* **7,** 15.

Vos A, Neubert A, Aylan O, Schuster P, Pommerening E, Muller T & Chivatsi DC. (1999). An update on safety studies of SAD B19 rabies virus vaccine in target and non-target species. *Epidemiology and infection* **123,** 165-175.

Waldrop TG, Eldridge FL, Iwamoto GA & Mitchell JH. (2010). Central Neural Control of Respiration and Circulation During Exercise. In *Comprehensive Physiology*. John Wiley & Sons, Inc.

Waller A. (1850). Experiments on the Section of the Glossopharyngeal and Hypoglossal Nerves of the Frog, and Observations of the Alterations Produced Thereby in the Structure of Their Primitive Fibres. *Philosophical Transactions of the Royal Society of London* **140,** 423-429.

Wang H & Wessendorf MW. (2002). Mu- and delta-opioid receptor mRNAs are expressed in periaqueductal gray neurons projecting to the rostral ventromedial medulla. *Neuroscience* **109,** 619-634.

Wang M, Orwar O, Olofsson J & Weber SG. (2010). Single-cell electroporation. *Analytical and Bioanalytical Chemistry* **397,** 3235-3248.

Wanner AA, Kirschmann MA & Genoud C. (2015). Challenges of microtome-based serial block-face scanning electron microscopy in neuroscience. *J Microsc* **259,** 137-142.

Weaver LC, Fry HK & Meckler RL. (1984). Differential renal and splenic nerve responses to vagal and spinal afferent inputs. *Am J Physiol* **246,** R78-87.

Weber F, Chung S, Beier KT, Xu M, Luo L & Dan Y. (2015). Control of REM sleep by ventral medulla GABAergic neurons. *Nature* **526,** 435-438.

Wei P, Liu N, Zhang Z, Liu X, Tang Y, He X, Wu B, Zhou Z, Liu Y, Li J, Zhang Y, Zhou X, Xu L, Chen L, Bi G, Hu X, Xu F & Wang L. (2015). Processing of visually evoked innate fear by a non-canonical thalamic pathway. *Nat Commun* **6,** 6756.

Wertz A, Trenholm S, Yonehara K, Hillier D, Raics Z, Leinweber M, Szalay G, Ghanem A, Keller G, Rozsa B, Conzelmann KK & Roska B. (2015). PRESYNAPTIC NETWORKS. Single-cell-initiated monosynaptic tracing reveals layer-specific cortical network modules. *Science* **349,** 70-74.

Westerhaus MJ & Loewy AD. (2001). Central representation of the sympathetic nervous system in the cerebral cortex. *Brain Res* **903,** 117-127.

White JG, Southgate E, Thomson JN & Brenner S. (1986). The structure of the nervous system of the nematode Caenorhabditis elegans. *Philosophical transactions of the Royal Society of London Series B, Biological sciences* **314,** 1-340.

Wickersham IR & Feinberg EH. (2012). New technologies for imaging synaptic partners. *Current opinion in neurobiology* **22,** 121-127.

Wickersham IR, Finke S, Conzelmann KK & Callaway EM. (2007a). Retrograde neuronal tracing with a deletion-mutant rabies virus. *Nat Methods* **4,** 47-49.

Wickersham IR, Lyon DC, Barnard RJ, Mori T, Finke S, Conzelmann KK, Young JA & Callaway EM. (2007b). Monosynaptic restriction of transsynaptic tracing from single, genetically targeted neurons. *Neuron* **53,** 639-647.

Willette RN, Barcas PP, Krieger AJ & Sapru HN. (1983a). Vasopressor and depressor areas in the rat medulla. Identification by microinjection of L-glutamate. *Neuropharmacology* **22,** 1071-1079.

Willette RN, Krieger AJ, Barcas PP & Sapru HN. (1983b). Medullary gamma-aminobutyric acid (GABA) receptors and the regulation of blood pressure in the rat. *J Pharmacol Exp Ther* **226,** 893-899.

Willette RN, Punnen S, Krieger AJ & Sapru HN. (1984). Interdependence of rostral and caudal ventrolateral medullary areas in the control of blood pressure. *Brain Research* **321,** 169-174.

Wojaczynski GJ, Engel EA, Steren KE, Enquist LW & Patrick Card J. (2015). The neuroinvasive profiles of H129 (herpes simplex virus type 1) recombinants with putative anterograde-only transneuronal spread properties. *Brain structure & function* **220,** 1395-1420.

Wouterlood FG, Bloem B, Mansvelder HD, Luchicchi A & Deisseroth K. (2014). A fourth generation of neuroanatomical tracing techniques: exploiting the offspring of genetic engineering. *Journal of neuroscience methods* **235,** 331-348.

Yasui Y, Tsumori T, Ando A, Domoto T, Kayahara T & Nakano K. (1994). Descending projections from the superior colliculus to the reticular formation around the motor trigeminal nucleus and the parvicellular reticular formation of the medulla oblongata in the rat. *Brain research* **656,** 420-426.

Yates BJ. (1992). Vestibular influences on the sympathetic nervous system. *Brain research Brain research reviews* **17,** 51-59.

Yates BJ & Miller AD. (1994). Properties of sympathetic reflexes elicited by natural vestibular stimulation: implications for cardiovascular control. *Journal of neurophysiology* **71,** 2087-2092.

Yates BJ, Smail JA, Stocker SD & Card JP. (1999). Transneuronal tracing of neural pathways controlling activity of diaphragm motoneurons in the ferret. *Neuroscience* **90,** 1501-1513.

Yates BJ, Yamagata Y & Bolton PS. (1991). The ventrolateral medulla of the cat mediates vestibulosympathetic reflexes. *Brain research* **552,** 265-272.

Yoder RM & Taube JS. (2014). The vestibular contribution to the head direction signal and navigation. *Frontiers in integrative neuroscience* **8,** 32.

Yonehara K, Farrow K, Ghanem A, Hillier D, Balint K, Teixeira M, Juttner J, Noda M, Neve RL, Conzelmann KK & Roska B. (2013). The first stage of cardinal direction selectivity is localized to the dendrites of retinal ganglion cells. *Neuron* **79,** 1078-1085.

Zagon A. (1995). Internal connections in the rostral ventromedial medulla of the rat. *J Auton Nerv Syst* **53,** 43-56.

Zhang J & Mifflin SW. (1998). Differential roles for NMDA and non-NMDA receptor subtypes in baroreceptor afferent integration in the nucleus of the solitary tract of the rat. *The Journal of physiology* **511 (Pt 3),** 733-745.

Zoccal DB, Simms AE, Bonagamba LG, Braga VA, Pickering AE, Paton JF & Machado BH. (2008). Increased sympathetic outflow in juvenile rats submitted to chronic intermittent hypoxia correlates with enhanced expiratory activity. *J Physiol* **586,** 3253-3265.

APPENDICIES